Department of
Industry and Resources

REPORT
99

MESOPROTEROZOIC SILL COMPLEXES IN THE BANGEMALL SUPERGROUP WESTERN AUSTRALIA: GEOLOGY, GEOCHEMISTRY, AND MINERALIZATION POTENTIAL

by P. A. Morris and F. Pirajno

Geological Survey of Western Australia

GEOLOGICAL SURVEY OF WESTERN AUSTRALIA

REPORT 99

MESOPROTEROZOIC SILL COMPLEXES IN THE BANGEMALL SUPERGROUP, WESTERN AUSTRALIA: GEOLOGY, GEOCHEMISTRY, AND MINERALIZATION POTENTIAL

by
P. A. Morris and F. Pirajno

Perth 2005

REFERENCE
The recommended reference for this publication is:
MORRIS, P. A., and PIRAJNO, F., 2005, Mesoproterozoic sill complexes in the Bangemall Supergroup, Western Australia: geology, geochemistry, and mineralization potential: Western Australia Geological Survey, Report 99, 75p.

National Library of Australia
Cataloguing-in-publication entry

Morris, P. A. (Paul Andrew), 1952–.
Mesoproterozoic sill complexes in the Bangemall Supergroup, Western Australia: geology, geochemistry and mineralization potential.

Bibliography.
ISBN 0 7307 8987 X

1. Sills (Geology) — Western Australia — Bangemall Basin.
2. Diabase — Western Australia — Bangemall Basin.
3. Mantle plumes — Western Australia — Bangemall Basin.
I. Pirajno, Franco, 1939–.
II. Geological Survey of Western Australia.
III. Title. (Series: Report (Geological Survey of Western Australia); 99).

551.88099413

ISSN 0508–4741

Grid references in this publication refer to the Geocentric Datum of Australia 1994 (GDA94). Locations mentioned in the text are referenced using Map Grid Australia (MGA) coordinates, Zone 50. All locations are quoted to at least the nearest 100 m.

Copy editor: L. Day
Cartography: M. Maron
Desktop publishing: K. S. Noonan

Published 2005 by Geological Survey of Western Australia
This Report is published in digital format (PDF) and is available online at www.doir.wa.gov.au/gswa/onlinepublications. Laser-printed copies can be ordered from the Information Centre for the cost of printing and binding.

Further details of geological publications and maps produced by the Geological Survey of Western Australia are available from:
Information Centre
Department of Industry and Resources
100 Plain Street
EAST PERTH, WESTERN AUSTRALIA 6004
Telephone: +61 8 9222 3459 Facsimile: +61 8 9222 3444
www.doir.wa.gov.au/gswa/onlinepublications

Cover photograph:
Dolerite outcrops capped by ferruginous duricrust, about 80 km west of the Glenayle Homestead, as seen from the Canning Stock Route in the Weld Spring area

Contents

Appendices

Figures

Tables

Mesoproterozoic sill complexes in the Bangemall Supergroup, Western Australia: geology, geochemistry, and mineralization potential

by

P. A. Morris and F. Pirajno

Abstract

Dolerite sills and less abundant mafic volcanic rocks are found throughout the Mesoproterozoic Bangemall Supergroup in central Western Australia. Sensitive high-resolution ion microprobe (SHRIMP) U–Pb geochronology and palaeomagnetism can be used to separate several intrusive events, with a 1070 Ma event being the most widespread. Whole-rock chemistry shows that two of these events in the western Bangemall Supergroup, dated at 1465 and 1070 Ma, can be separated in terms of field relations and absolute concentrations of some trace elements at the same level of magma evolution, incompatible trace-element ratios, and rare-earth element (REE) chemistry. This chemical fingerprinting means that other sills can be confidently attributed to one of the two intrusion events, and shows that the majority of the 1465 Ma sills intrude older parts of the Bangemall Supergroup, whereas the 1070 Ma sills are found in younger parts of the stratigraphy. This temporal relationship between sill age and sedimentation is consistent with the presence of plastically deformed country-rock xenoliths adjacent to sill margins, and vesiculation and fluidization at sill margins indicate that the sills were intruded into unconsolidated sediments.

The 1070 Ma sills and related volcanic rocks cover an area of approximately 1.5 million km^2, extending from Western Australia into South Australia and the Northern Territory, that forms the Warakurna Large Igneous Province (LIP). The sills are variably fractionated in terms of magnesium number (Mg#; defined as molar 100 [MgO/(MgO + FeO)], Ni, and Cr contents, and show uniform incompatible-element ratios and REE patterns. The exception to this is localized sills in parts of the eastern Bangemall Supergroup that have been modelled in terms of contamination of magma by about 10% Yilgarn Craton granitic material coupled with about 20% fractionation of clinopyroxene and plagioclase. Variations in chalcophile element concentrations with contamination point to some potential for magmatic sulfide mineralization.

Available isotope data, the overlap of some Nd model ages with a Palaeoproterozoic subduction event in the western Bangemall Supergroup, and the subduction signature of both the 1465 and 1070 Ma dolerites throughout the Bangemall Supergroup, with the enrichment in low field-strength elements (LFSE) relative to high field-strength elements (HFSE), indicate melting of a subduction-modified mantle source. Other studies on coeval intrusive and extrusive rocks of the western Musgrave Complex, and in the Northern Territory and South Australia, have also argued for a source modified by subduction processes.

The emplacement of the Warakurna LIP is postulated to be the result of a mantle plume that impinged onto the base of the lithosphere at about 1100 Ma. This timing is roughly coincident with other large mafic igneous events, notably the Umkondo LIP in southern Africa and the Keweenawan LIP in North America. These mafic igneous events also coincide with the assembly of the Rodinia supercontinent and suggest that a superplume may have been active at that time.

The mineral potential of the Warakurna LIP, which encompasses the Giles mafic–ultramafic intrusive rocks, includes magmatic nickel – platinum group element (PGE) deposits of the Noril'sk type, magmatic-hydrothermal deposits related to felsic anorogenic magmatism with which most LIPs are associated, and hydrothermal vein deposits. The Bangemall Supergroup sill complexes are prospective for all of these ore deposit types.

KEYWORDS: Warakurna Large Igneous Province, dolerite, mineralization, Bangemall Supergroup, mantle plume.

Introduction

Large igneous provinces are produced by the rapid emplacement of usually mafic magma that is commonly preserved as extensive flood-basalt provinces, many of which are in excess of one million km^2 (Coffin and Eldholm, 1994; Fig. 1). Apart from mafic igneous rocks emplaced at constructive plate margins, LIPs are the most common type of continental mafic rocks found at the Earth's surface (Coffin and Eldholm, 1994), and LIPs represent anomalous conditions when large amounts of mafic magma are produced and emplaced in a short period of time. As many LIPs are associated with mantle plumes (White and McKenzie, 1995; Anderson et al., 1992; Johnston and Thorkelson, 2000), they can provide information on mantle dynamics and chemistry. With increasingly precise and accurate geochronological methods, LIPs offer the opportunity to assess changes in mantle chemistry over time. Some LIPs host world-class mineralization, such as the Cu–Ni and PGE deposits of the Noril'sk region (Arndt et al., 2003; Duzhikov et al., 1992; Lightfoot and Hawkesworth, 1997; Lightfoot et al., 1990; Naldrett, 1992) and magmatic and hydrothermal mineral deposits associated with the Midcontinent Rift System (Nicholson et al., 1992). The rapid emplacement of such large volumes of magma can also have significant effects on both the biosphere and atmosphere. Rampino et al. (1988) have suggested that eruption of the Paraná–Etendeka flood basalts may be linked to mass extinctions at the Jurassic–Cretaceous boundary. They also noted that flows in excess of 700 km^3, such as those associated with the Columbia River Basalt, could modify the atmosphere by releasing significant quantities of sulfuric volatiles and carbon dioxide.

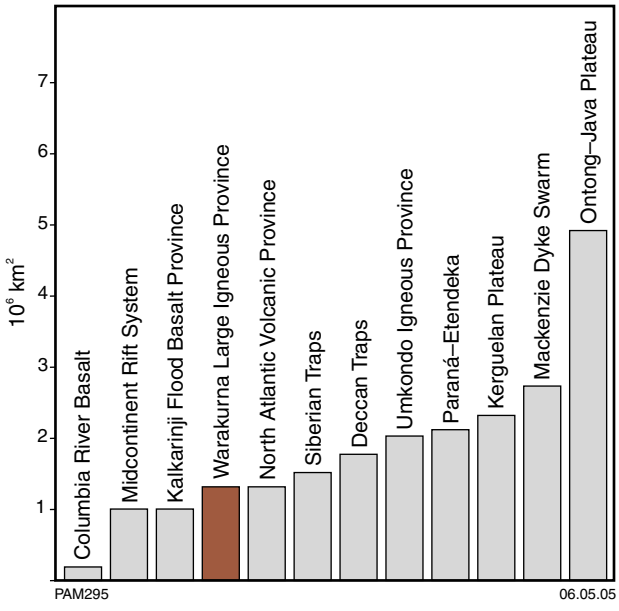

Figure 1. Histogram showing the estimated area of the Warakurna LIP in relation to other LIPs. Data from Wingate et al. (2004), Glass (2002), Coffin and Eldholm (1993, 1994), Peate (1997), Tolan et al. (1989), Lurie and Masaitis (1964), Zolutukhin and Al'Mukhamedov (1988), Ernst and Buchan (1997), and Mahoney (1988)

Phanerozoic LIPs are usually found as extensive continental flood-basalt sequences (e.g. Deccan Traps: Sharma, 1997; Columbia River Basalt: Hooper, 1997), but due to erosion and tectonic processes pre-Phanerozoic LIPs are usually only represented by intrusions or layered complexes (Ernst and Buchan, 1997). The Palaeo- to Neoproterozoic Earaheedy, Edmund, Collier, and Officer sedimentary basins of central Western Australia were intruded by large volumes of mafic magma as sills and dykes over a distance of about 1300 km along an east-southeast trend. The ages of these mafic rocks cluster around 1465, 1070, 826, and 510 Ma (Wingate and Giddings, 2000; Wingate, 2002, 2003; Wingate et al., 2004). This indicates that four major thermal events resulted in the emplacement of LIPs along what was probably a major zone of crustal weakness formed by the Capricorn Orogen and Musgrave Complex (Fig. 2). This Report focuses on the mafic igneous rocks that were emplaced at about 1070 Ma. These rocks form part of a LIP that extends east into the Northern Territory and South Australia and covers an area of approximately 1.5 million km^2 (Wingate et al., 2004; Fig. 3). It has been termed the Warakurna Large Igneous Province by Wingate et al. (2004), as its putative centre is located near the settlement of Warakurna, close to the Western Australia – South Australia border. In terms of area, the Warakurna LIP (Figs 1 and 3) is of the same magnitude as the North Atlantic Volcanic Province, and the Siberian and Deccan Traps. A significant part of the Warakurna LIP in Western Australia comprises dolerite sills that intrude Mesoproterozoic sedimentary rocks of the Bangemall Supergroup (Martin et al., 1999), as shown in Figure 2. This Report deals with the disposition, petrography, chemistry, and petrogenesis of these sills.

Despite the availability of geological maps covering the area of the Warakurna LIP, and several reports discussing the geology of the Bangemall Supergroup (Chuck, 1984; Muhling and Brakel, 1985; Williams, 1990), it has only recently been shown that many sills found in the Bangemall Supergroup can be attributed to a single, widespread intrusive event (Wingate et al., 2004). There are three main reasons for this. Firstly, in the western part of the Bangemall Supergroup, 1:250 000-scale mapping (e.g. Daniels, 1965) emphasized the sedimentary component of the Bangemall Supergroup, noting the presence of units with dolerite sills, but not showing the actual extent of the dolerite. Only on recent 1:100 000-scale maps (e.g. Copp et al., 1999) is the actual extent of the dolerite shown (Fig. 4). Secondly, in the eastern part of the Bangemall Supergroup (the Glenayle area, informally referred to here as the eastern Bangemall Supergroup; Fig. 2), where outcrop is less well developed, recently acquired high-quality aeromagnetic data and detailed regolith mapping have indicated a greater extent of dolerite in the Bangemall Supergroup than previously thought. For example, in the northern part of STANLEY*, aeromagnetic data show a much wider distribution of dolerite than that

* Capitalized names refer to standard 1:250 000 map sheets, unless otherwise indicated

indicated by the few scattered outcrops. The extent of dolerite has also been shown by regolith mapping in the same area (Morris et al., 2000), where a thin sheet of iron-rich sandplain derived from the weathering of dolerite is extensively developed between scattered dolerite outcrops. Thirdly, the recognition that these widely spaced sills belong to one intrusive event is the result of precise dating of mafic igneous rocks and the application of palaeomagnetism to identify rocks with similar magnetic declination (Wingate, 2002, 2003). Earlier attempts at dating dolerites used techniques unsuited to samples that had undergone weathering or low-grade metamorphism (e.g. Rb–Sr and K–Ar techniques), or involved indirect dating using phases associated with sill intrusion (e.g. K–Ar dating of glauconite in sedimentary rocks adjacent to sills; Goode and Hall, 1981).

This Report addresses some of the issues that have arisen from these recent advances in the understanding of the disposition, extent, and age of the Bangemall Supergroup sills. SHRIMP U–Pb dating of zircon ($ZrSiO_4$) and baddeleyite (ZrO_2) has shown that there were two periods of dolerite intrusion in the Bangemall Supergroup during the Mesoproterozoic: one at about 1465 Ma and one at 1070 Ma (Wingate, 2002, 2003). In the western Bangemall Supergroup, sills of both ages are present, but as zircon and baddeleyite are not found in sufficient abundance for reliable dating in all sills, it would not be possible to date every sill in order to assign it to an intrusive event. Wingate (2002, 2003) has used palaeomagnetism to group sills emplaced during the same igneous event, arguing that, of the two intrusive events (1465 and 1070 Ma), the 1070 Ma event is the most widespread, whereas the 1465 Ma event is confined to older parts (pre-1465 Ma) of the stratigraphy in the western Bangemall Supergroup. The use of palaeomagnetism as a dating tool is assessed in relation to sill chemistry, and how it relates to the two intrusive events.

This Report also evaluates whether whole-rock chemistry can be used to develop chemical fingerprints of the two intrusive events by analysing sills that have been accurately and precisely dated (i.e. by SHRIMP), or whether sills can be assigned to one of the two intrusive events based on stratigraphy.

A feature of the Bangemall Supergroup sills is the lack of evidence for feeder systems. Gravity modelling in the Glenayle area (Morris et al., 2003) has provided evidence for a 36 km-wide and 3 km-thick laccolith-like body from which overlying dolerite sills may have been derived. This modelling has been facilitated by the availability of more detailed gravity measurements, based on a 4 × 4 km grid. Generally, gravity measurements over the Bangemall Supergroup are widely spaced, and feeder systems in the western Bangemall Supergroup may be present. If the source of the Warakurna LIP is centred on the Western Australia – South Australia border, as suggested by Wingate et al. (2004), then lateral magma transport in the order of 1500 km would have to have taken place to account for sills in the western Bangemall Supergroup. The chemistry of the sills may provide some insight into the degree of magma homogeneity over large areas, which in turn may have implications for magma transport processes (Ernst and Buchan, 1997).

Volcanic rocks and feeder dykes of the Giles intrusions in the Musgrave Complex (Glikson et al., 1996), and the Stuart and Kulgera dykes of the Northern Territory (Zhao and McCulloch, 1993a,b) — which are part of the Warakurna LIP (Wingate et al., 2004) — have been attributed to melting of subduction-modified asthenospheric mantle, possibly induced by mantle plume activity. In this Report, the whole-rock and isotope chemistry of the Bangemall Supergroup sills is evaluated in terms of the mantle source, and whether crustal contamination is an important process. The terms Musgrave Complex and Giles intrusions are utilized in this Report in accordance with the terminology for tectonic units used in Western Australia (Tyler and Hocking, 2002).

Regional geology

Comprehensive discussions of the sedimentary component of the Bangemall Supergroup (previously Bangemall Group) have been given elsewhere (Chuck, 1984; Muhling and Brakel, 1985; Williams, 1990; Martin and Thorne, 2002; 2004), and discussion here is restricted to that relevant to the understanding of the Bangemall Supergroup dolerite sills.

Stratigraphy of the western Bangemall Supergroup

Sedimentary rocks of the Mesoproterozoic Edmund and Collier Groups, which make up the Bangemall Supergroup (Martin and Thorne, 2002), were deposited in an intracratonic basin located between the Pilbara and Yilgarn Cratons (Fig. 2). The sedimentary component of the Edmund Group comprises carbonate and siliciclastic rocks approximately 3900 m thick, whereas the overlying Collier Group is dominated by siliciclastic sedimentary rocks totalling about 2300 m in thickness (Martin et al., 1999). The two groups are separated by a low-angle unconformity. Bangemall Supergroup rocks unconformably overlie lithologies that were deformed and/or metamorphosed during the 1830–1780 Ma Capricorn Orogeny (Tyler and Thorne, 1990; Occhipinti et al., 1999; Cawood and Tyler, 2004). SHRIMP U–Pb dating of detrital zircons has shown that the Edmund Group sedimentary rocks must be younger than 1688 ± 18 Ma, whereas the Collier Group sedimentary rocks were deposited after 1352 ± 89 Ma (Cawood, P. A., and Nemchin, A. A., 2004, written comm.).

The lithostratigraphy of the Bangemall Supergroup has undergone several revisions since its recognition as a separate lithological association by Woodward (1891). The three main stratigraphies proposed for these rocks (Chuck, 1984; Muhling and Brakel, 1985; Williams, 1990) have been summarized by Martin and Thorne (2002), who argued that none of these stratigraphic schemes could be applied throughout the depositional basin due to lateral facies changes and gradational boundaries between units. The stratigraphic scheme adopted here (Martin et al., 1999; Martin and Thorne, 2002; Fig. 5) is based on 1:100 000-scale mapping on parts of Edmund and Turee Creek in the northwestern part of the supergroup that has resulted

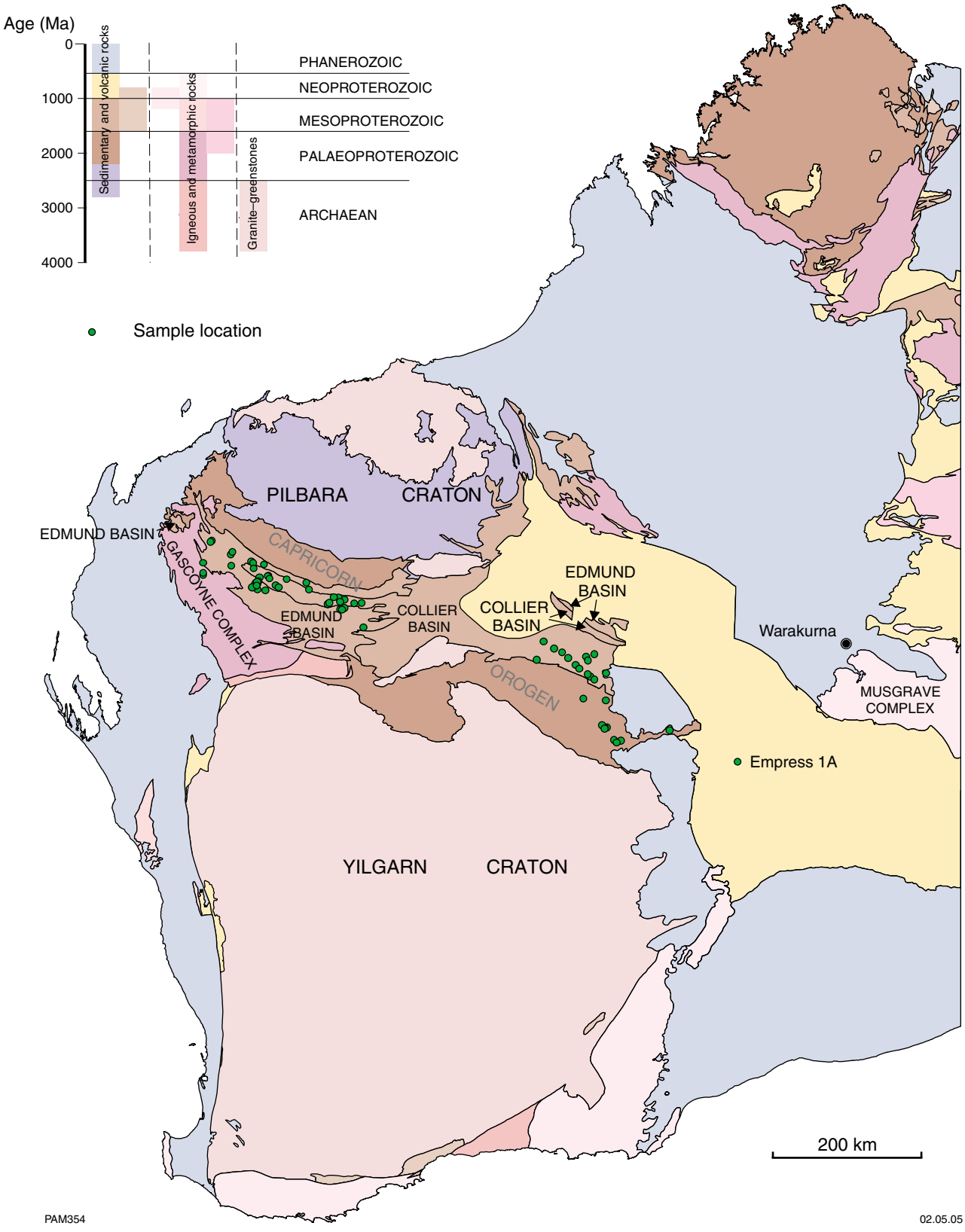

Figure 2. Simplified geology of Western Australia (Myers and Hocking, 1998) showing the extent of the Bangemall Supergroup in relation to other major tectonic elements. The Bangemall Supergroup comprises sedimentary rocks deposited throughout the Collier and Edmund Basins. The Musgrave Complex contains 1070 Ma rocks of the Warakurna LIP. Also shown are sample locations

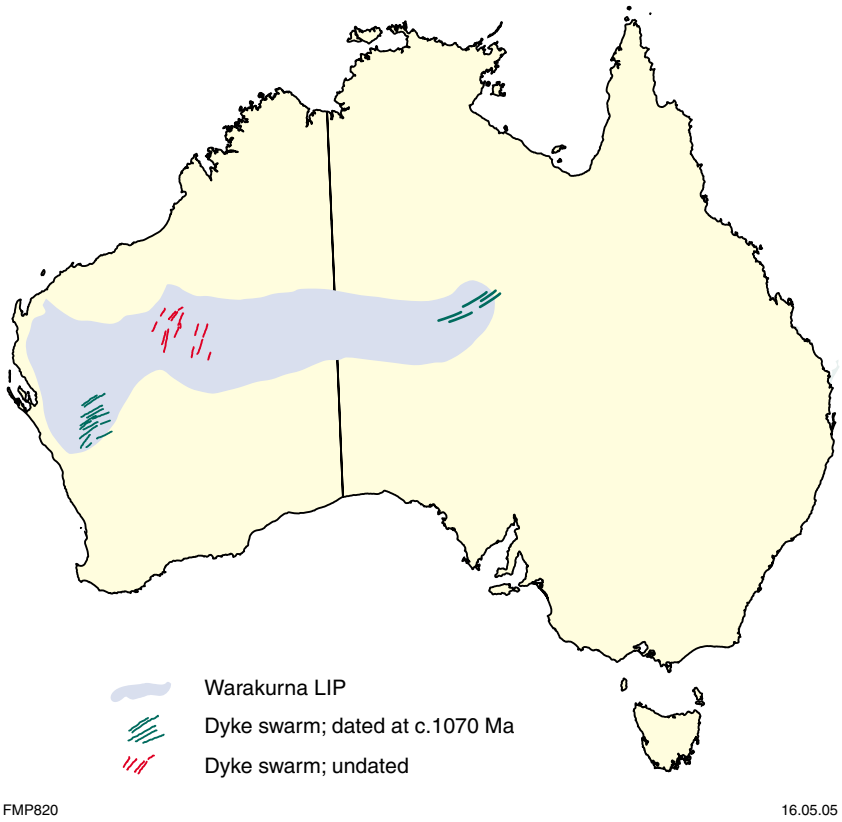

Figure 3. Extent of the Warakurna LIP and distribution of the associated dyke swarms

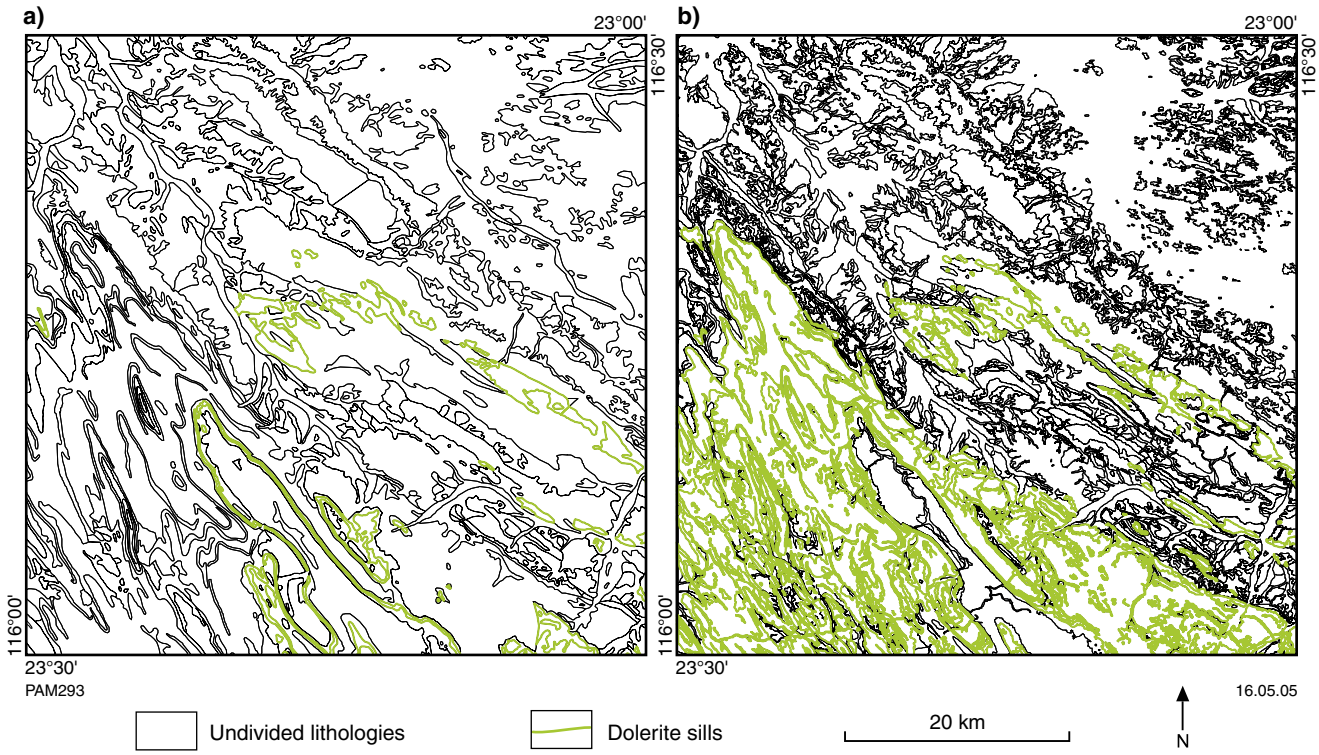

Figure 4. Geology of Ullawarra (1:100 000), showing the extent of dolerite sills from: a) 1:250 000-scale mapping of Daniels (1965); b) 1:100 000-scale mapping of Copp et al. (1999)

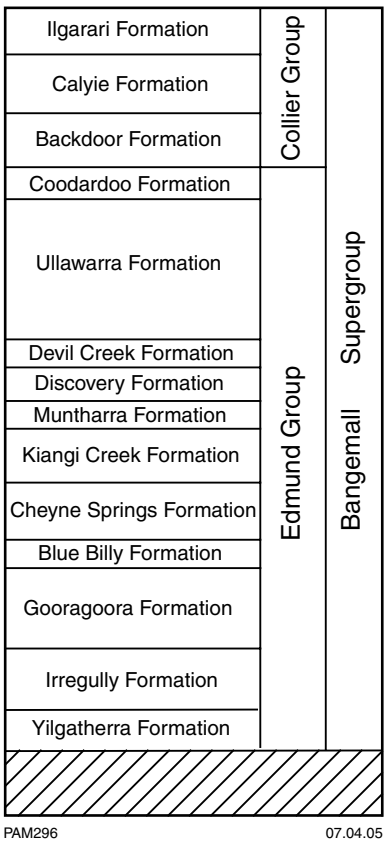

Figure 5. Stratigraphy of the western part of the Bangemall Supergroup (Martin et al., 1999)

in the redefinition of some lithological units and the abandonment or renaming of others. A comprehensive discussion of the stratigraphy and basin evolution relevant to the Bangemall Supergroup has been given by Martin and Thorne (2004).

Stratigraphy of the eastern Bangemall Supergroup

Establishing stratigraphic relations between the western and eastern parts of the Bangemall Supergroup has been hindered by the relatively poor exposure and general lack of age control in the latter, and the lack of detailed mapping of Bangemall Supergroup rocks between the two areas. Two groups of rocks have been identified in the eastern Bangemall Supergroup, the Scorpion and Salvation Groups (Hocking and Jones, 1999; Hocking et al., 2000), which are in fault contact. The Scorpion Group consists of coastal deposits of cross-bedded and rippled sandstone and siltstone, with interbedded stromatolitic dolomite and evaporitic lithologies. Although the stromatolite forms have not been studied in detail, and microstructures have been largely destroyed by diagenetic processes, the forms observed are similar to those found in the Irregully Formation of the Edmund Group in the western Bangemall Supergroup.

The Salvation Group comprises the Coonabildie Formation and the overlying Brassey Range Formation. The former consists of coastal and fluvial sandstone, and siltstone, with local shale and mudstone, and a basal massive to banded chert unit. The Brassey Range Formation consists of fluvial and coastal deposits represented by cross-bedded sandstone and less common siltstone.

Dolerite sills

Western Bangemall Supergroup

Muhling and Brakel (1985) provided a comprehensive discussion of the lithologies, stratigraphy, and likely depositional environment of the then Bangemall Group, including the distribution, outcrop pattern, and petrography of the dolerite sills. They estimated that sills outcrop over an area of about 143 000 km^2, with individual sills traceable for more than 60 km and reaching in excess of 100 m in thickness. In some areas, sills probably account for up to 60% of the stratigraphic thickness as shown on the geological maps of the area (Figs 6a–d). Figure 6 also shows the locations of the western Bangemall Supergroup samples discussed in this Report. Although most sills are concordant, in the Mount Vernon area on Mount Egerton two dolerite sills transgress a 1700 m thickness of the Fords Creek Shale (Backdoor Formation of Martin and Thorne, 2002; fig. 4).

The sills are most commonly found in fine-grained siliciclastic units and chert such as the Ullawarra Formation of the Edmund Group on Edmund. Muhling and Brakel (1985) argued that sills are more abundant in these finer grained lithologies because intrusion was easier into fissile units. However, there is some evidence that the sediments were only partly lithified when the sills were intruded. Although country rock xenoliths are uncommon, plastically deformed shale inclusions have been recorded in the Mount Vernon area (Muhling and Brakel, 1985), suggesting that the sediments were only partly consolidated before dolerite intrusion. Daniels (1969) reported fine-grained amygdaloidal tops to sills, as well as plastically deformed fragments of the surrounding sedimentary rocks, consistent with near-surface emplacement of dolerite into partially lithified sediments. Martin (2003) described peperite and associated fluidization adjacent to a sill that intrudes the upper part of the Edmund Group and the lower part of the Collier Group sedimentary rocks, and concluded that the sill was intruded into variably lithified sediments.

In terms of regional distribution, Muhling and Brakel (1985) pointed out that dolerite sills were more common in the western and eastern parts of the Bangemall Basin (now the Edmund and Collier Basins) compared with the central part. They argued that as dolerite sills did not extend beyond the basin margins, sill emplacement and sedimentation were closely related. However, Wingate et al. (2004) have discussed a dolerite dyke intruding the Palaeoproterozoic Woongarra Rhyolite (about 75 km north of the western Bangemall Supergroup) that has a primary magnetization identical to that of the 1070 Ma Bangemall Supergroup sills. Similarly, east-northeasterly

trending mafic dykes within Archaean granitic rocks of the northwest Yilgarn Craton (the Muggamurra dyke swarm of Myers et al., 1996) include SHRIMP U–Pb baddeleyite and zircon ages of 1075 ± 10 Ma (Wingate, M. T. D., 2004, written comm.). Thus, there is some evidence that the 1070 Ma intrusive event may have transgressed the Bangemall Supergroup basin boundary, although, to date, intrusive rocks found outside of the basin are restricted to dykes. Thus, Muhling and Brakel's (1985) assertion that sills were confined to the depositional basin still stands.

Within the Bangemall Supergroup, dykes are less common than sills. Most dykes are 1–2 m wide, but dykes up to 50 m wide and 15 km long have been recorded (Muhling and Brakel, 1985). The dykes belong to two generations, one of which appears to feed sills, whereas the other crosscuts the sills. The ages of these dykes are not clear, although the relatively common dykes that feed sills in the Backdoor Formation (formerly the Fords Creek Shale) must belong to the 1070 Ma event. Bangemall Supergroup rocks are also cut by dykes of the 755 Ma Mundine Well dyke swarm (Wingate and Giddings, 2000), and it is possible that some dykes that crosscut sills are part of this unit.

Eastern Bangemall Supergroup

A series of sills in the Glenayle area, to the north of the c. 1800 Ma Earaheedy Basin, intrude dominantly siliciclastic sedimentary rocks of the Bangemall Supergroup (Fig. 7). This sill complex extends for about 150 km east-southeast and about 60 km in a northerly direction. Its western margin is overlain by sedimentary rocks of the Officer Basin, whereas to the east, the sill complex is overlain by a veneer of Permian glacigene sedimentary rocks of the Paterson Formation, and Neoproterozoic rocks of the Officer Basin. The southern margin of the sill complex is in fault contact with the Earaheedy Group along the Salvation and Glenayle Faults. The total thickness of sills making up the Glenayle sill complex is unknown because exposures are essentially at one stratigraphic level. Geophysical data suggest that the sill complex may extend to depths of 3–4 km (Morris et al., 2003). A possible geometry, reconstructed with the aid of geophysical data and a cross section from Glenayle (1:100 000; Pirajno and Hocking, 2002), is shown in Figure 8. Numerous northeasterly and west-northwesterly trending dykes cut the sill complex.

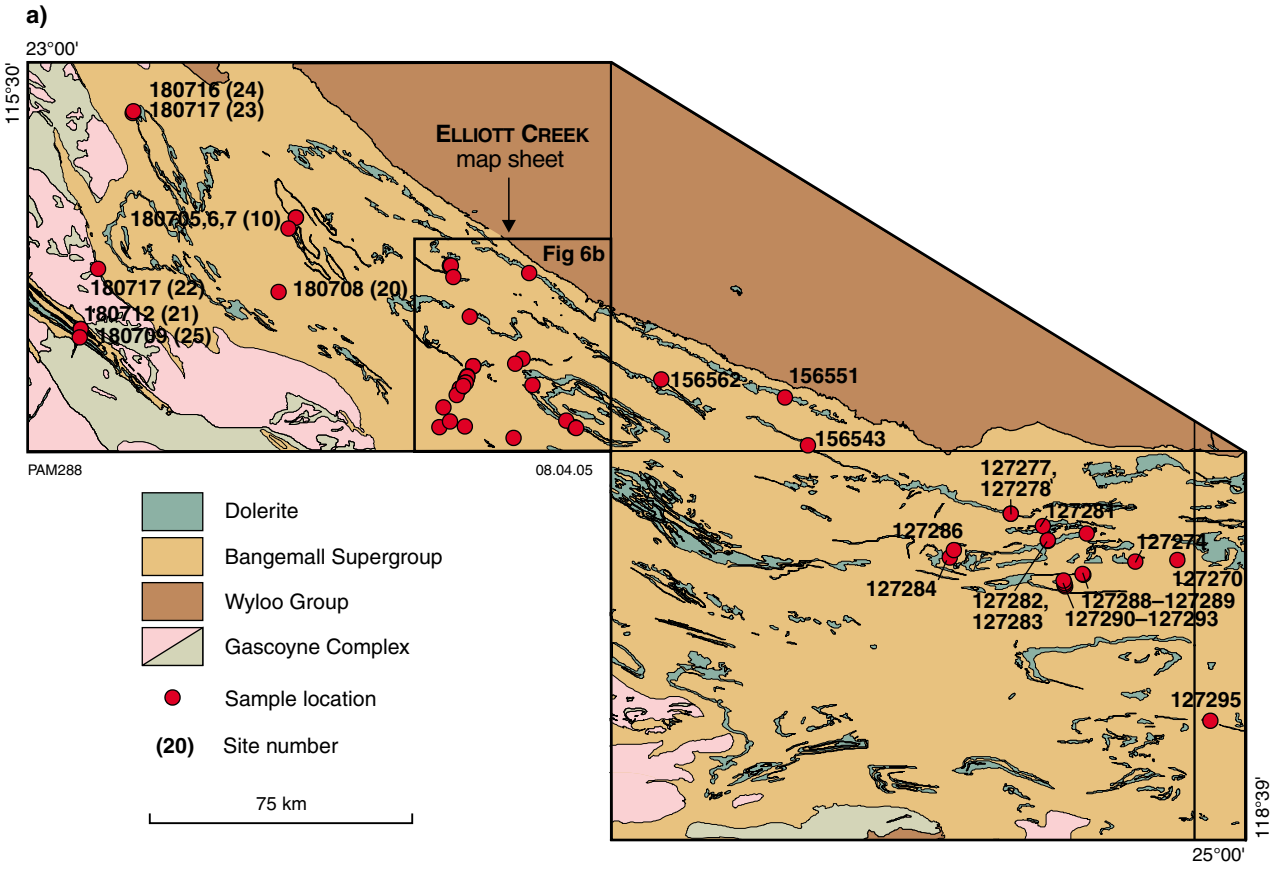

Figure 6. Sample location maps for the western Bangemall Supergroup showing: a) an overview of the western Bangemall Supergroup (Vanderhor and Flint, 2001), and the location of more detailed Figure 6b; b) an overview of the sample locations in the central portion of the western Bangemall Supergroup on Elliott Creek (1:100 000), and the locations of the more detailed Figure 6c and d; c) detailed locations on the northwestern part of Elliott Creek (1:100 000); d) detailed sample locations on the southwestern portion of Elliott Creek (1:100 000). Geology for b–d based on Martin et al. (2004). For each sample, the GSWA number is shown and, where available, Wingate's (2002) site number. A complete list of samples and their locations is given in Table 2

b)

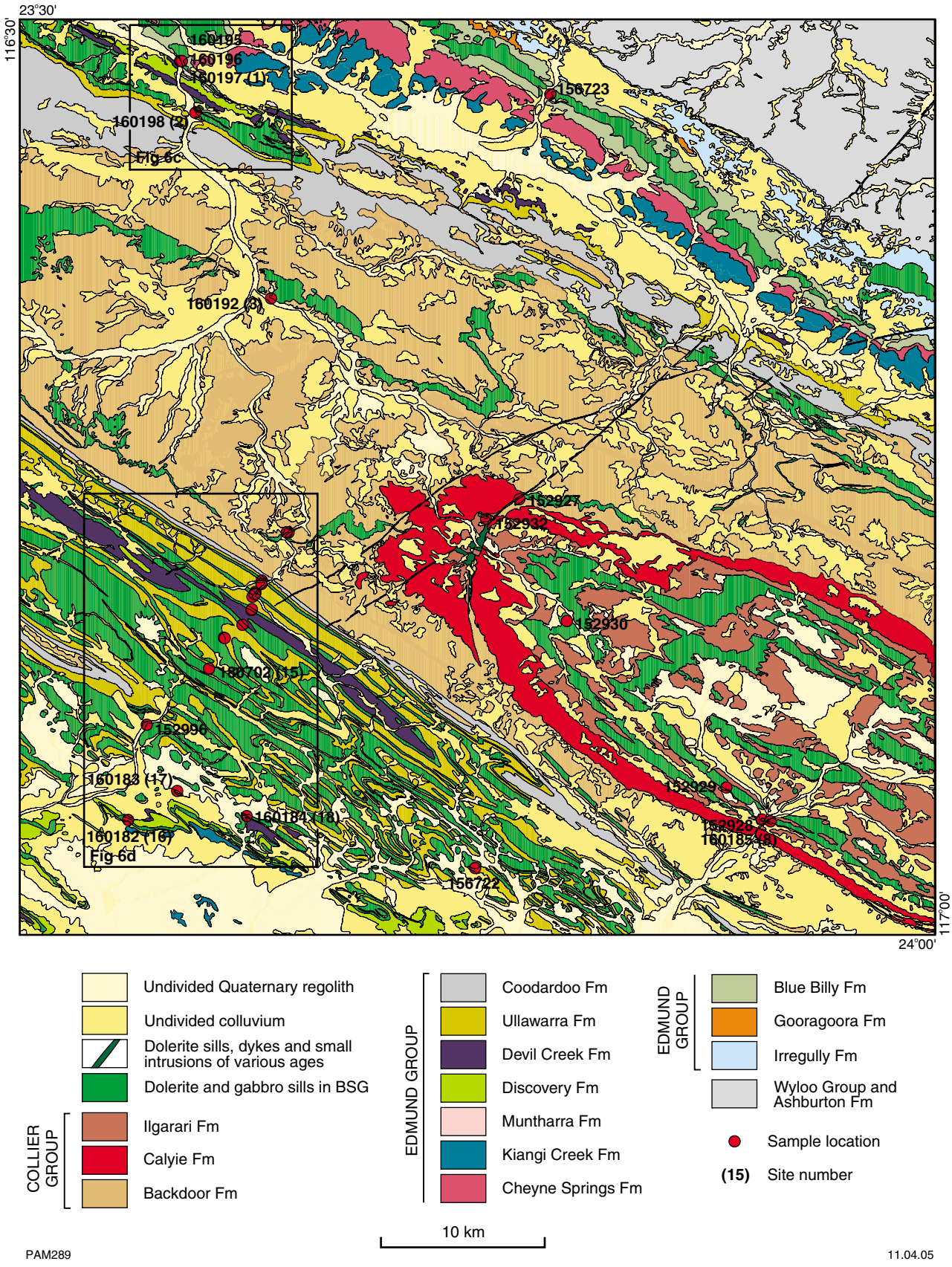
23°30'
116°30'
160195
160196
160197 (1)
160198 (2)
Fig 6c
156723
160192 (3)
152927
152932
152930
160192 (15)
152996
160183 (17)
160184 (18)
160182 (16)
Fig 6d
156722
152929
152928
160185 (19)
24°00'
117°00'
Undivided Quaternary regolith
Undivided colluvium
Dolerite sills, dykes and small intrusions of various ages
Dolerite and gabbro sills in BSG
COLLIER GROUP
Ilgarari Fm
Calyie Fm
Backdoor Fm
EDMUND GROUP
Coodardoo Fm
Ullawarra Fm
Devil Creek Fm
Discovery Fm
Muntharra Fm
Kiangi Creek Fm
Cheyne Springs Fm
EDMUND GROUP
Blue Billy Fm
Gooragoora Fm
Irregully Fm
Wyloo Group and Ashburton Fm
Sample location
(15) Site number
10 km
PAM289
11.04.05

c)

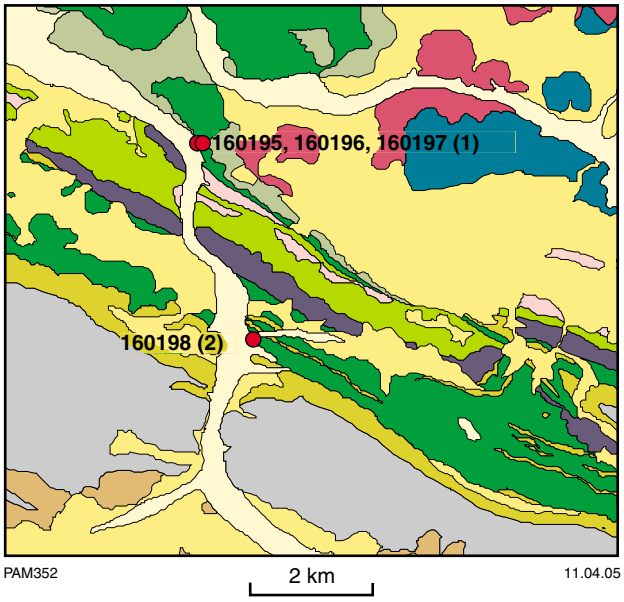
160195, 160196, 160197 (1)
160198 (2)
PAM352
2 km
11.04.05

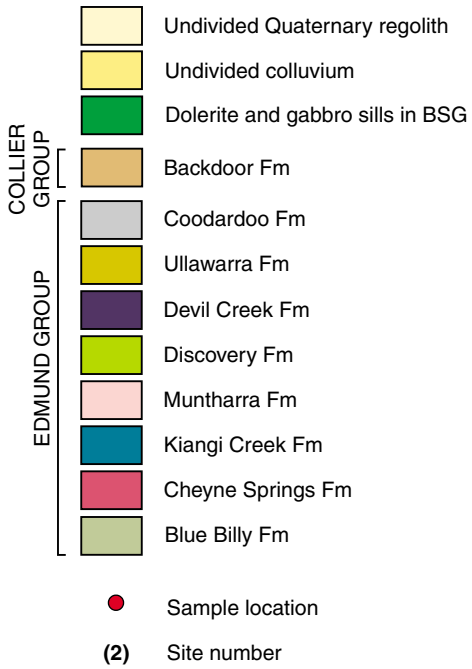
Undivided Quaternary regolith
Undivided colluvium
Dolerite and gabbro sills in BSG
COLLIER GROUP
Backdoor Fm
EDMUND GROUP
Coodardoo Fm
Ullawarra Fm
Devil Creek Fm
Discovery Fm
Muntharra Fm
Kiangi Creek Fm
Cheyne Springs Fm
Blue Billy Fm
Sample location
(2) Site number

d)

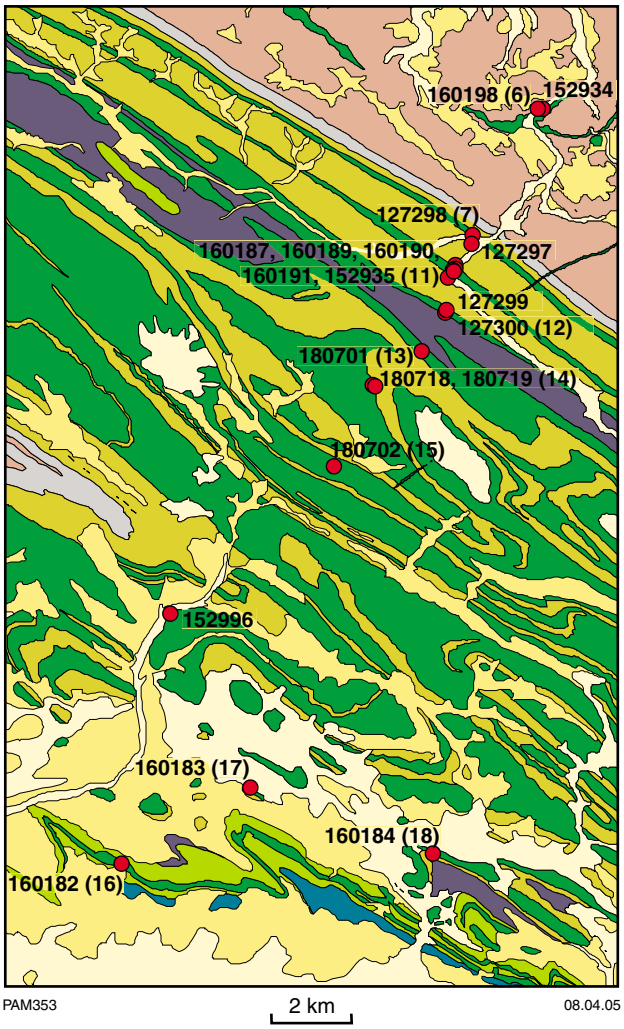
160198 (6)
152934
127298 (7)
160187, 160189, 160190
127297
160191, 152935 (11)
127299
127300 (12)
180701 (13)
180718, 180719 (14)
180702 (15)
152996
160183 (17)
160184 (18)
160182 (16)
PAM353
2 km
08.04.05

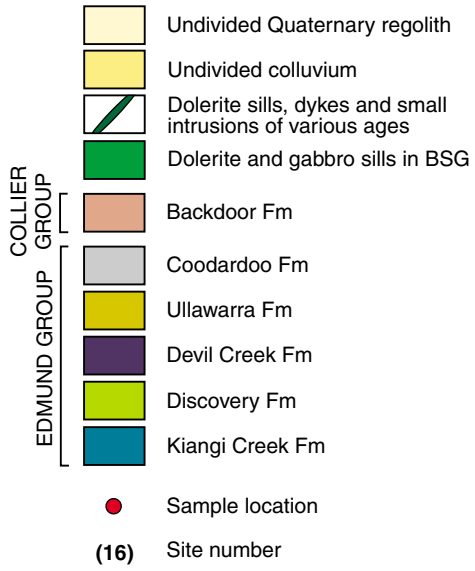
Undivided Quaternary regolith
Undivided colluvium
Dolerite sills, dykes and small intrusions of various ages
Dolerite and gabbro sills in BSG
COLLIER GROUP
Backdoor Fm
EDMUND GROUP
Coodardoo Fm
Ullawarra Fm
Devil Creek Fm
Discovery Fm
Kiangi Creek Fm
Sample location
(16) Site number

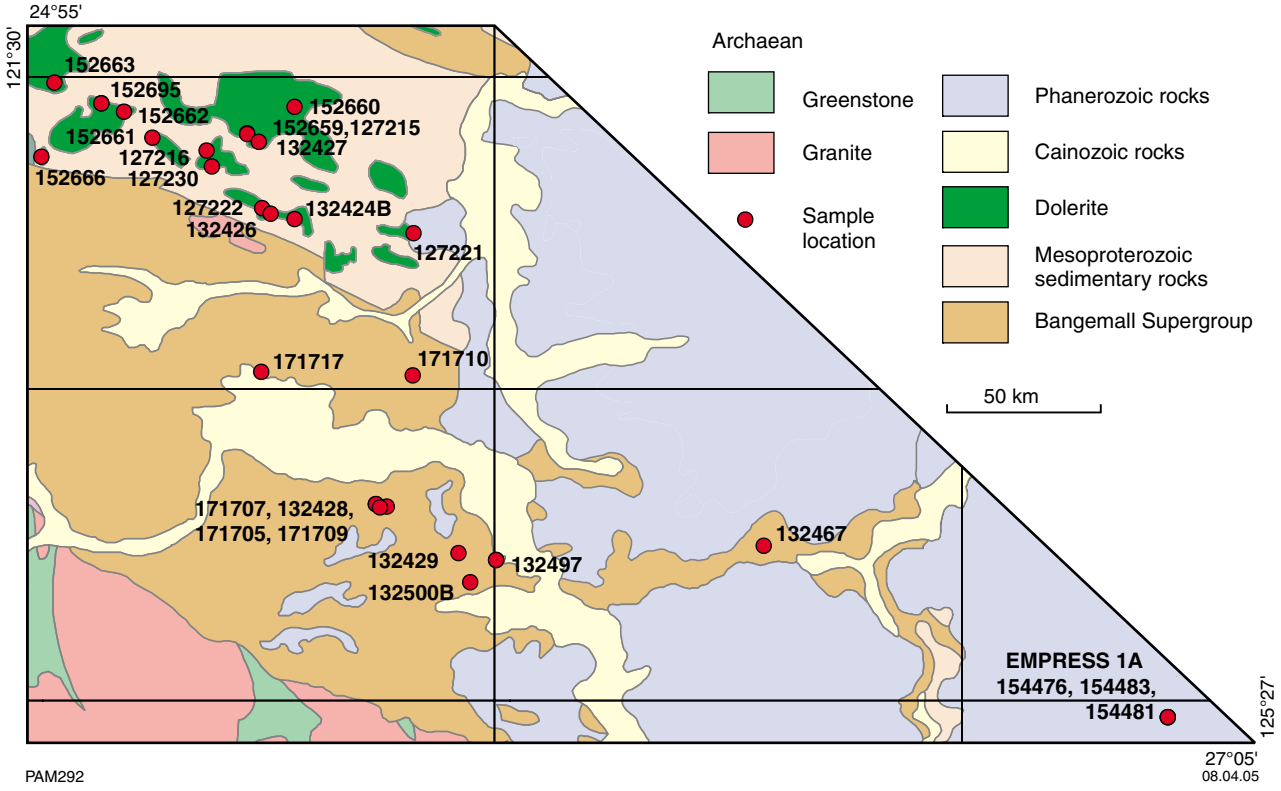

Figure 7. Sample location map for the eastern Bangemall Supergroup (modified from Vanderhor and Flint, 2001)

Individual sills range in thickness from a few metres to more than 100 m. As the country rocks are dominantly siliciclastic, contact metamorphic effects are poorly developed, but local melt patches are observed along the contact with some sills. These sills have been grouped as the Glenayle Dolerite (Pirajno and Hocking, 2001, 2002), which is intruded by aphanitic to very fine-grained dolerite sills and dykes that have been referred to as the Prenti Dolerite by Pirajno and Hocking (2002). The Prenti Dolerite is petrographically similar to sills that intrude the Earaheedy Group. The relationship between, and main features of, the Glenayle and Prenti Dolerites are shown in Figure 9. A typical Glenayle Dolerite sill is usually characterized by an upper granophyric zone that grades downward towards zones that contain only minor, interstitial granophyre. Sills thicker than 50 m usually have a central zone or scattered pods of gabbro. Chilled (fine-grained) margins are commonly recognized.

Some circular features on GLENAYLE (1:100 000) and MUDAN (1:100 000; northwestern part of STANLEY) appear to be floored by Prenti-type dolerite. Similar features have been noted in the Karoo large igneous province (South Africa) where Chevalier and Woodford (1999) carried out a morphotectonic analysis of ring structures associated with dolerite sills. They suggested that the mechanism of emplacement and formation of a ring structure takes place when a sill initially intrudes as an inclined sheet (feeder

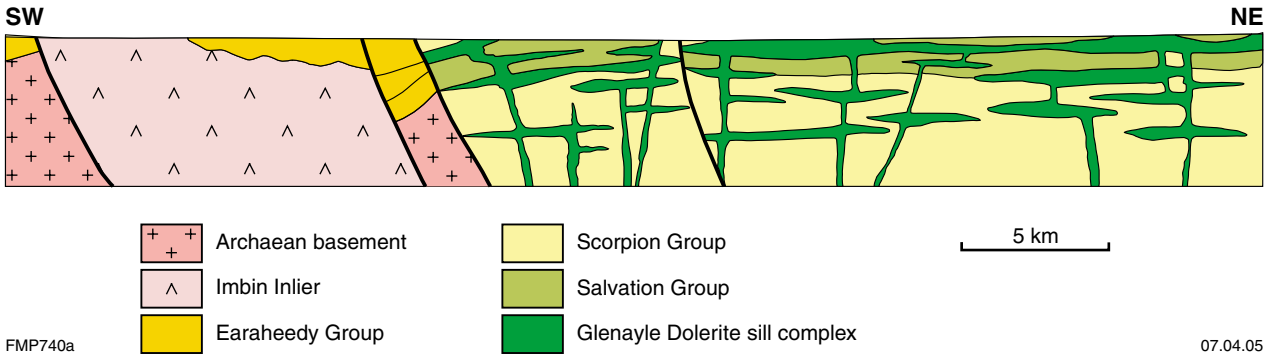

Figure 8. Cross section showing a schematic architecture of the Glenayle sill complex (eastern Bangemall Supergroup) in the Glenayle area (modified from Pirajno and Hocking, 2001, 2002)

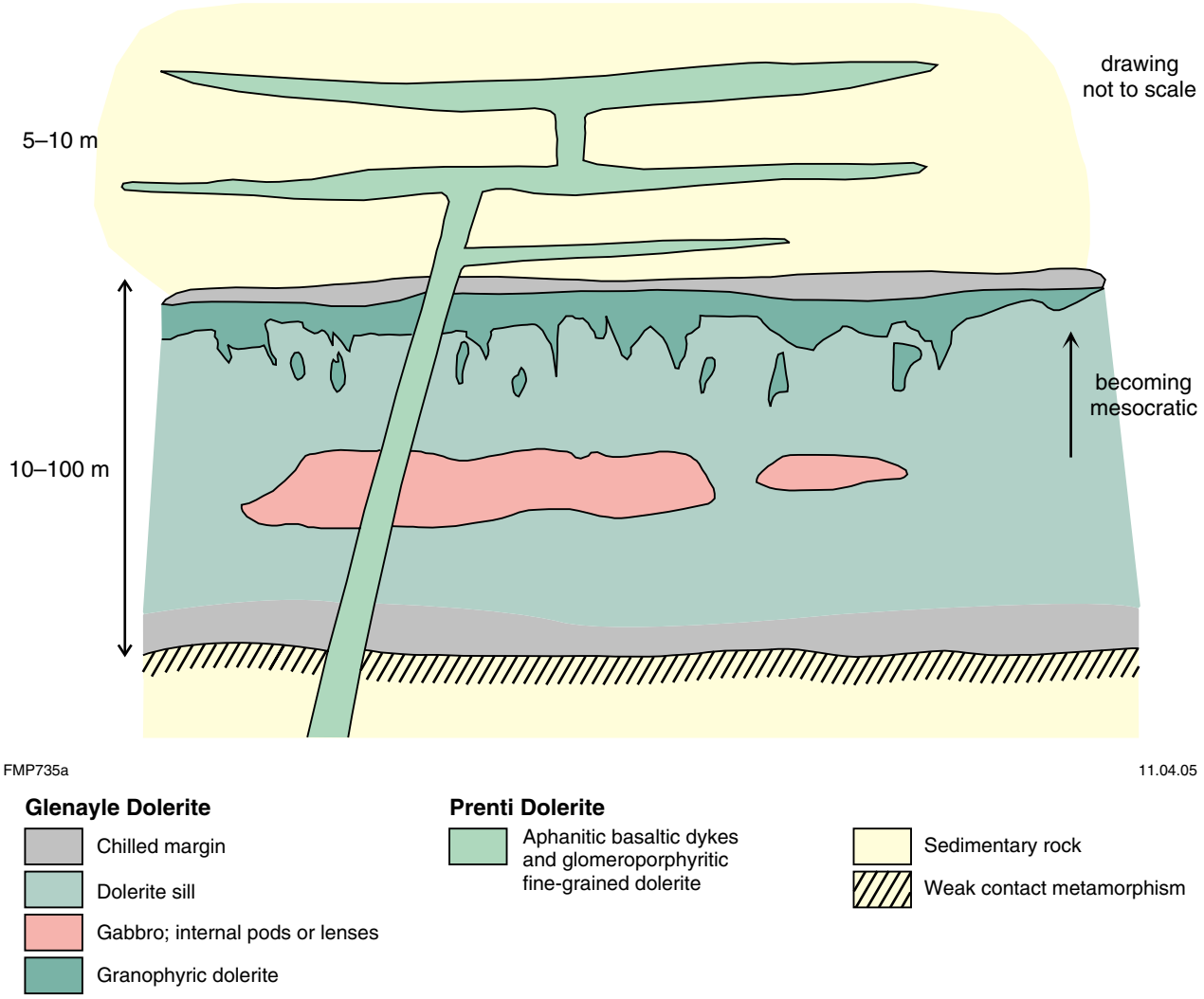

Figure 9. Schematic diagram showing the lithology and mutual relations between the Glenayle and Prenti Dolerites in the eastern Bangemall Supergroup

dyke). This sheet passes upward into a nearly flat-lying sill that uplifts the sedimentary strata and propagates outward as an outer sill; the upwarping of the sedimentary strata would create a fracture at a lower level, thereby allowing the propagation of an inner sill (Chevalier and Woodford, 1999, fig. 9). The end result is a 'trumpet-like' geometry. These authors also suggested that the Karoo sills and associated ring structures may be linked to a regional along-strike curvature that results from the interaction of the two active main directions from a triple junction (east–west right lateral and north-northwest in the Karoo case).

Mechanisms and controls on sill intrusion

A knowledge of the shape of the intrusions is important in order to understand the mechanics of sill emplacement. In general, sills are emplaced through upward movement of magma along fractures or faults (dykes), commonly from feeding centres that are predetermined by regional basement structure or discontinuities. These same basement structures may also control sedimentary basin formation (Leaman, 1995). Dykes are injected either through existing structures such as faults or they can generate a propagating fracture. Numerical simulations suggest that dyke injection can be rapid (greater than 1 m/s; Turcotte et al., 1987). The fundamental driving force causing a body of melt to rise from its source region is its buoyancy, because the liquid state is always less dense than the surrounding solid materials. Therefore, the emplacement of sill complexes may be controlled by a buoyancy level. The concept of a neutral buoyancy zone is based on the idea that a silicate melt rises through the lithosphere and crust because of its density contrast with the surrounding material, and stops where it reaches a level of equal density (Glazner and Usler, 1988). In this model, melts reach the base of the crust and stall because the rising melts have the same density as the crust, thus creating a zone of neutral buoyancy. The melts would pond at the lithosphere–crust boundary, and from these ponded melts, dykes would propagate upward into the overlying sedimentary cover.

Geochronology of sills and spatially related rocks

Western Bangemall Supergroup

The Bangemall Supergroup unconformably overlies Archaean and Palaeoproterozoic rocks, and is in turn overlain by Neoproterozoic rocks in the east, and by Palaeozoic–Cainozoic rocks in the west (Fig. 2). Age constraints on sill emplacement are provided by ages of underlying lithologies, detrital zircon ages from Bangemall Supergroup sedimentary rocks, and crystallization ages of sills that intrude the Edmund and Collier Groups. The underlying Capricorn Formation has a SHRIMP U–Pb zircon age of 1804 ± 7 Ma (Hall et al., 2001), whereas granitic rocks of the Gascoyne Complex, and those on WYLOO, have SHRIMP U–Pb zircon ages of 1797 ± 8 Ma and 1786 ± 5 Ma respectively (Nelson, 1995; Krapez and McNaughton, 1999). Pearson et al. (1995) reported a SHRIMP U–Pb zircon age of 1674 ± 6 Ma for the Dingo Granite (now Dingo Creek Granite, Martin et al., 2002; dated at 1674 ± 8 Ma by Nelson, 2002.) and ultrabasic sills in the Gifford Creek area that also underlie the Bangemall Supergroup. SHRIMP U–Pb zircon dates of between 1670 and 1620 Ma for various granitic rocks of the Gascoyne Complex have been reported by Nelson (1998, 2002) and Sheppard and Swager (1999).

Wingate (2002) reported SHRIMP U–Pb zircon and baddeleyite ages from the granophyric parts of five dolerite sills from the Edmund Group in the western Bangemall Supergroup. The combined data for three of these sills produced an age of 1070 ± 6 Ma, whereas the combined data for the two remaining sills indicated an older emplacement event at c. 1465 Ma (Table 1). Similar though less precise ages were reported for felsic rocks from near Mount Palgrave (1080 ± 80 Ma; Rb–Sr isochron) by Compston and Arriens (1968), and a Rb–Sr isochron age of 1098 ± 42 Ma has been reported for altered rhyolite from Tangadee by Gee et al. (1976). Goode and Hall (1981) provided a K–Ar age of 1050 Ma for glauconite adjacent to an undated dolerite of the Manganese Group, which Muhling and Brakel (1985) equated with the Backdoor Formation.

Thus, the Edmund Group sedimentary rocks must have been deposited after 1620 Ma, with deposition completed by 1465 Ma (the age of the oldest sill group). The Collier Group sedimentary rocks are constrained by detrital zircon chronology and the age of sills to between 1352 and 1070 Ma. Combining the results of the direct dating of the sills and the detrital zircon chronology, it is likely that sills intruding the Collier Group must have been emplaced after 1352 Ma and most likely during the 1070 Ma event, and sills intruding the Edmund Group could belong to either the 1070 or 1465 Ma event.

Eastern Bangemall Supergroup

The available age determinations for the Glenayle and Prenti Dolerites include U–Pb baddeleyite ages of 1066 ± 14 and 1068 ± 20 Ma (Wingate, 2003). A younger whole-rock K–Ar age of 968 ± 19 Ma (Nelson, 2002) may represent the effects of Ar loss. A whole-rock K–Ar age of 1058 ± 13 Ma from basaltic rocks at about 1600 m in drillhole GSWA Empress 1A in the Officer Basin (Carlsen and Grey, 1998; Stevens and Apak, 1999) is within analytical error of the SHRIMP ages for the Glenayle and Prenti Dolerite sills. Compston (1974) reported a whole-rock Rb–Sr age of 1050 Ma for a Prenti Dolerite sill in the easternmost part of the Earaheedy Basin.

Detrital zircon chronology shows that the Salvation Group was deposited after 1200 Ma, suggesting that it might be a time equivalent of the Collier Group in the western Bangemall Supergroup (Nelson, 2002).

Dolerite sills

Western Bangemall Supergroup

For the purposes of this study, sills intruding the western Bangemall Supergroup sedimentary rocks can be divided into three broad groupings, based on their age of intrusion or the stratigraphic position of the rocks they intrude. The first group comprises two sills intruding the Edmund Group that were dated by Wingate (2002), with the combined data providing an age of c. 1465 Ma. The second group consists of sills dated at c. 1070 Ma and sills intruding the Collier Group sedimentary rocks that, according to constraints imposed by detrital zircon chronology, are considered to be part of the c. 1070 Ma

Table 1. SHRIMP U–Pb zircon or baddeleyite ages for the Bangemall Supergroup sills

Sample	*Site*	*Stratigraphic position*	*Minerals dated*	*Mean $^{207}Pb/^{206}Pb$ age (Ma)*
169011	1	Edmund Group, western Bangemall Supergroup	zircon and baddeleyite	1071 ± 8
WANC	7	Edmund Group, western Bangemall Supergroup	zircon and baddeleyite	1067 ± 14
156750	10	Edmund Group, western Bangemall Supergroup	baddeleyite	1068 ± 22
WANH	11	Edmund Group, western Bangemall Supergroup	zircon	≥1449 ± 5
156751	21	Edmund Group, western Bangemall Supergroup	zircon and baddeleyite	1465 ± 3
152661	D	Eastern Bangemall Supergroup	baddeleyite	1068 ± 20
171741	B	Eastern Bangemall Supergroup	baddeleyite	1063 ± 21

NOTE: Site designations are from Wingate (2002, 2003)

intrusive event. The third group comprises sills intruding the Edmund Group sedimentary rocks that may belong to either the 1465 or 1070 Ma event. Samples that make up the three groups are summarized in Table 2. Many of the samples are from the same sites used by Wingate (2002) for his dating and/or palaeomagnetism work in the western Bangemall Supergroup. The distribution of analysed samples from the western Bangemall Supergroup that are discussed in this Report is shown on Figure 6a–d.

Eastern Bangemall Supergroup

Based on available SHRIMP U–Pb baddeleyite dating of sills and on detrital zircon geochronology of rocks they intrude, it is assumed that all sills in the Glenayle area belong to the 1070 Ma intrusion event. The locations of analysed sill samples are shown in Figure 7, and their locations are also given in Appendix 1.

Field relations and petrography of the dolerite sills

The field relations and petrography of sills from the western Bangemall Supergroup have been discussed by Muhling and Brakel (1985) and Wingate (2002), as well as by other authors. Dolerites intruding sedimentary rocks of the Bangemall Supergroup have been metamorphosed to greenschist (locally amphibolite) facies, and comprise roughly equal proportions of pyroxene (dominantly augite, less commonly orthopyroxene or pigeonite) and labradoritic plagioclase, with minor amounts of opaque oxide (dominantly Fe–Ti oxides with subordinate sulfides). Late-stage intergrowths of quartz and alkali feldspar (granophyre) include apatite, zircon, and baddeleyite. All sills have been altered to some extent, with sericitization of feldspar, and alteration of pyroxene to amphibole and chlorite. The following discussion emphasizes the disposition and petrography of the sills for which the ages are known either through direct dating or stratigraphy.

1465 Ma dolerite sills of the western Bangemall Supergroup

Dolerite at site 11 near Coodardo Well (Wingate, 2002; Figs 6d and 10) consists of an approximately 175 m-thick sill (Wingate, 2002) intruding shale and thinly bedded quartz-rich sandstone of the Ullawarra Formation. The upper 50 cm-thick margin of the sill is more fine grained than the sill interior, due to chilling of the sill adjacent to the country rock. This upper contact of the sill with the country rock is sharp, although within 50 cm of the sill margin are spherical to ovoid ?varioles up to 0.5 cm in diameter that appear as 3–4 mm diameter depressions (Fig. 11).

In thin section, the fine-grained sill margin (GSWA 160187) is largely aphyric, with thin feldspar laths now partly replaced by sericite and amorphous ?clay. Bladed and wispy chlorite is found as patches between feldspar laths. Chlorite-filled patches are a possible replacement after subhedral clinopyroxene. Some stubby clinopyroxene prisms have been replaced by amphibole, and scattered opaque-oxide grains are now replaced by ?goethite. Varioles, up to 1.5 mm in diameter, are filled with wispy, bladed, pale-green amphibole and chlorite, with the latter occurring occasionally as well-developed sheaves. The rim of some varioles is marked by a higher concentration of granular opaque oxide. The boundaries between the varioles and the host rock can be both sharp and diffuse (Fig. 12).

Sample GSWA 160187 is typical of the central parts of the sill, comprising interlocking grains of plagioclase and clinopyroxene showing ophitic to subophitic texture. Wingate (2002) noted a grain size of this sill of approximately 10 mm, but GSWA 160189 has few grains greater than 3 mm in length. The clinopyroxene (probably augite) is pale brown, unzoned, and locally altered along cleavages on the margin to pale-green amphibole and chlorite. Blocky plagioclase grains up to 2 mm long are usually totally replaced by sericite and amorphous ?clay. Scattered opaque-oxide grains are altered, and show well-developed exsolution features. Wingate (2002) described these as ilmenite lamellae surrounded by leucoxene or maghemite. Interstices contain minor late-stage alkali feldspar, quartz, and chlorite, with development of acicular apatite. Wingate (2002) reported interstitial granophyric intergrowths of quartz and alkali feldspar.

The adjacent siliciclastic sedimentary rock is fine grained and dominated by quartz (Fig. 13a). Grains are angular to subangular, with minor angular to tabular plagioclase (<5% by volume; Fig. 13a) that is unzoned and usually fresh. Accessory amounts of interstitial ?chlorite are found between some quartz grains. Locally developed bedding-parallel horizons contain weakly birefringent ?clay (Fig. 13b). Rare crosscutting veins are usually micaceous, although one vein is composed of carbonate.

At site 21 (Wingate, 2002; Fig. 6a), a 200 m-thick sill intrudes fine-grained sedimentary rocks of the Discovery Formation (incorrectly assigned to the Ullawarra Formation in Wingate, 2002, appendix 2) on the northeastern limb of the Mangaroon Syncline. In outcrop, the dolerite is blocky and jointed (Fig. 14), mesocratic and equigranular, with some parts appearing to be slightly more leucocratic. Samples for both geochemistry and petrography were collected from nearby palaeomagnetic sample holes.

In thin section, the dolerite (GSWA 180712) is coarse grained (up to 8 mm in grain size according to Wingate, 2002) and consists of plagioclase enclosed by clinopyroxene (Fig. 15). The clinopyroxene grains are blocky, subhedral, and unzoned, with alteration to pale-green amphibole, and fine-grained chlorite and some sericite commonly along the cleavages. Biotite is poorly developed. In sample GSWA 180713, a well-developed alteration zonation was observed on the margins and along the cleavages of the clinopyroxene. This alteration comprises chlorite, biotite, and minor sericite. Plagioclase grains are oligoclase to andesine ($An_{28–32}$; on twin extinction) and are altered along the cleavage to sericite. Most grains are cracked. The opaque oxide grains now

Table 2. Summary of samples from the western Bangemall Supergroup

GSWA no.	*Site*	*Palaeomagnetic character*	*Age (Ma)*	*Latitude*	*Longitude*	*Chemical designation (Ma)*
COLLIER GROUP						
Ilgarari Formation						
160185	8	A	–	23°56'16"	116°54'40"	1070
152928	–	–	–	23°56'12"	116°54'23"	1070
152929	–	–	–	23°55'09"	116°53'12"	1070
152930	–	–	–	23°49'41"	116°47'59"	1070
152932	–	–	–	23°46'20"	116°45'19"	1070
152933[a]	–	–	–	23°45'44"	116°46'18"	?
127270	–	–	–	24°16'40"	118°27'26"	1070
127274	–	–	–	24°16'52"	118°20'54"	1070
127281	–	–	–	24°11'27"	118°06'40"	1070
127282	–	–	–	24°13'47"	118°07'22"	1070
127283	–	–	–	24°13'35"	118°07'24"	1070
127284	–	–	–	24°16'14"	117°52'15"	1070
127286	–	–	–	24°15'09"	117°52'58"	1070
Backdoor Formation						
160192	3	A	–	23°39'05"	116°38'15"	1070
160198	6	AB	–	23°46'47"	116°38'46"	1070
152927	–	–	–	23°45'41"	116°46'25"	1070
152934	–	–	–	23°46'47"	116°38'50"	1070
127276	–	–	–	24°09'19"	118°01'34"	–
127277	–	–	–	24°09'32"	118°01'42"	1070
127278	–	–	–	24°09'36"	118°01'42"	1070
156562	–	–	–	23°48'51"	117°07'46"	1070
EDMUND GROUP						
Ullawarra Formation						
127298	7	AB	1067	23°48'21"	116°37'57"	1070
160199	7	AB	1067	23°48'22"	116°38'04"	1070
160200	7	AB	1067	23°48'22"	116°37'59"	1070
127296	7	–	1067	23°48'22"	116°38'04"	–
180705	10	A	1068	23°23'55"	116°11'25"	1070
180706	10	A	1068	23°23'54"	116°11'25"	1070
180703	10	–	1068	23°23'48"	116°11'33"	–
180704	10	–	1068	23°23'47"	116°11'32"	–
160187	11	B	>1449	23°48'43"	116°37'44"	1465
160189	11	B	>1449	23°48'46"	116°37'44"	1465
160190	11	B	>1449	23°48'47"	116°37'42"	1465
160191	11	B	>1449	23°48'54"	116°37'38"	1465
160186	11	B	>1449	23°48'44"	116°37'44"	1465
160188	11	–	>1449	23°48'43"	116°37'44"	–
152935	11	B	>1449	23°48'49"	116°37'43"	1465
160193	2	AB	–	23°32'59"	116°35'46"	1070
180718	14	AB	–	23°50'14"	116°36'42"	1465
180719	14	AB	–	23°50'15"	116°36'44"	1465
180702	15	AB	–	23°51'15"	116°36'13"	1465
160184	18	B	–	23°56'06"	116°37'27"	1465
180708	20	AB	–	23°35'23"	116°08'44"	1465
160183	17	B	–	23°55'16"	116°35'10"	1465
180707	19	AB	–	23°25'33"	116°10'17"	1465
127297	–	–	–	23°48'28"	116°37'56"	1465
127290	–	–	–	24°20'45"	118°10'06"	1465
127291	–	–	–	24°20'30"	118°09'57"	1465
127292	–	–	–	24°20'14"	118°09'55"	1465
127293	–	–	–	24°19'51"	118°09'53"	1465
156722	–	–	–	23°57'47"	116°44'58"	1465
156543	–	–	–	23°58'58"	117°30'23"	1070
152996	–	–	–	23°53'06"	116°34'10"	1465
Devil Creek Formation						
180701	13	B	–	23°49'48"	116°37'19"	1465
127299	12	AB	–	23°49'20"	116°37'37"	1465
127300	12	AB	–	23°49'18"	116°37'37"	1465
Discovery Formation						
160182	16	B	–	23°56'14"	116°33'34"	1465
180712	21	B	1465	23°41'04"	115°38'16"	1465
180713	21	B	1465	23°41'04"	115°38'18"	1465

Table 2. (continued)

GSWA no.	*Site*	*Palaeomagnetic character*	*Age (Ma)*	*Latitude*	*Longitude*	*Chemical designation (Ma)*
Discovery Formation (cont.)						
180714	21	B	1465	23°41'04"	115°38'17"	1465
127287A	–	–	–	24°19'09"	118°13'03"	–
127287B	–	–	–	24°19'09"	118°13'03"	–
127288	–	–	–	24°18'58"	118°12'51"	1465
127289	–	–	–	24°18'50"	118°12'49"	1465
127294	–	–	–	24°12'37"	118°13'21"	1070
127295	–	–	–	24°41'27"	118°32'25"	1465
Kiangi Creek Formation						
180715	23	B	–	23°07'43"	115°46'13"	1465
180716	24	B	–	23°07'25"	115°46'23"	1465
180709	25	AB	–	23°42'22"	115°38'07"	1465
156734	–	–	1782	23°04'16"	116°02'20"	–
Blue Billy Formation						
160195	1	AB	1071	23°31'17"	116°35'16"	1070
160196	1	AB	1071	23°31'17"	116°35'17"	1070
160197	1	AB	1071	23°31'17"	116°35'20"	1070
156551	–	–	–	23°51'35"	117°26'49"	1070
156723	–	–	–	23°32'28"	116°47'20"	1070
Yilgatherra Formation						
180717	22	B	–	23°31'48"	115°40'53"	1465

SOURCES: Martin and Thorne (2002); Wingate (2002)

NOTE: (a) 152933 is possibly from the Mundine Well dyke swarm (Wingate and Giddings, 2000)

PAM 304 05.08.04

Figure 10. A sill dated at older than 1449 ± 5 Ma (Wingate, 2002; site 11) intruding the Ullawarra Formation near Coodardo Gap (exposed in a stream bed at MGA 462199E 7366432N). Pack is approximately 50 cm high

PAM 305 15.04.05

Figure 11. Varioles (arrowed) showing negative relief, developed approximately 50 cm from the upper sill margin (upper right of photograph) at site 11 (Wingate, 2002; MGA 462196E 7366520N)

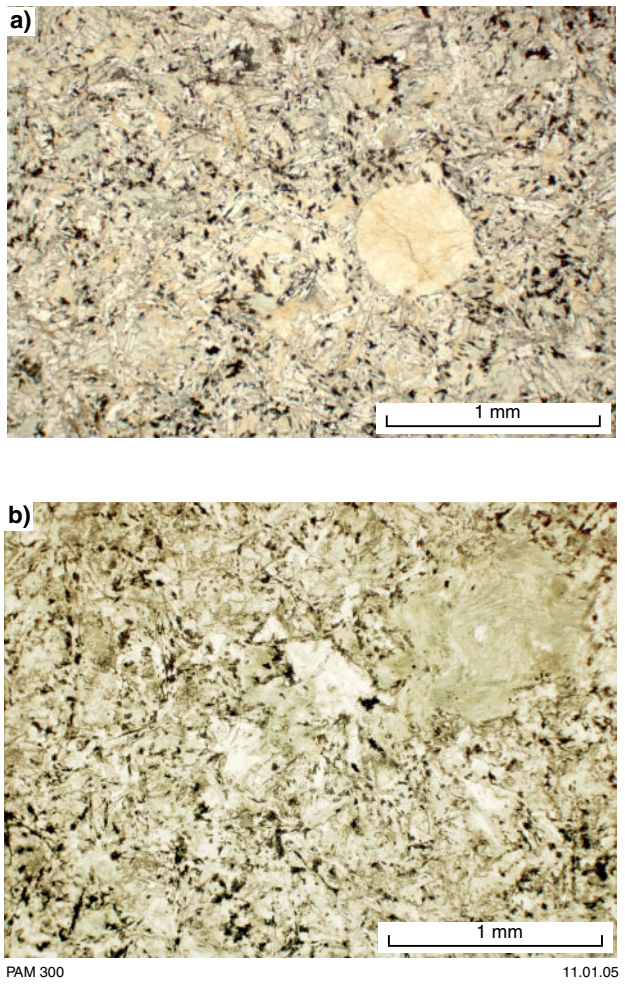

Figure 12. a) Photomicrograph of a variole developed in the margin of a 1465 Ma sill (GSWA 160186; MGA 462186E 7366520N) at site 11 (Wingate, 2002). Plane-polarized light. Note the sharp contact between the variole margin and host; b) another variole in the same sill (GSWA 160187) at the same location. Plane-polarized light. Note the diffuse margin between the variole and host

comprise leucoxene or maghemite with ilmenite lamellae (Wingate, 2002). The plagioclase in GSWA 180714 is andesine ($An_{45–50}$), which is slightly fresher than GSWA 180712, with weak sericitization of the plagioclase. Opaque oxides are less altered and partly enclose the plagioclase. Wingate (2002) recorded the development of minor late-stage alkali feldspar and quartz, with acicular apatite needles.

1070 Ma sills of the western Bangemall Supergroup

Dolerite from site 1 (Wingate, 2002; Fig. 6c) is exposed on the northeastern side of Irregully Creek, where it intrudes shale and mudstone of the Blue Billy Formation (Edmund Group) about 1.9 km north of Strama Bore (Wingate, 2002). The dolerite is conformable with the country rock, with no apparent alteration along the sill or sediment margin. A 10 cm-thick quartz vein is subparallel to the bedding in the sediment about 1.5 m below the lower contact of the sill. The upper contact is obscured by shale float.

The three dolerite samples examined petrographically from this site are all similar. Pale-brown to colourless clinopyroxene grains up to 1.5 mm in diameter are occasionally twinned, and locally altered to pale-green amphibole and chlorite (GSWA 160195). Some clinopyroxene is partly enclosed by skeletal grains of opaque oxide up to 1 mm in diameter. Wingate (2002) recorded exsolution lamellae of either orthopyroxene or pigeonite in some clinopyroxene grains from this site. Most plagioclase (andesine; $An_{40–43}$) encloses or partly encloses clinopyroxene and is cloudy, with sericite developed in small patches. Stubby apatite grains are found in some plagioclase. In GSWA 160196, plagioclase is partly enclosed by clinopyroxene, and well-developed acicular apatite is found in plagioclase grains (Fig. 16).

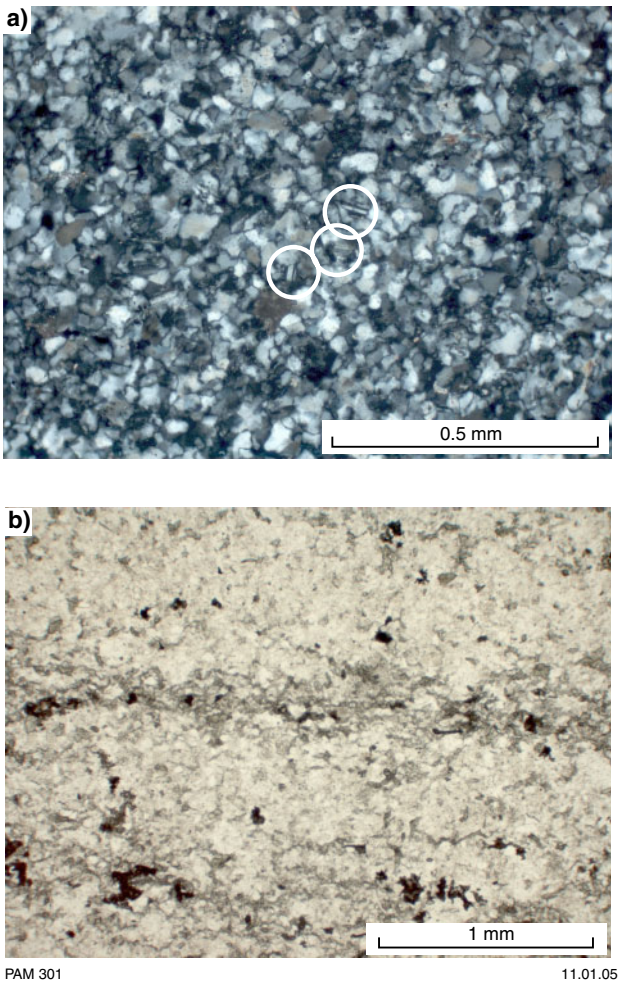

Figure 13. a) Photomicrograph of a fine-grained, well-sorted, quartz-dominated sedimentary rock (GSWA 160188; MGA 462196E 7366520N) intruded by a 1465 Ma sill at site 11 (Wingate, 2002). Cross-polarized light. Fresh plagioclase laths are circled; b) as above, but incipient bedding is shown by thin ?clay-rich horizons. Plane-polarized light

PAM 302 05.08.04

Figure 14. Jointed dolerite sill intruding the Discovery Formation at site 21 (MGA 361160E 7380051N; 1465 ± 3 Ma, Wingate, 2002) showing palaeomagnetic sampling holes. Global positioning system is 16 cm long

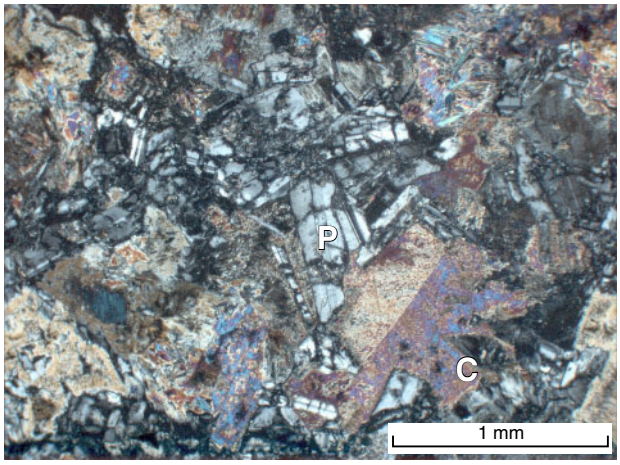

PAM 303 11.01.05

Figure 15. Photomicrograph of intergranular texture shown by dolerite GSWA 180712 at site 21 (MGA 361160E 7380051N; 1465 ± 3 Ma, Wingate, 2002). Plagioclase (P) is variably sericitized and clinopyroxene (C) is twinned. Cross-polarized light

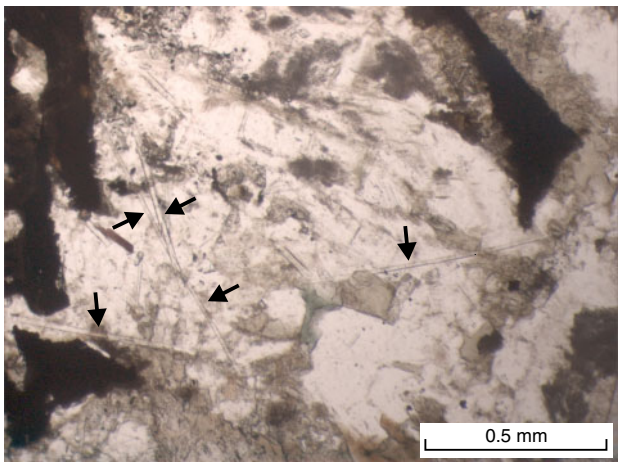

PAM 297 11.01.05

Figure 16. Photomicrograph of acicular apatite (arrowed) in late-stage feldspar (GSWA 160196; MGA 457949E 7398692N) from Wingate's (2002) site 1 (1071 ± 8 Ma). Plane-polarized light

GSWA 160197 is slightly coarser grained, which may account for the development of late-stage intergrowths of quartz and alkali feldspar. This sample also contains small isolated carbonate patches.

At site 7 (Wingate, 2002), dolerite intrudes the Ullawarra Formation (Edmund Group) at Coodardo Gap (Fig. 6d). The sill is approximately 340 m thick. Although the lower contact is poorly exposed, the upper contact with the surrounding sedimentary rocks is usually sharp, although brecciation is locally developed and comprises a chaotic mixture of dolerite and siliciclastic sedimentary rock. It is possible that this represents intrusion of the sill into unconsolidated sediments, but it may also represent solid-state intrusion accompanied by abundant fluids. A 50 cm-thick zone of finer grained dolerite is developed on the sill margin, although within about 20 m of the upper contact the sill is quite coarse grained (grain size about 1–2 mm). Sedimentary rock at the sill contact is characterized by abundant development of secondary carbonate (Fig. 17).

The fine-grained upper contact of the sill (GSWA 160199) is quite strongly altered, with well-developed chlorite (after clinopyroxene), and sericite (after plagioclase). Both clinopyroxene and plagioclase (as individual grains or pseudomorphs) are in roughly equal proportions. The clinopyroxene grains are anhedral and are usually replaced by chlorite, although some are elongate. Wingate (2002) noted that some clinopyroxene grains had exsolution lamellae of orthopyroxene or pigeonite. Most plagioclase grains (oligoclase–andesine; $An_{30–32}$) are wispy and less than 0.5 mm long, and form masses between less common acicular plagioclase and clinopyroxene. These patches of wispy feldspar support apatite needles. Elongate plagioclase grains up to 1 mm long are usually partly altered to sericite. Late-stage quartz patches are developed, and opaque oxides are seen as scattered anhedral granules. Further away from the sill margin (GSWA 160198), the dolerite is fresher and more coarse grained. Interlocking

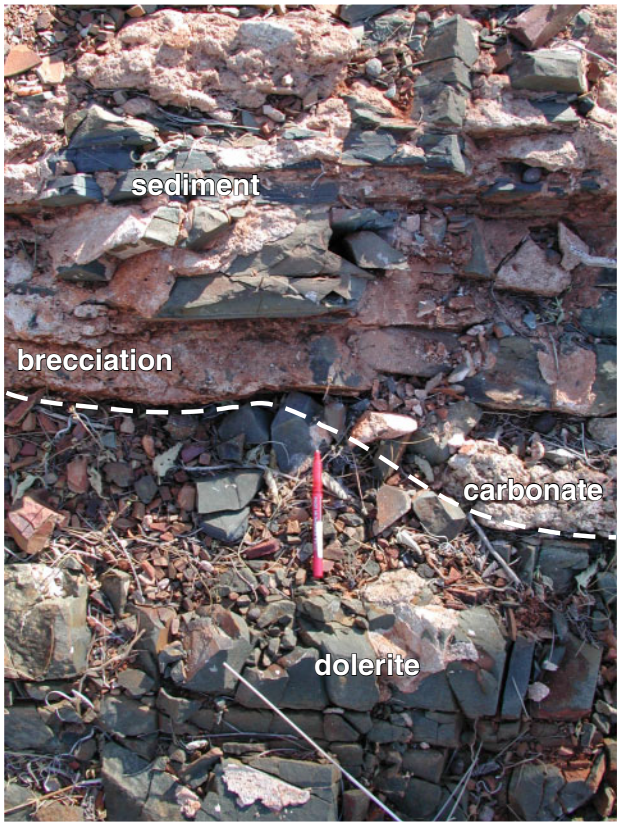

PAM 298 11.01.05

Figure 17. Subhorizontal dolerite sill in contact with thinly bedded siliciclastic sedimentary rock of the Ullawarra Formation at site 7 (MGA 462760E 7367177N; 1067 ± 14 Ma; Wingate, 2002). Brecciation and secondary carbonate are developed along the sediment–sill contact

colourless to pale-brown clinopyroxene is enclosed by blocky, fresh oligoclase–andesine ($An_{28–37}$). Biotite flakes are developed adjacent to clinopyroxene when in contact with opaque oxides, which are skeletal. Rare grains of orthopyroxene are weakly zoned. GSWA 160200 is similar, with clinopyroxene up to 2 mm and plagioclase up to 3 mm in size. Patches of granophyre contain accessory amounts of zircon. The clinopyroxene is cracked, with incipient alteration to a brown, birefringent mineraloid along the cleavages.

At site 10, an approximately 100 m-thick dolerite sill intrudes siliceous sedimentary rocks of the Ullawarra Formation (Edmund Group) near Curran Well (Wingate, 2002; Fig. 6a). The sill consists of rounded meso- to leucocratic dolerite outcrop in and adjacent to a stream channel. The sill appears to be texturally and mineralogically homogeneous.

In thin section (GSWA 180705, 180706), the dolerite is even grained and consists of clinopyroxene partly enclosing plagioclase, with well-developed late-stage patches of granophyre (Fig. 18). The clinopyroxene is up to 1.5 mm in diameter (GSWA 180705, 180706), pale brown to colourless, unzoned, and is incipiently altered to pale green-blue amphibole and chlorite on the margin, with biotite alteration of clinopyroxene in GSWA 180706. Individual clinopyroxene grains are locally twinned and intergrown with fresh blocky to skeletal opaque oxide. Plagioclase grains (andesine; $An_{34–41}$) are elongate to tabular and unzoned, variably sericitized, and labradoritic. Some late-stage feldspar is completely altered to sericite in GSWA 180705. In GSWA 180706, late-stage feldspar is intergrown with quartz and encloses needles of apatite, and late-stage clinopyroxene is replaced by wispy chlorite. In GSWA 180705, some secondary amphibole is rimmed by biotite and minor epidote.

Discussion

Although 1465 and 1070 Ma sills cannot be separated in terms of field relations, and variations in modal mineralogy and texture in thin section, there are some subtle differences between the two sill intrusion events. Most 1465 Ma sill samples examined appear to be more altered, particularly in terms of chlorite and amphibole after clinopyroxene. In contrast to the 1465 Ma sills, the 1070 Ma sills usually have some late-stage pockets of intergrown quartz and feldspar that occasionally enclose acicular apatite and locally zircon. Accessory amounts of biotite are also found in some cases. However, it is clear that the degree of alteration or the amount of late-stage quartz and feldspar cannot be reliably used to separate sills into different intrusion events, as sills of the same age can be variably altered, and the amount of late-stage quartz–feldspar is in part determined by the thickness and cooling time of the sill.

1070 Ma sills of the eastern Bangemall Supergroup

Three dolerite units (the Glenayle, Mingol, and Prenti Dolerites) can be recognized amongst the 1070 Ma sills

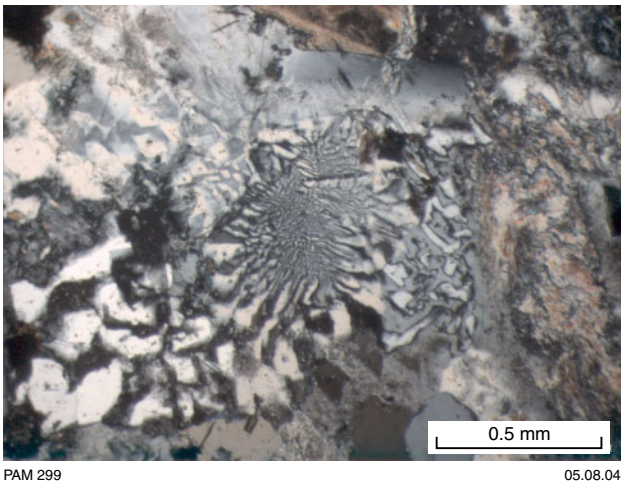

PAM 299 05.08.04

Figure 18. Photomicrograph of intergrown quartz and alkali feldspar (GSWA 180705; MGA 417261E 7412113N) showing the runic form typical of granophyre at site 10 (1068 ± 22 Ma; Wingate, 2003), intruding the Ullawarra Formation shale at Curran Well. Cross-polarized light

in the eastern Bangemall Supergroup, based on variations in texture and mineralogy. The Glenayle Dolerite can be further subdivided into three formal members, as discussed below.

Glenayle Dolerite

The Glenayle Dolerite consists of fine- to medium-grained dolerite sills and dykes. Three different types of dolerite have been recognized on the basis of the amount of granophyre present and the proportions of Fe–Ti oxides. These types have been given member status by Pirajno and Hocking (2002). However, subsequent work has shown that these dolerite units may represent different levels of exposure within a single sill. The Parker Range Member is a fine- to medium-grained dolerite containing distinct millimetre-scale blebs of pink granophyre and locally abundant Fe–Ti oxides. The Yallum Hill Member is a medium- to coarse-grained dolerite, which is locally mesocratic, with patches of granophyre, and plagioclase-rich bands up to 10 cm thick. The Weld Spring Member is very fine to medium grained, with abundant (typically 5–7%) disseminated Fe–Ti oxides and minor sulfides (pyrite and chalcopyrite). The Weld Spring Member is discussed below.

The mineralogy of the Glenayle Dolerite is dominated by plagioclase and clinopyroxene, with or without orthopyroxene, and interstitial granophyre is usually developed. Plagioclase (usually about 50% by volume of most samples) ranges from An_{60} to An_{72} (labradorite) according to optical determinations on albite and combined Carlsbad-albite twins. Augite (35% by volume of most samples) is accompanied occasionally by pigeonite or enstatite. Textures range from typically ophitic to intergranular. The amount of granophyre increases towards the tops of the sills (Fig. 9), where it can account for 20–30% by volume. Accessory minerals include the Fe–Ti oxides ilmenite and titanomagnetite, quartz, and apatite. Alteration phases include biotite, hornblende, chlorite, smectite, sericite, and prehnite. Baddeleyite is present as inclusions in hydrous minerals such as biotite and hornblende. Accessory amounts of sulfides contain grains usually less than 0.05 mm in diameter (commonly around 0.01 mm) consisting of pyrite and less common chalcopyrite.

Iron–titanium oxides, including ilmenite, magnetite, and titanomagnetite, account for less than one up to 10% by volume. Ilmenite is present as skeletal crystals up to 1 mm long that locally have well-developed hematite exsolution lamellae. Average magnetic susceptibility of the Glenayle Dolerite, based on 40 measurements, is 2918×10^{-5} SI.

A typical country rock (GSWA 152680; MGA 354818E 7229413N) consists of a thermally metamorphosed medium-grained sandstone containing an aggregate of quartz grains up to 0.5 mm across. These grains are unstrained, commonly have rounded cores, and are cemented by optically continuous silica overgrowths. Brown clay has partly replaced feldspar grains and there are aggregates of interstitial, decussate red-brown biotite, also partially altered to clay. Opaque oxides form irregular areas or patches, some up to 7 × 4 mm, in addition to veins of black iron or ?manganese oxide. Bedding laminations are not clearly visible in thin section, but in hand specimen the oxide spots are aligned parallel to the layering, yet the veins are at a high angle to the layering. The small, colourless, high-relief and isotropic grains that are present are probably garnets, which are accompanied by scattered, rounded zircon grains. GSWA 161224 (MGA 372370E 7225920N) is a thermally metamorphosed sandstone containing quartz, sericite, prehnite (partly altered to clay), euhedral pink garnet (Fig. 19), and possible pyrophyllite.

Weld Spring Member

The Weld Spring Member occupies an approximately circular area, about 30 km in diameter, at the intersection of the Bullen, Trainor, Nabberu, and Stanley, with most of the outcrop on northwest Stanley (Fig. 20). In both outcrop and hand specimen, the dolerite has disseminated spots that are shown in thin section to be Fe–Ti oxides (Fig. 21a). Locally, crude layering can be seen in the outcrops (Fig. 21b). The Weld Spring Member is probably a dolerite sheet that is inclined towards the southwest, as the northern section that represents the upper part of the sill is granophyre rich (Fig. 21c,d), whereas the southern section that represents the lower part of the sill is granophyre poor (Fig. 20), but relatively rich in sulfides and Fe–Ti oxides. In thin section, the southern part of this dolerite sheet contains plagioclase laths, less common clinopyroxene, and conspicuous ilmenite and titanomagnetite up to 5 mm across (Fig. 22a,b). The titanomagnetite has ilmenite exsolution lamellae along the (111) planes. Diagnostic of the Weld Spring Member are disseminated skeletal crystals and poikilitic ilmenite blebs 4–5 mm across and about 5–7% by volume that appear as phenocrysts in hand specimen and give the rock a spotted

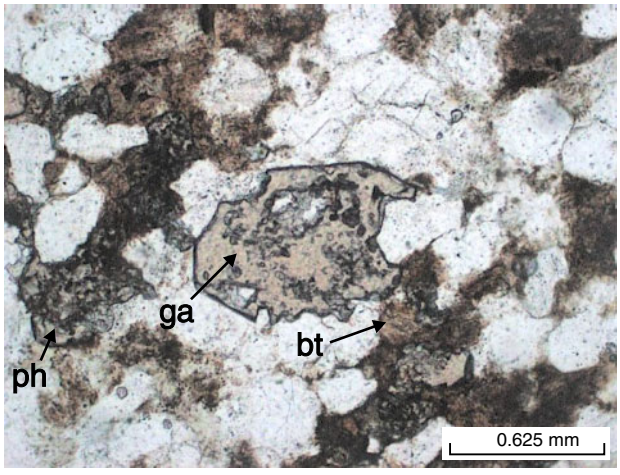

Figure 19. Photomicrograph of GSWA 161224 showing pink garnet porphyroblast (ga) and quartz grains with interstitial prehnite (ph) and biotite (bt), partly altered to clay (dark material). Both the garnet and the prehnite are the result of thermal metamorphism of Salvation Group sandstone, due to the intrusion of dolerite. Plane-polarized light

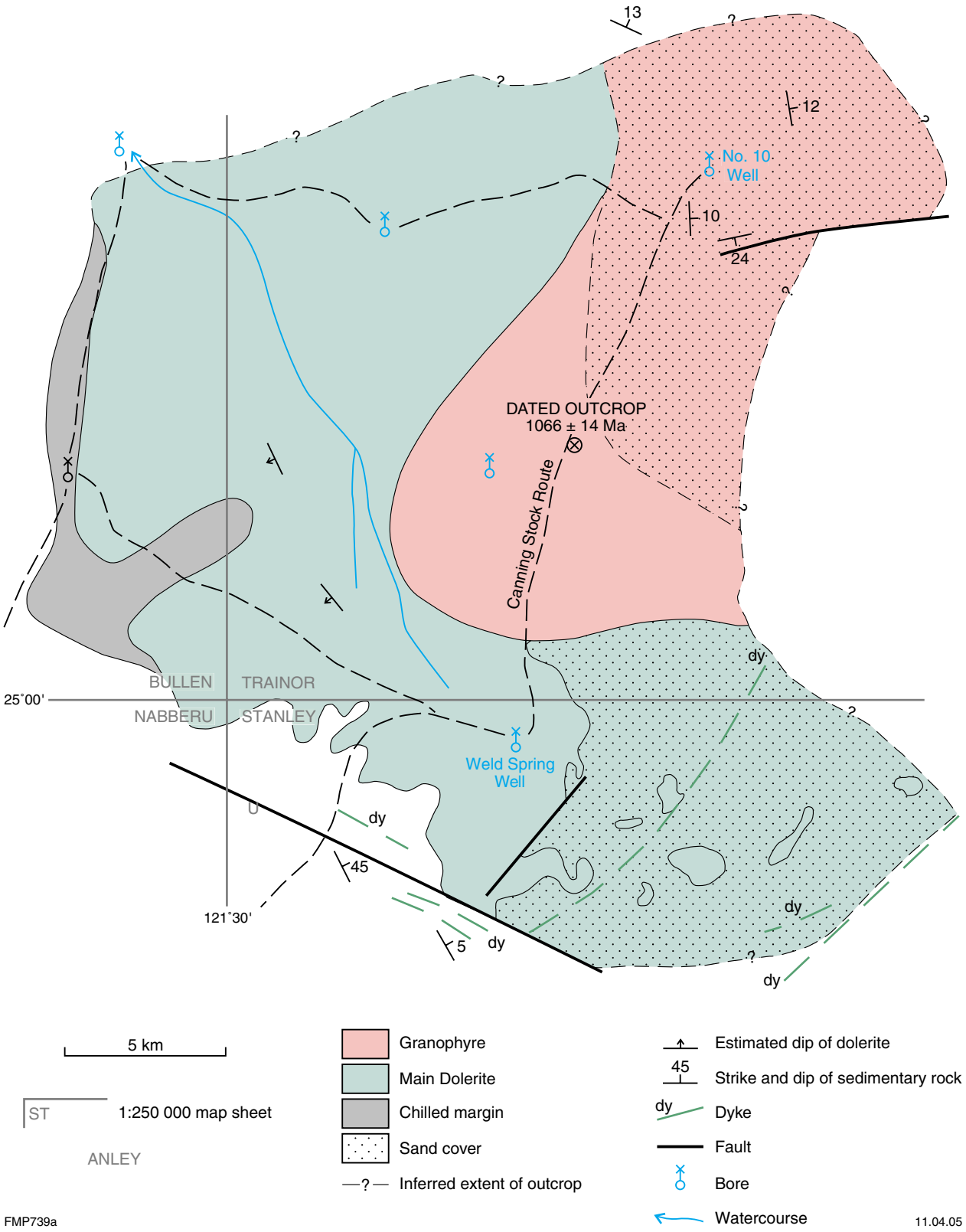

Figure 20. Interpreted solid geology map of parts of the Weld Spring Dolerite sill (northwest STANLEY), based on geological mapping (Pirajno and Hocking, 2001; Pirajno, unpublished data) and aeromagnetic data. The sill or sheet is inclined to the southwest (dip unknown)

Figure 21. Selected outcrop features of the Weld Spring Dolerite: a) porphyritic appearance due to disseminated Fe–Ti oxides; b) crude magmatic layering; c) granophyre veinlet cutting through the dolerite, with interstitial granophyre; d) locally a sharp boundary separates the granophyric dolerite from dolerite with only minor interstitial granophyre

appearance (Fig. 21a). The plagioclase is labradorite ($An_{54–62}$), and accounts for 55–60% of each sample. The clinopyroxene (augite) grains are 1–2 mm long, twinned, hour-glass zoned, and account for about 35% by volume of the dolerites. They are incipiently altered to chlorite and anthophyllite, with the latter also found as fine needles and brown, radial, fibrous aggregates. Minor pigeonite is present, with alteration parallel to a sub-basal parting or to fractures at a high angle to the c-axis. Quartz forms small interstitial grains (2–3%). Patches of dark-brown cloudy material are the result of iron-oxide weathering. Small blebs of pyrite and subordinate chalcopyrite are accessory minerals. Some sulfides are found in ilmenite grains. Some chalcopyrite grains are rimmed by bornite. Magnetite appears to have been replaced by maghemite, with residual lamellae of ilmenite up to 0.2 mm wide (Fig. 22a), and separate lobate to dendritic aggregates of ilmenite and clays. Red-brown biotite and small sheaves of prehnite are present as minor alteration phases. Rare pale-green to greenish-brown amphibole is found either mantling pyroxene or as separate small prisms, in addition to biotite flakes up to 0.4 mm long. Apatite needles are present in the groundmass (Fig. 22c). Alteration to clays and microcrystalline sphene is seen locally, especially adjacent to opaque oxide patches. Minor late-magmatic quartz and granophyre up to 1 mm in diameter are present, with associated accessory apatite.

The northern section of the Weld Spring Member is characterized by abundant granophyre and more abundant brown hornblende and chlorite as alteration minerals (Fig. 22d,e,f). The latter is more abundant and contains inclusions of baddeleyite crystals (about 100 μm long) with distinct pleochroic haloes (Fig. 22f). The presence of this baddeleyite has enabled a precise U–Pb age determination for the dolerite of 1066 ± 14 Ma (Wingate, 2003).

Mingol Dolerite

The Mingol Dolerite is found on Lee Steere (1:100 000; Hocking and Pirajno, 2004), where it forms scattered east-trending outcrops extending for about 6 km; however, aeromagnetic data indicate that the dolerite has a subsurface extent of 15 km (east–west) by 7 km (north–south) and is associated with northwest-trending aeromagnetic lineaments that have been interpreted as

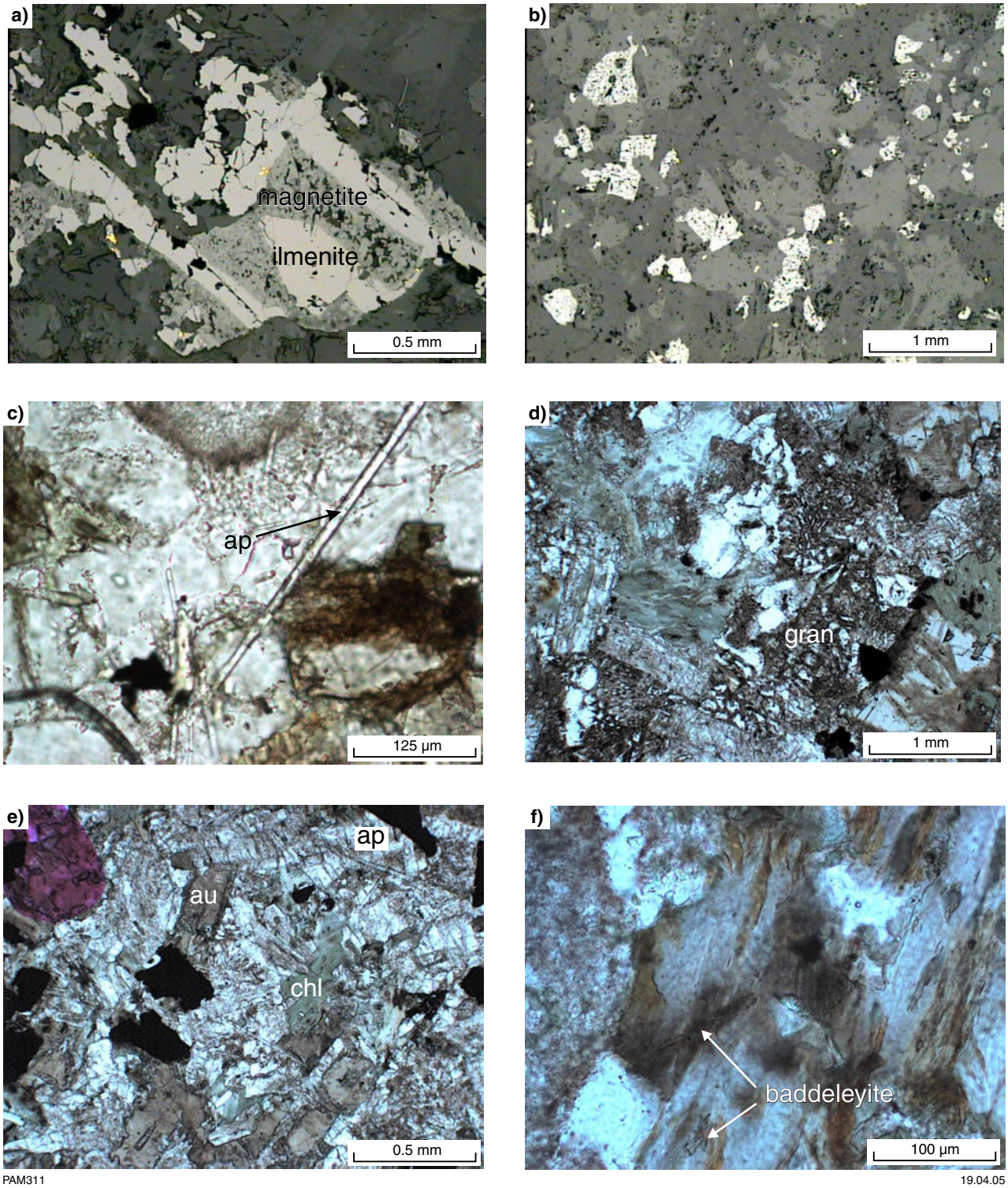

Figure 22. **Photomicrographs of the Weld Spring Dolerite: a) GSWA 152663B containing magnetite (darker grey) with ilmenite exsolution bodies (lighter grey) and small specks of chalcopyrite (yellow). Reflected light; b) GSWA 1717734D containing disseminated titanomagnetite crystals. Reflected light; c) GSWA 152674 containing apatite (ap) needles in granophyre. Plane-polarized light; d) GSWA 171732 containing interstitial granophyre (gran). Plane-polarized light; e) GSWA 171734A containing plagioclase laths and augite crystals (au) cloudy with sericitic, chloritic (chl), and brown clay alteration; apatite needles (ap); and interstitial granophyre. Plane-polarized light; f) GSWA 171732 containing green hornblende associated with chlorite and pumpellyite. Hornblende contains inclusions of baddeleyite surrounded by pleochroic haloes due to radioactive damage. Plane-polarized light**

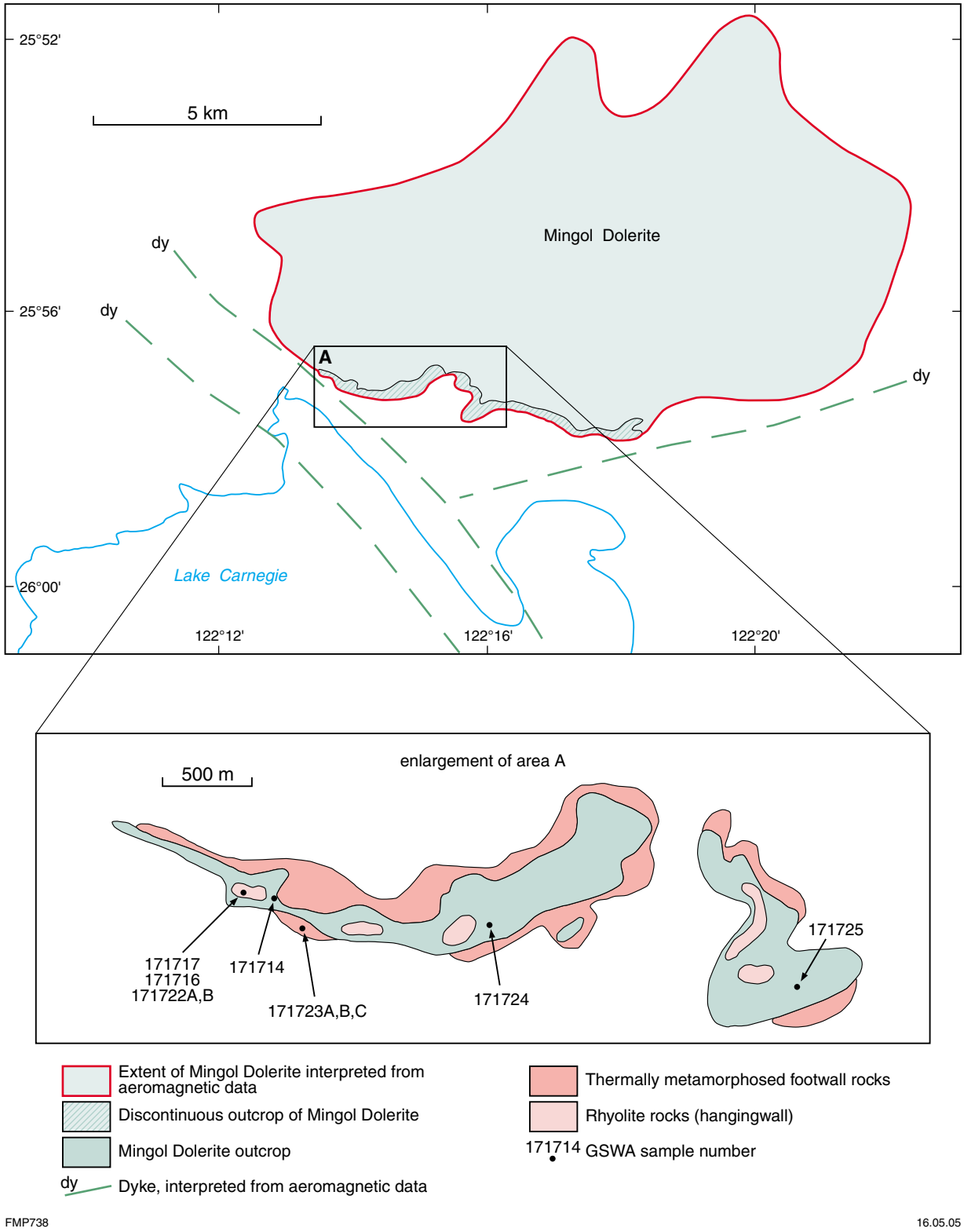

Figure 23. Simplified geological map of the Mingol Dolerite on Lee Steere (1:100 000; Hocking and Pirajno, 2004), showing scattered remnants of rhyolitic rocks in the hangingwall

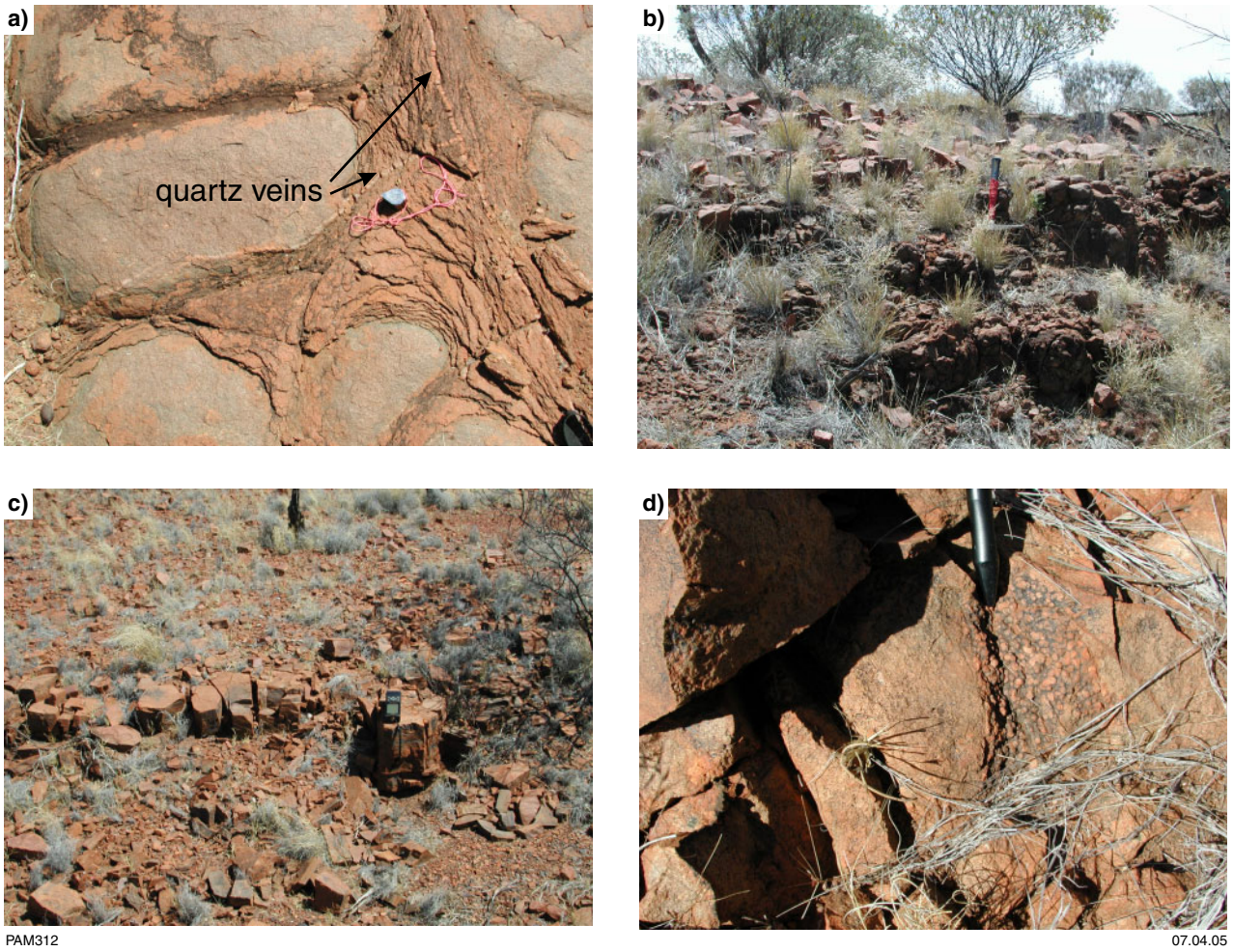

Figure 24. Selected features of Mingol Dolerite outcrops: a) spheroidal weathering of the dolerite. Note the crosscutting, post-weathering quartz veinlets; b) contact of the dolerite and overlying rhyolitic rock; c) reddish-brown rhyolitic rock; d) spherulitic textures developed in rhyolite

mafic dykes (Fig. 23). The thickness of the sill(s) is unclear. Field evidence indicates that individual dolerite sills may be only 1 or 2 m thick, but considering the intensity of the aeromagnetic signature it is possible that the Mingol Dolerite consists of a number of thin metre-sized sheets. At one outcrop (MGA 425845E 7130008N) the magnetic susceptibility of this dolerite has been measured at 4660×10^{-5} SI. These thin sills are intruded subparallel to the bedding into limestone and sandstone units of the Wongawol Formation of the Earaheedy Group. In hand specimen, the Mingol Dolerite ranges from a coarse-grained gabbroic rock to a very fine, aphanitic or glassy material, probably representing the chilled margins of sills. In places, the dolerite has characteristic spheroidal weathering, with quartz veins cutting through the weathered material (Fig. 24a), thus implying post-weathering circulation of silica-rich fluids.

The Mingol Dolerite is overlain by scattered remnants of a dense, massive, reddish-brown rhyolitic rock (Figs 23 and 24b,c) that locally contains numerous angular lithic fragments, thus imparting a breccia-like appearance. The rhyolitic rock with lithic fragments suggests mixing and splitting of the Wongawol Formation limestone and sandstone beds in a brittle environment, implying that a volatile-charged felsic melt applied considerable pressure to the overlying rocks and caused fragmentation. At one locality (MGA 425105E 7130049N), the rhyolitic rock outcrops as a sheet about 0.5 m thick, with sharp contacts with the limestone (hangingwall) and the dolerite (footwall). At this same locality, this rhyolitic sheet is spatially associated with a thin dyke of the same material that is probably a feeder.

The Mingol Dolerite is characterized by ophitic to intersertal or intergranular textures with some interstitial devitrified glass (Fig. 25a). The essential minerals are plagioclase and augite, with the former pervasively and selectively altered to quartz and sericite. Chlorite is also common and is mostly interstitial or replacing silicate minerals. Locally there are zones of feathery crystallites of feldspar showing a quench texture. Disseminated opaque oxide, up to about 10% by volume, includes anhedral pyrite, and Fe–Ti oxides (ilmenite and titanomagnetite) showing low-temperature oxidation and replacement to maghemite. Tiny blebs (<0.01 mm) of chalcopyrite are also present (Fig. 25b). In places, the Fe–Ti oxides clearly post-date the augite crystals.

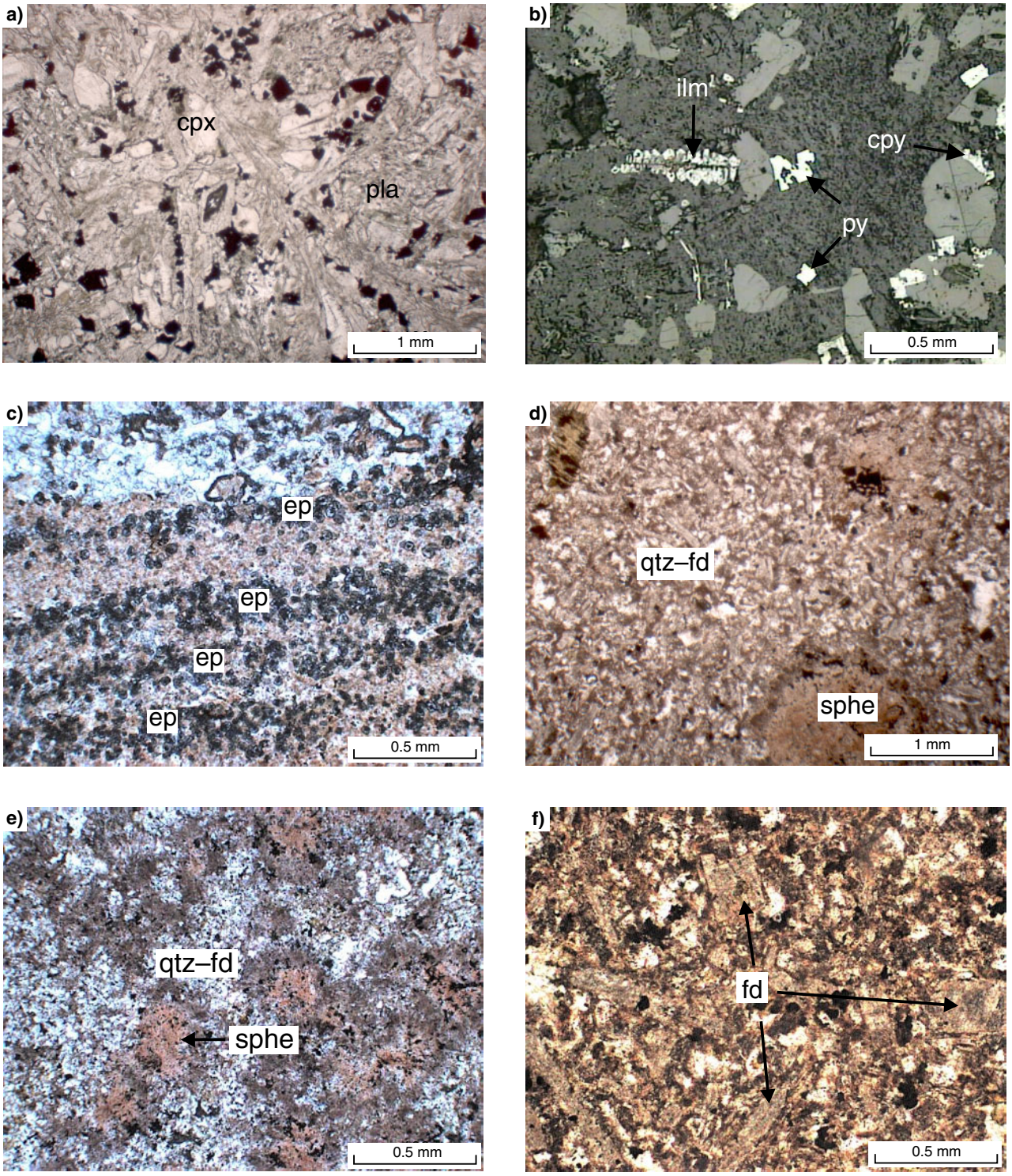

Figure 25. Photomicrograph of the Mingol Dolerite showing: a) GSWA 171724 containing altered dolerite, sericitized plagioclase (pla), clinopyroxene (cpx), and disseminated Fe–Ti oxides. Plane-polarized light; b) GSWA 171717 containing altered dolerite (sericitized and silicified in part), with skeletal ilmenite (ilm), pyrite (py), and minor chalcopyrite (cpy). Reflected light; c) GSWA 171723B containing hangingwall metamorphosed limestone (calc-silicate) composed of brown-coloured laminae of dusty quartz-grain aggregates interlayered with laminae of epidote (ep) and ?carbonate (calcite) material. Plane-polarized light; d) rhyolitic rocks showing spherulite (sphe) and quartz–feldspar felsitic (qtz–fd) groundmass. Plane-polarized light; e) rhyolitic rock showing spherulites (sphe) and quartz–feldspar groundmass (qtz–fd). Plane-polarized light; f) rhyolitic rock (GSWA 171716) showing a fine-grained felsitic assemblage composed of quartz and feldspar (fd). Plane-polarized light

The emplacement of the Mingol Dolerite produced thermal metamorphism of the wall rocks. Limestone units of the Wongawol Formation were metamorphosed to pale-green marble and calc-silicate rocks (Fig. 25c). The marble is composed of recrystallized calcite (grain size from 60 to about 180 µm) with bands and zones of quartz, albite, orthoclase, and epidote.

The rhyolitic rock is characterized by spherulites (Figs 24d and 25d,e) containing radial aggregates of fibrous and acicular red-brown feldspar that form a framework within which are quartz, K-feldspar, chlorite and prehnite crystals. These crystals are surrounded by fine dusty material that is largely unidentifiable due to the abundance of fluid inclusions. Apart from the spherulites, there are two types of feldspar: clear albite and dusty alkali feldspar that is possibly adularia (Fig. 25f), both of which are associated with quartz and prehnite sheaves. Locally there are elongated zones with abundant feldspar microlites associated with quartz and needle-like or slender prismatic crystals of pale-green biotite. Some amygdales are present that are lined with K-feldspar and cored with prehnite sheaves. Quartz-rich zones are elongated and contain round sandstone or siltstone fragments. Crosscutting quartz and albite veinlets have also been observed. The spherulites can be attributed to feldspar nucleation accompanied by the growth of contact mineral phases such as biotite, and recrystallization of the quartz grains to develop a dusty, brown-coloured quartz aggregate. The interstitial material (originally ?clay) has formed chlorite and/or prehnite. The thermal metamorphic assemblage can be summarized as quartz–K-feldspar–plagioclase–biotite. The origin of this unusual rock is not known, but it is possible that it may be the result of localized crustal melting caused by the emplacement of dolerite sills in the region. The Mingol rhyolitic rock is the only example in the region of a silicic subvolcanic rock associated with the Glenayle Dolerite sill complex.

Prenti Dolerite

The Prenti Dolerite consists of aphanitic to very fine-grained dolerite sills and dykes (Pirajno and Hocking, 2002) that crosscut the Glenayle Dolerite. On MUDAN (1:100 000) and GLENAYLE (1:100 000), the Prenti Dolerite floors some of the circular features described previously. To the south, sills of Prenti Dolerite up to 30–40 m thick intrude along the bedding planes of the Earaheedy Group rocks on VON TREUER (1:100 000) and WINDIDDA (1:100 000; Fig. 26). Separation of the Prenti Dolerite from fine-grained chilled margins of the Glenayle Dolerite is difficult in the field, but in thin section the glomeroporphyritic texture that typifies the Prenti rocks is diagnostic.

The Prenti Dolerite is mineralogically simple, comprising roughly equal proportions of plagioclase and granular augite (partially replaced by chlorite and biotite), with an intergranular glomeroporphyritic texture, defined by bunches of fresh plagioclase crystals, set in a groundmass of clinopyroxene and plagioclase with interstitial devitrified glass (Fig. 27a). Optically, the plagioclase compositions range from labradorite to bytownite ($An_{56–70}$). Accessory minerals include chlorite and biotite as alteration phases replacing augite (Fig. 27b). In some samples, disseminated Fe–Ti oxides occupy up to 10% of the rock (Fig. 27c). It is unclear whether the

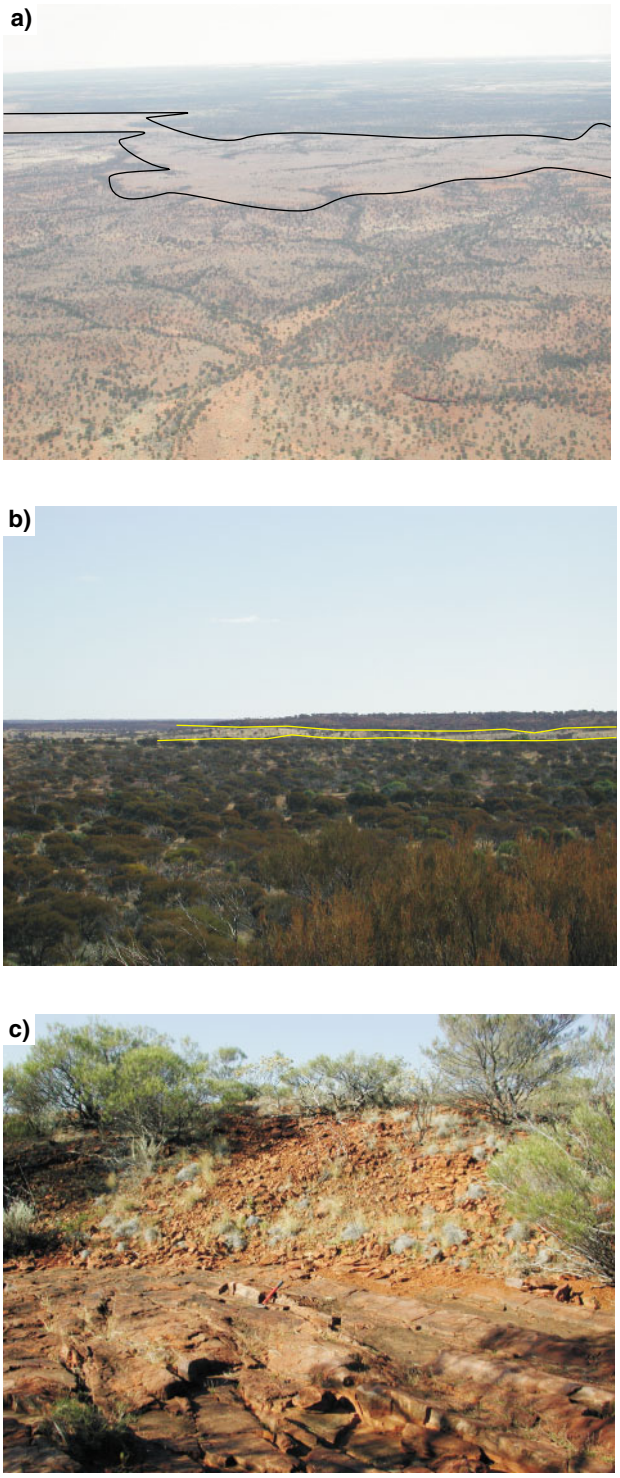

Figure 26. a) Aerial photograph of a sill of the Prenti Dolerite (outlined) intruding Earaheedy Group rocks on VON TREUER (1:100 000; southeastern Earaheedy Basin); b) view of the same sill from the ground; c) outcrop of the Prenti Dolerite in contact with ripple-marked sandstone of the Chiall Formation (Earaheedy Group)

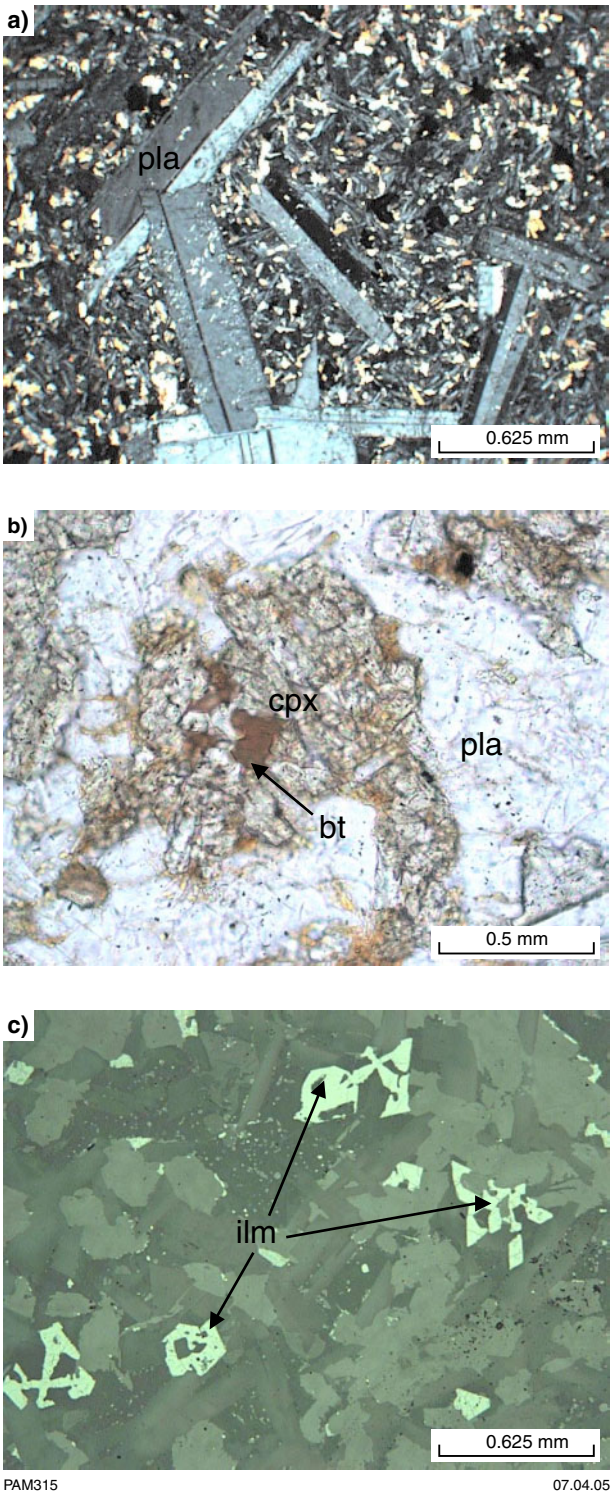

Figure 27. Photomicrographs of the Prenti Dolerite showing: a) GSWA 171705 which has glomeroporphyritic texture with clusters of plagioclase crystals and a groundmass that is mainly plagioclase and clinopyroxene. Cross-polarized light; b) GSWA 132411 from the floor of a circular structure on Glenayle that contains plagioclase (pla) and clinopyroxene (cpx) in a fine-grained intergranular texture. Clinopyroxene is locally altered to brown biotite (bt). Plane-polarized light; c) GSWA 132424 showing disseminated skeletal ilmenite (ilm) crystals in aphanitic dolerite. Reflected light

Glenayle and Prenti Dolerites are comagmatic or represent separate magmatic events.

Geochemistry

Sample collection, preparation, and analysis

Ninety-four samples have been analysed for this Report. Twenty-five samples are from sills dated at 1070 Ma or intruding the Collier Group in the western Bangemall Supergroup. Twenty-seven samples are from 1070 Ma sills in the eastern Bangemall Supergroup, and three are from the Empress 1A drillhole in the Officer Basin (Stevens and Apak, 1999). A further eight samples are from the two sills dated at 1465 Ma by Wingate (2002; sites 11 and 21). Thirty samples have also been analysed from sills intruding the Edmund Group, which could belong to either the 1465 or 1070 Ma intrusive event. One sample (GSWA 159233) is from a crosscutting dyke on Edmund (1:100 000). This sample has tentatively been assigned to the 1070 Ma event, but could be part of the 755 Ma Mundine Well dyke swarm (Wingate and Giddings, 2000). Due to the equivocal parentage of this sample, it has not been plotted on the element variation diagrams. The chemistry of all the sills discussed in this Report has been compiled as a .csv digital dataset that is available on the Department's website (Appendix 1). The average compositions of sill groupings discussed below are shown in Table 3.

Approximately 3 kg of the more mafic and finer grained parts of the sills were collected, if possible, in order to minimize the effects of fractional crystallization. Each sample was slabbed using a diamond saw in the Geological Survey of Western Australia's (GSWA's) Carlisle laboratory, and any vein or weathered material was removed. Saw marks were ground off using a carborundum lap, and samples were thoroughly washed and dried. Approximately 1 kg of material was crushed in a modified Nugget jaw crusher. For each sample, a small amount of slabbed material was crushed and rejected, then the remainder of the sample was reduced to a nominal particle size of about 0.5 cm. After crushing of each sample, the crusher was cleaned with compressed air and a wire brush; after every five samples, the crusher jaws were removed, cleaned with high-pressure water, and dried.

Approximately 250 g of crushed material was milled for approximately 90 seconds in a Tema tungsten-carbide ring mill to produce a talcum-powder grade pulp, with approximately 50 g of powder reserved for analysis.

Of the 94 analyses discussed here, 68 (72%) were analysed at Geoscience Australia's (GA) Canberra laboratory, 17 (18%) at the Australian National University (ANU), and nine (10%) at ANU and the University of Queensland. Analyses of GSWA's internal Bunbury Basalt reference material (BB1), analysed with the dolerites, are given in Appendix 2.

Analyses carried out by GA comprise major element oxides and some trace elements analysed by X-ray

Table 3. Average composition of sill groupings

	1070 Ma western Bangemall Supergroup (n = 22)	*1070 Ma eastern Bangemall Supergroup (n = 27)[a]*	*Low-Th/Nb 1070 Ma eastern Bangemall Supergroup (n = 19)*	*High-Th/Nb 1070 Ma eastern Bangemall Supergroup (n = 8)*	*1465 Ma western Bangemall Supergroup (n = 8)*	*Sills intruding Edmund Group (western Bangemall Supergroup) with 1465 Ma chemistry (n = 25)*	*Sills intruding Edmund Group (western Bangemall Supergroup) with 1070 Ma chemistry (n = 5)*
				Percentage			
SiO_2	50.96	52.62	52.17	53.68	49.50	49.41	52.04
TiO_2	2.02	1.91	1.87	1.98	1.54	1.55	1.75
Al_2O_3	13.15	13.54	13.51	13.61	13.72	13.97	13.65
Fe_2O_3[b]	14.69	13.39	13.68	12.70	13.37	12.99	13.94
MnO	0.19	0.18	0.18	0.17	0.25	0.21	0.19
MgO	4.91	4.86	5.11	4.27	6.04	5.96	4.69
CaO	9.04	8.25	8.54	7.56	9.99	9.88	9.01
Na_2O	2.39	2.50	2.50	2.50	2.04	2.17	2.42
K_2O	1.15	1.49	1.30	1.95	1.09	0.91	1.18
P_2O_5	0.24	0.22	0.22	0.23	0.22	0.22	0.22
SO_3	0.23	0.14	0.12	0.33	0.32	0.40	0.19
LOI	1.77	1.04	0.90	1.34	1.78	2.71	1.63
Total	**100.74**	**100.13**	**100.11**	**100.31**	**99.87**	**100.38**	**100.91**
				Parts per million			
As	2.13	1.69	1.87	1.03	26.77	1.95	2.83
Ba	344	489	507	445	338	291	346
Be	1.07	1.14	1.09	1.50	1.07	0.85	1.19
Bi	0.20	2.86	0.58	8.20	–	–	–
Cd	0.11	0.25	0.25	0.25	0.12	0.17	0.12
Co	55	60	60	–	–	44	50
Cr	95	55	68	29	149	143	52
Cs	2.00	4.08	5.00	0.85	1.55	1.84	1.41
Cu	167	125	146	76	65	107	166
Ga	22	22	21	22	19	19	22
Ge	1.66	1.48	1.61	1.20	2.16	1.75	1.63
Hf	4.71	5.43	4.86	6.64	2.97	3.05	4.31
Mo	0.8	1.3	1.5	1.0	0.9	0.8	0.8
Nb	11.58	10.70	9.85	12.73	10.04	9.63	9.59
Ni	99	83	94	59	63	79	93
Pb	7.46	14.06	12.05	18.84	2.97	3.98	8.87
Rb	39	56	46	80	29	28	41
S	86	46	18	78	–	95	40
Sb	0.13	0.18	0.19	0.13	0.42	0.30	–
Sc	29	29	30	28	40	35	28
Sn	1.89	2.11	2.10	2.14	1.34	1.28	2.13
Sr	240	273	273	276	213	212	230
Ta	0.66	0.75	0.64	1.24	0.67	0.60	0.57
Th	4.79	8.61	5.63	14.94	2.01	1.93	5.23

U	0.67	1.17	0.74	2.38	0.40	0.39	0.73
V	331	304	313	284	328	318	313
Y	36	33	33	34	26	27	32
Zn	110	100	100	100	99	108	103
Zr	181	192	180	220	117	122	167
La	21.11	27.37	23.07	37.57	16.52	14.78	20.54
Ce	45.95	58.88	51.96	75.33	34.81	31.78	44.34
Pr	6.00	7.17	6.77	8.02	4.49	4.14	5.66
Nd	26.19	28.87	26.68	33.51	19.10	18.00	24.44
Sm	6.27	6.85	6.46	8.18	4.16	4.25	5.72
Eu	1.94	1.95	1.90	2.17	1.57	1.53	1.78
Gd	6.40	6.58	6.61	6.22	4.29	4.35	5.91
Tb	1.04	1.03	1.04	0.94	0.69	0.72	0.95
Dy	6.19	6.44	6.29	7.10	4.28	4.44	5.69
Ho	1.26	1.23	1.24	1.14	0.90	0.94	1.17
Er	3.35	3.51	3.45	3.76	2.57	2.62	3.09
Tm	0.45	0.43	0.43	–	–	0.29	0.42
Yb	2.87	3.02	2.96	3.28	2.34	2.34	2.72
Lu	0.43	0.44	0.43	0.49	0.35	0.36	0.42
				Ratios			
Mg#	39.64	41.42	42.34	39.24	47.14	47.50	39.95
FeO/MgO	2.9	2.6	2.5	2.9	2.1	2.0	2.7
Th/Nb	0.429	0.705	0.516	1.154	0.198	0.197	0.549
$(La)_{CN}$	89.1	115.5	97.3	158.5	69.7	62.4	86.7
$(La/Yb)_{CN}$	5.3	6.5	5.7	10.0	5.0	4.5	5.4
$(La/Sm)_{CN}$	2.2	2.5	2.3	3.3	2.5	2.3	2.3
$(Gd/Yb)_{CN}$	1.9	1.9	1.9	2.0	1.5	1.5	1.8
Eu/Eu*	0.94	0.89	0.90	0.84	1.15	1.09	0.94
Ti/Zr	68	61	63	56	82	83	63
Zr/Y	5.0	5.8	5.5	6.6	4.5	4.4	5.2

NOTES: For some sill groupings, not all samples have been analysed for all analytes (especially REE)
(a) excludes Empress 1A samples
(b) all Fe as Fe_2O_3

fluorescence (XRF) on a fused glass disc and a pressed powder pellet, following the methodology of Norrish and Hutton (1969) and Norrish and Chappell (1977). At GA's laboratory, the remaining trace elements, and the rare earth elements (La–Lu) were analysed by inductively coupled plasma mass spectrometry (ICP-MS) using a solution prepared by dissolving the XRF glass disc, as described by Eggins et al. (1997) and Pyke (2000). ICP-MS and XRF calibration is checked by the routine analysis of eight international reference materials: DNC-1, DTS-1, GSP-2, RGM-1, SCO-1, W-2, BHVO-1, and AGV-1. The GSWA reference material BB1 was analysed with batches of unknowns, along with duplicates of one of more samples. As BB1 is a new reference material, there are no consensus values, and the results presented in Appendix 2 can only be used to assess precision. Based on 21 analyses of the BB1 reference material, most major element oxides have a percent relative standard deviation (RSD%) of less than 4, whereas trace elements and REE with concentrations greater than ten times the detection level have RSD% less than 10 (most less than 5).

Major and trace element analysis at ANU also involved XRF analysis of fused glass discs and pressed powder pellets, as described by Morris (2000). Rare earth elements and some trace elements were analysed by ICP-MS using the method of Eggins et al. (1997), who noted that the RSD% is near 1 for elements with a mass greater than 80 atomic mass units (amu), and 1–4% for elements with mass less than 80 amu. These data, and the few standard analyses reported, show that analytical precision is of the same order as analysis at GA. ICP-MS analysis at the University of Queensland includes dissolution of the sample at elevated temperatures before analysis, as described in Morris (2000).

Analyte nomenclature

Saunders et al. (1980) divided elements with bulk distribution coefficients (D) less than 1 into two groups based on their radius/ionic charge. High field-strength elements (HFSE) have a radius/charge of less than 0.2, and include Zr, Hf, Ti, P, Nb, and Ta. Low field-strength elements (LFSE), also known as large-ion lithophile elements (LILE; Schilling, 1973) have a radius/charge greater than 0.2, and include Cs, Rb, K, Ba, Sr, Th, Pb, and U. In terms of charge/ionic radius, the rare earth elements and Y belong to the LFSE, as they have radius/charge values between 0.3 and 0.34 (Saunders et al., 1980). However, Y and the REE are often discussed with the HFSE as they show a similar behaviour to this group. Saunders et al. (1980) noted the relative immobility of the HFSE, Y, and REE compared to the LFSE. It should be noted that there is still some conflict in assignment of elements to the different groups. For example, Rollinson (1993; fig. 4.2) assigned Pb as both a HFSE and LFSE, and also assigned Th and U as HFSE.

Assessment of element mobility

Interpretation of major, trace, and rare-earth element variations relies on precise and accurate determination of analyte concentrations (Hall and Plant, 1992), and the determination of to what extent analyte concentrations have been affected by synmagmatic processes such as seafloor alteration or interaction with intruded sedimentary rocks, or by post-magmatic processes such as weathering and metamorphism. Petrographic examination of dolerites from the Bangemall Supergroup shows that some have undergone up to greenschist-facies metamorphism, with localized alteration of some clinopyroxene to chlorite and amphibole, variable sericitization of feldspar, and alteration of some opaque oxide grains to leucoxene and maghemite (Wingate, 2002, 2003, this Report). Some dolerites contain small amounts of epidote and calcite.

Most studies of element mobility in mafic igneous rocks (Winchester and Floyd, 1976; Pearce, 1976; Gélinas et al., 1982; Ludden et al., 1982) have examined volcanic successions, so direct comparison of these results with dolerites may not always be warranted. This is particularly the case when considering the influence of texture on alteration. Gélinas et al. (1982) have pointed out that although temperature, the presence and type of fluid, and the host rock mineralogy influenced the extent of alteration, rocks with metastable or immature textures (e.g. skeletal crystals and aphanitic texture) are more prone to alteration. For igneous rocks in general, published studies (Rollinson (1993) and references therein) suggest that alkaline earth and large-ion lithophile elements in particular (e.g. Rb, Na, K, Ba, and Sr) are more likely to be mobile than high field-strength and rare earth elements (e.g. Ti, Zr, Y, P, Nb, and La–Lu). However, conflicting results have been produced from studies of the same rock types under similar metamorphic conditions (Hynes, 1980), strengthening the argument for a case-by-case assessment.

Bearing in mind that direct comparisons between element behaviour in volcanic and plutonic rocks may not always be possible due to the influence of texture on mobility, it is useful to review some published work on major and trace element mobility. Gélinas et al. (1982) examined the major element variations in Archaean metavolcanic rocks that had undergone seafloor alteration. They found that secondary chlorite resulted from hydration and the substitution of MgO and FeO for CaO in ferromagnesian minerals. Alteration of feldspar resulted in the redistribution of Al_2O_3, CaO, Na_2O , and K_2O (often resulting in the generation of excess Al_2O_3), and albite and clinozoisite resulted from the breakdown of calcic plagioclase. Gélinas et al. (1982) argued that under greenschist-facies conditions MgO and FeO were mobile. In a study of the same rocks, Ludden et al. (1982) examined the behaviour of trace elements. They noted that the HFSE Zr and Ti, and Y and REE were immobile, and that even under extreme conditions when REE were remobilized during fluid-induced carbonation and K-metasomatism, Zr/Y and Ti/Zr ratios remained unchanged. They also found that at all levels of alteration, Rb and Ba, and to a lesser extent Sr, were mobile.

Wood et al. (1976) also noted that under zeolite-facies conditions, Si, Mg, K, Rb, Sr, and the LREE were mobilized in Tertiary basalts from Iceland, but Ti, P, Zr, Y, Nb, Ta, Hf, and some of the REE were well correlated, implying limited mobility.

These studies indicate the immobility of elements such as Ti, P, Zr, Y, and Nb relative to LILE elements. As a general statement, the HFSE (Zr, Hf, Ti, P, Nb, and Ta), Y, and REE can be considered to be less mobile than the LFSE (Cs, Rb, K, Ba, Sr, Th, U, and Pb).

Assessment of element mobility in the Bangemall Supergroup dolerites

The approach taken to determining the extent of element mobility in the Bangemall Supergroup dolerites is to examine the covariance of likely immobile elements, and then assess the relative mobility of other elements. In all cases, the major element values have been recalculated to 100% loss on ignition (LOI) free. The six-digit sample numbers shown in these element-variation diagrams are GSWA sample numbers. Both Ti and Zr (Fig. 28a) show a positive correlation for most samples, although the slope of the 1070 Ma western Bangemall Supergroup (WBSG) sill analyses (slope = 67; r = 0.80, where r is the correlation coefficient) is steeper than that of the sills intruding the Edmund Group (slope = 31; r = 0.73). However, the shallower slope of the sills intruding the Edmund Group may be influenced by samples such as GSWA 180709 that has scattered elongate grains of zircon, and less common baddeleyite, which accounts for its higher Zr concentration. Four samples lie off the main trend at lower Ti and higher Zr, including GSWA 180709, and one sample (GSWA 127286) plots at higher Ti. This sample has an unusually high proportion of titanomagnetite that is present as scattered anhedral grains up to 1 mm in diameter, which are enclosed by clinopyroxene.

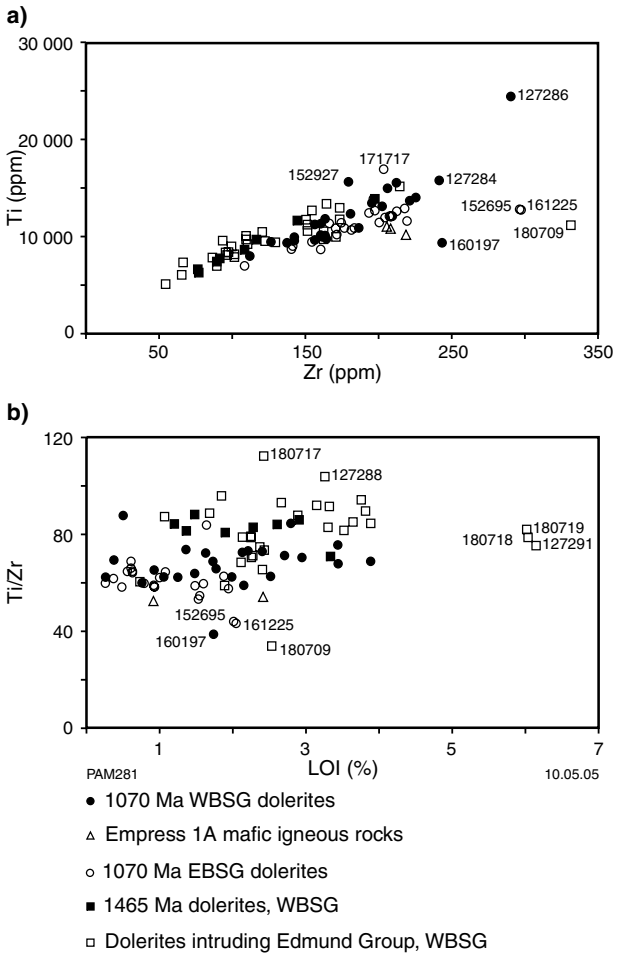

Figure 28. Bivariate plots showing: a) Ti (converted from TiO_2 %) versus Zr; b) Ti/Zr versus LOI

When Ti/Zr is plotted against volatile content (LOI as an indicator of alteration), the separation of 1070 Ma western Bangemall Supergroup and 1070 Ma eastern Bangemall Supergroup (EBSG) samples (lower Ti/Zr) from the 1465 Ma western Bangemall Supergroup and sills intruding the Edmund Group (higher Ti/Zr) is apparent, regardless of volatile content (Fig. 28b). The four samples with high Zr in Figure 28a (GSWA 152695, 161225, 160197, and 180709) have an expected low Ti/Zr compared with other samples, although in most cases Ti/Zr is constant within sill groupings regardless of volatile content.

If Zr and Y are relatively immobile even under fluid-present alteration conditions (as suggested by Ludden et al., 1982), then the ratios of these elements should be largely unaffected by post-magmatic alteration. This was found to be the case, as Zr/Y shows little variation regardless of volatile content (Fig. 29a), with values clustering around 5 for 1070 Ma western Bangemall Supergroup samples. The 1465 Ma western Bangemall Supergroup sill samples and samples from sills intruding the Edmund Group show a slightly wider range in Zr/Y, with most values less than 5. Three samples (GSWA 180718, 180719, and 127291) lie in the same Zr/Y range but have notably higher volatile contents. A group of eight 1070 Ma eastern Bangemall Supergroup sills, one Empress 1A sample (GSWA 155481), and an Edmund Group sill sample (GSWA 180709) plot at Zr/Y greater than 6 above the main group. As they have similar volatile contents to the other samples, the high Zr/Y is unlikely to be an alteration effect. This introduces another factor in determining the relative mobility of elements by graphical means and by analogy with published studies; elements usually considered to be mobile during metamorphism or alteration such as Rb, Sr, Cs, La, Ba, K, Na, and the LREE (La–Sm) are also found in relatively high concentrations in crustal rocks (Taylor and McLennan, 1985; Rudnick and Fountain, 1995; Rollinson, 1993; Peate, 1997). Thus, if dolerites have been crustally contaminated, or have been derived by melting of a mantle source into which a crustal component has been introduced prior to melting, they may have elevated concentrations of some or all of these elements. In a similar fashion to Zr/Y, there is a limited range in La/Sm versus volatile content (Fig. 29b), and samples with high Zr/Y (GSWA 152965 and 161225) also have high La/Sm. As elevated La/Sm can also reflect crustal input, there is some evidence that elevated concentrations of some LFSE and LREE could reflect input of a crustal component rather than alteration.

Low field-strength elements such as Rb and Sr show only a crude positive correlation (Fig. 29c), which suggests that they may have undergone some post-magmatic

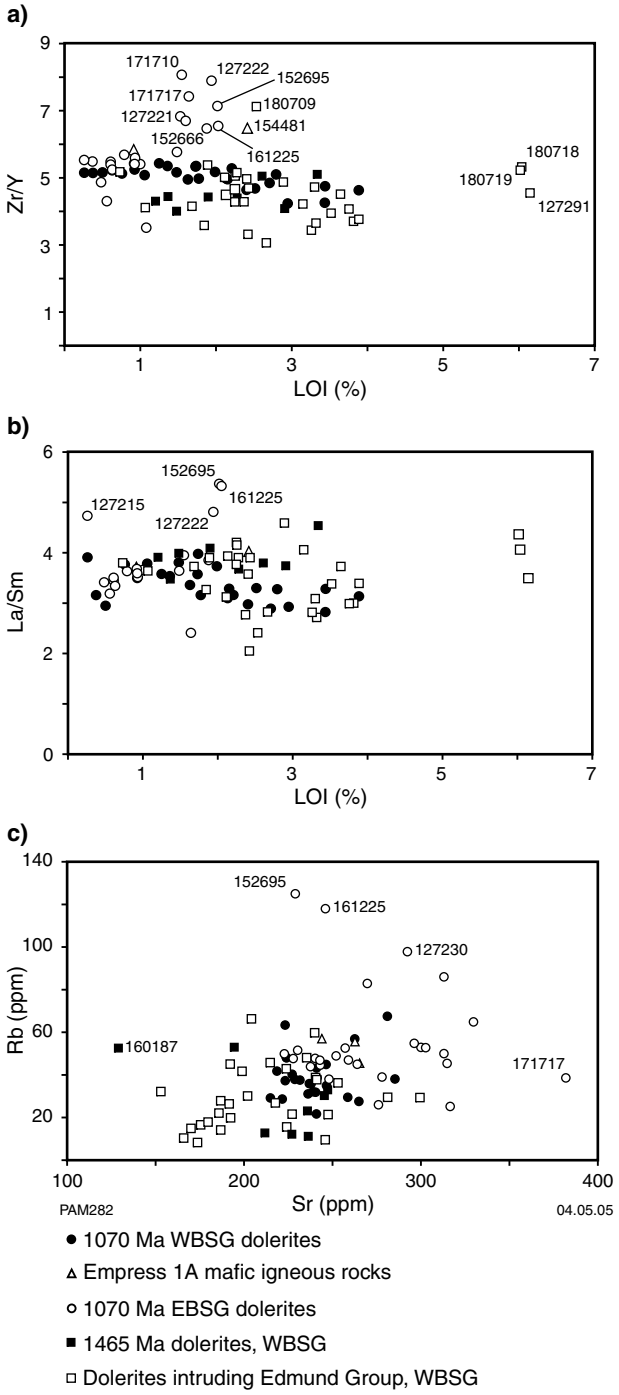

Figure 29. Bivariate plots showing: a) Zr/Y versus LOI; b) La/Sm versus LOI; c) Rb versus Sr

redistribution. However, the two samples with the highest Rb content (GSWA 152695 and 161225) also have high Zr/Y and La/Sm, so it is possible that the elevated Rb contents may not be entirely due to alteration. The majority of the 1465 Ma western Bangemall Supergroup sills and those intruding the Edmund Group sedimentary rocks have Rb contents less than the 1070 Ma western Bangemall Supergroup sills, which could reflect either different alteration regimes within the two sets of sills, or different magmatic concentrations.

The mobility of the LFSE elements Na and K is shown by the wide variation in the Na_2O/K_2O ratio independent of volatile content (Fig. 30a), especially in the 1465 Ma western Bangemall Supergroup and sills intruding the Edmund Group. This is consistent with Wingate's (2002) assertion, and petrographic examination carried out in this study, that the 1465 Ma sills appear to be more altered than the 1070 Ma sills. The Na_2O/K_2O ratio only shows a narrow range (near 2) for volatile contents less than 1%, suggesting that both oxides become more mobile with increasing amount of alteration. Samples from the 1070 Ma western Bangemall Supergroup and eastern Bangemall Supergroup sills also show some scatter regardless of volatile content, but generally cluster between a Na_2O/K_2O of 1 to 3. In this case, samples with high Zr/Y and La/Sm do not have anomalously high or low Na_2O/K_2O, so variable Na_2O/K_2O reflects alteration rather than precrystallization processes.

In thin section, most opaque oxide grains have undergone some alteration (Wingate, 2002, 2003), although this is not apparent in Fe_2O_3/FeO – volatile relations (Fig. 30b), where most 1070 Ma western Bangemall Supergroup sills, 1465 Ma western Bangemall Supergroup sills, and sills intruding the Edmund Group

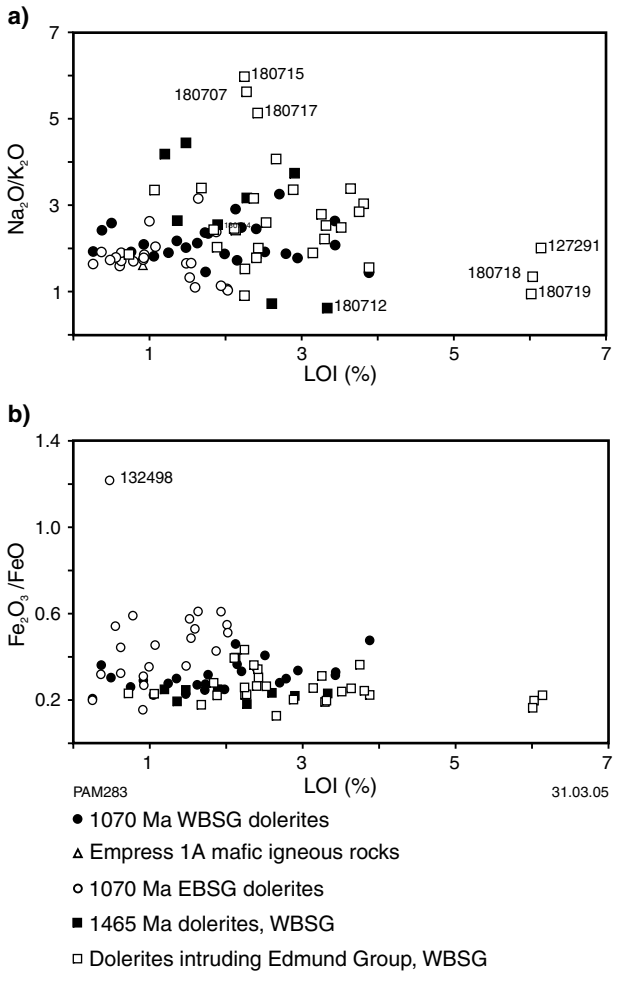

Figure 30. Bivariate plots showing: a) Na_2O/K_2O versus LOI; b) Fe_2O_3/FeO versus LOI

plot at about an Fe_2O_3/FeO of 0.2 – 0.4. The 1070 Ma eastern Bangemall Supergroup sills show a wide range, and have higher Fe_2O_3/FeO ratios, consistent with a more oxidized (altered) nature. GSWA 132498 has Fe_2O_3/FeO greater than or equal to 1; this sample is petrographically similar to other eastern Bangemall Supergroup dolerites in this area. Most samples have Fe_2O_3/FeO between 0.2 and 0.4, and although most mid-oceanic-ridge basalt (MORB) values are lower (0.15 – 0.24), continental flood-basalt values are highly variable (0.15 – 1.24) and bracket the Bangemall Supergroup dolerite range (Wilson, 1989). However, the range in Fe_2O_3/FeO values for some continental flood basalts (e.g. Columbia River Basalt) could, in part, reflect the influence of titanomagnetite crystallization.

From this assessments of element behaviour, HFSE such as Zr, Hf, Ti, P, Nb, and Ta are likely to have remained immobile during greenschist-facies metamorphism. In contrast, LFSE such as Rb, Sr, Na, and K, and ratios of these elements, show some scatter, part of which may be due to post-magmatic alteration. The development of secondary chlorite and amphibole could affect FeO and MgO contents, although the localization of this alteration style to the margins of clinopyroxene probably means that, overall, MgO and FeO (and hence Mg#) have not been significantly modified from igneous values. This is further supported by expected oxide and trace element versus Mg# relations discussed below. The covariance of immobile element pairs (e.g. Zr and Y) with other elements (e.g. LREE, and some LFSE such as Rb) suggests that some element variations may be due to crustal input. However, this cannot account for variations in elements such as Na and K. Alteration, shown by the aberrant behaviour of LFSE such as Rb, K, and Na, is more apparent in the 1465 Ma western Bangemall Supergroup sills and the majority of the sills that intrude the Edmund Group sedimentary rocks. Elevated contents of LFSE and LREE in some Glenayle Dolerite samples most probably reflect some degree of crustal contamination rather than post-magmatic alteration.

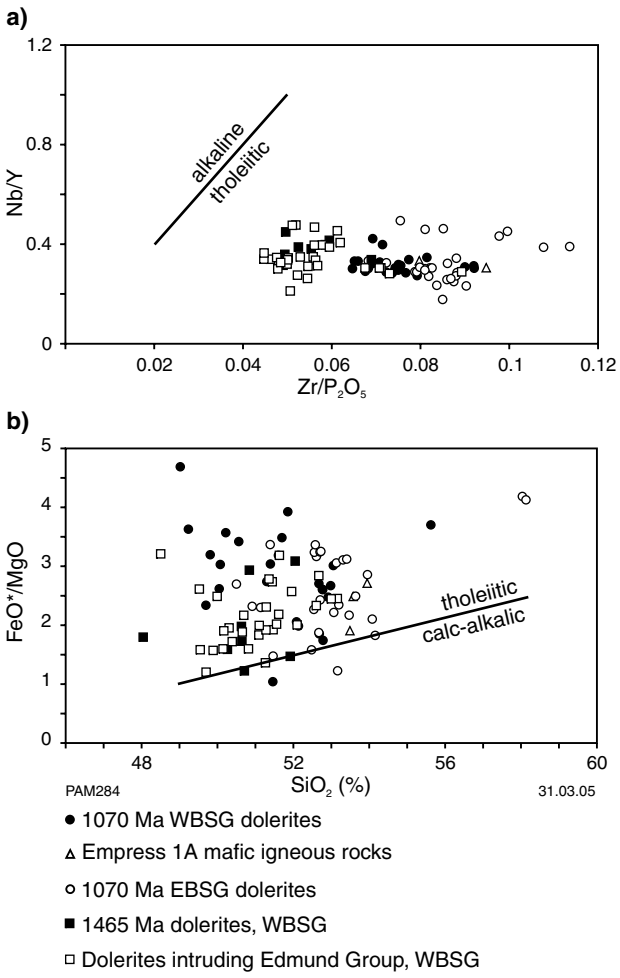

Figure 31. a) Nb/Y versus Zr/P_2O_5 discriminant diagram (Winchester and Floyd, 1976) showing that the Bangemall Supergroup dolerite sills are all tholeiitic. Note the separation of most 1465 Ma western Bangemall Supergroup sills and sills intruding the Edmund Group from the 1070 Ma sills; b) FeO^*/MgO (all Fe as FeO) versus SiO_2. Tholeiitic–calc-alkalic discriminant line has the equation $FeO^*/MgO = 0.1562 \times SiO_2 - 6.685$ (Gill, 1981)

Classification

Due to the likely mobility of alkaline earth elements such as Na and K, classification schemes such as alkalies–iron–magnesium (AFM; Irvine and Baragar, 1971) and total alkalies–silica (TAS; Le Maitre, 2002) have been avoided in preference to schemes that employ relatively immobile elements. Winchester and Floyd (1976), amongst others, have shown that immobile trace elements and some major element oxides can be used in the classification of mafic volcanic rocks that have been metamorphosed up to amphibolite facies. In terms of Nb/Y versus Zr/P_2O_5 (Winchester and Floyd, 1976), the sill samples plot as tholeiites, subparallel to the Zr/P_2O_5 axis (Fig. 31a). It is worth noting on this figure that all but one analysis from the 1465 Ma western Bangemall Supergroup sills and all but five sills intruding the Edmund Group plot at Zr/P_2O_5 less than 0.06, whereas the remaining analyses plot at higher Zr/P_2O_5 values, and seven 1070 Ma eastern Bangemall Supergroup sills plot at slightly higher Nb/Y. This suggests that there may be some fundamental separation of the sills in terms of which parts of the stratigraphy they intrude. This is further evaluated below. Almost all the samples are tholeiitic in terms of FeO^*/MgO versus SiO_2 (Fig. 31b); where FeO^* is all Fe calculated as FeO, following Miyashiro (1974) and Gill (1981).

Division of continental flood basalts into high-Ti and low-Ti suites has been reported for several provinces, although the chemical criteria for separating such groups varies between studies. The significance of high- and low-Ti basalts is that the former are probably derived from melting at higher pressure, whereas the latter reflect derivation from the shallower continental lithospheric mantle. Peate (1997) identified high- and low-Ti groups in the Paraná–Etendeka province based on a Ti/Y value of 310, whereas Xiao et al. (in press) have separated high- and low-Ti mafic rocks of China's Emeishan LIP at Ti/Y equal to 500. In both cases, there are natural breaks

at these Ti/Y levels that facilitate subdivision; however, this is not the case for the dolerites from the Bangemall Supergroup (Fig. 32), which show no natural break. These dolerites are low-Ti in terms of Xiao et al.'s (in press) division, but high-Ti in terms of the criteria used by Peate (1997), and the value of such subdivision is questionable. The geographic separation of magma types with different Ti contents led Peate (1997) to suggest that spatially separate mantle sources were being tapped. Xiao et al. (in press) explained the difference in Ti contents in terms of lithospheric versus asthenospheric mantle contributions.

Major and trace element variations

As SiO_2 shows a limited range of about 10%, major and trace element variations are shown in relation to magnesium number (Mg#), which ranges from 27 to 63. Magnesium number is an indicator of fractional crystallization since Mg# decreases when ferromagnesian minerals are removed from the magma. Most samples from sills dated at 1465 Ma in the western Bangemall Supergroup and those intruding the Edmund Group sedimentary rocks have higher Mg# than both the 1070 Ma western Bangemall Supergroup and Glenayle sills. However, the 1070 Ma western Bangemall Supergroup and eastern Bangemall Supergroup sills overlap in terms of Mg# with the 1465 Ma sills and sills intruding the Edmund Group, and span the complete Mg# interval of all samples analysed. All sill samples are fractionated relative to primary mantle-derived liquids, which have Mg# between 68 and 72 (Frey et al., 1978). Some trace elements are at uniformly low levels in all samples analysed, others show little variation with Mg#, and in some cases there are insufficient data to draw conclusions (F, SO_3, As, Bi, Cd, Ge, Mo, and S). Although all data are given in Appendix 1, not all element variations are discussed below.

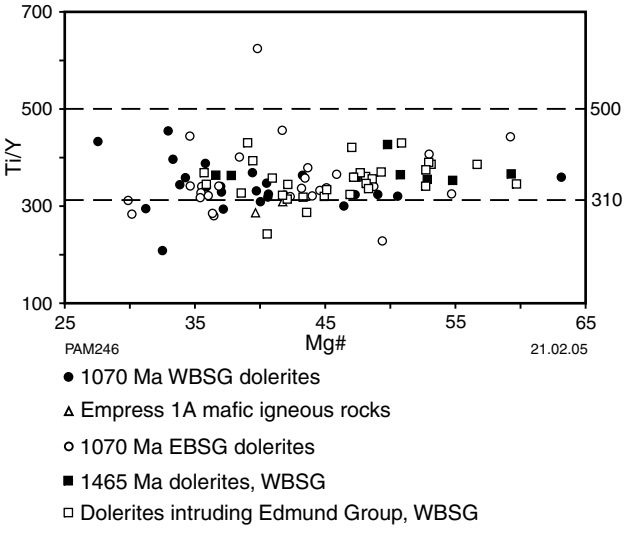

Figure 32. Bivariate plot showing Ti/Y versus Mg#. Lines at Ti/Y equal to 500 and 310 separate low- and high-Ti basaltic rocks from the Emeishan (Xiao et al., in press) and Paraná–Etendeka (Peate, 1997) provinces respectively

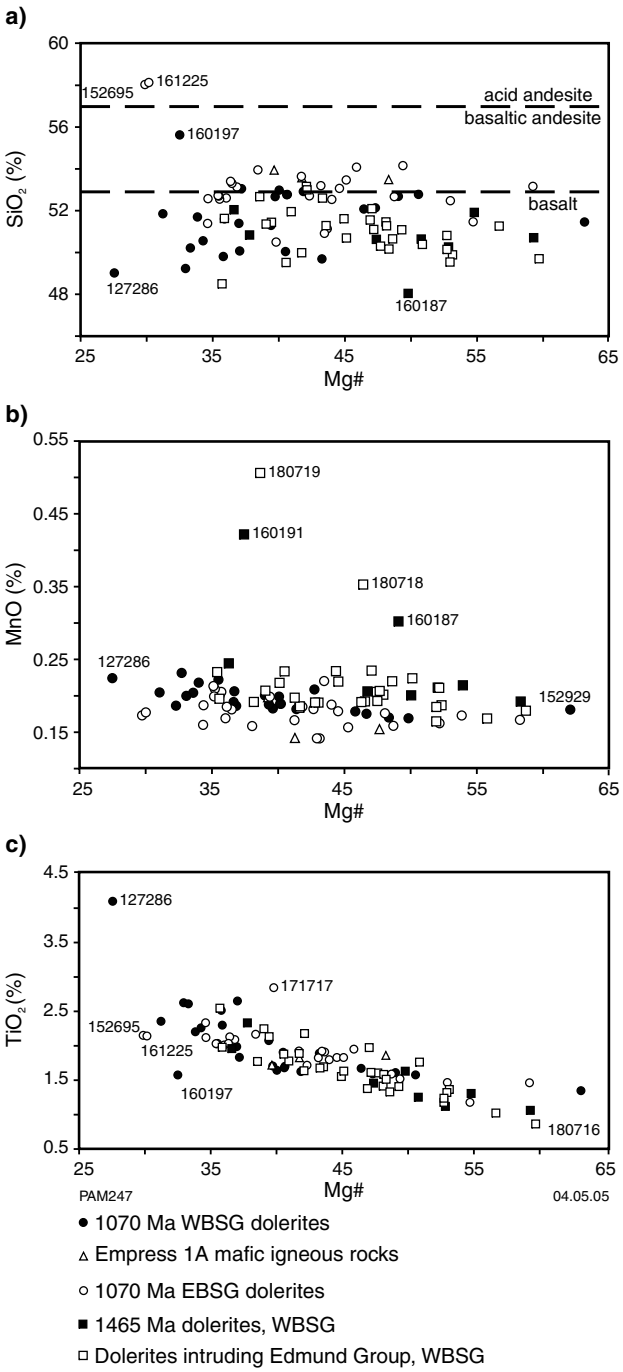

Figure 33. Bivariate plots showing: a) SiO_2 versus Mg#. Dotted lines separate basalt, basaltic andesite, and acid andesite in terms of SiO_2 content (Gill, 1981); b) MnO versus Mg#; c) TiO_2 versus Mg#

Both SiO_2 and MnO show little correlation with Mg# (Fig. 33a,b). The SiO_2 values range from about 48 to 58%, and in terms of SiO_2 divisions used for volcanic rocks (Gill, 1981) most samples plot as basalts (less than 53% SiO_2), a few plot as basaltic andesites (53–57% SiO_2), and two Glenayle sill samples (GSWA 152695 and 161225) plot as acid andesites. The 1465 Ma western Bangemall Supergroup sills, sills intruding the Edmund Group, and the 1070 Ma western Bangemall Supergroup samples all

have similar SiO_2 contents, but most 1070 Ma eastern Bangemall Supergroup sills have higher SiO_2 contents at a given Mg#. As with most element variation diagrams, the three Empress 1A samples plot with the 1070 Ma eastern Bangemall Supergroup samples.

MnO contents are usually less than 0.25% (Fig. 33b), and show little variation with Mg#, although four samples from sills intruding the Edmund Group sedimentary rocks have higher MnO contents, and the 1465 Ma western Bangemall Supergroup sills and most sills intruding the Edmund Group have higher MnO contents than other samples.

Four oxides (TiO_2, Na_2O, K_2O, and P_2O_5) are negatively correlated with Mg#. The TiO_2 values (Fig. 33c) vary between about 0.9 and 3%, and three samples with a low Mg# lie off the main trend (GSWA 161225, 152695, and 160197). For all data, TiO_2 shows a strong negative correlation with Mg# (r = -0.79), which means that the different sill groupings cannot be separated based on TiO_2 content at a given Mg#. Compared to TiO_2, Na_2O (Fig. 34a) shows a weaker negative correlation with Mg# (r = -0.34), and K_2O (Fig. 34b) shows a similar degree of correlation with Mg# as Na_2O, with two samples with high K_2O (GSWA 152695, 2.97%; GSWA 161225, 2.96%) also having high Na_2O and SiO_2. As discussed previously, some of the scatter in Na_2O and K_2O can be attributed to post-magmatic alteration, but the crude negative correlation of both Na_2O and K_2O with Mg# implies some magmatic control. There is a well-developed negative correlation between P_2O_5 and Mg# (r = -0.60), and the different dolerite groups cannot be separated in terms of P_2O_5 content (Fig. 34c).

Both Al_2O_3 (r = 0.57) and CaO (r = 0.67) are positively correlated with Mg# (Fig. 35). GSWA 152929 has unusually low Al_2O_3, which could reflect the high clinopyroxene to plagioclase ratio seen in thin section. Five samples, including one from Empress 1A, have lower CaO contents than other samples, and form a loose array subparallel to other samples. Most 1465 Ma western Bangemall Supergroup sill analyses have higher CaO for a given Mg#, but there is no clear separation of dolerite groups in terms of Al_2O_3.

Of the trace elements, only two show little correlation with Mg#; both Ba and Sc show a wide scatter (Fig. 36a,b), with Sc contents appearing to be higher in the Edmund Group sills, and Sr contents generally lower.

Only Cr (Fig. 36c, r = 0.73) and Ni (Fig. 37a, r = 0.61) are positively correlated with Mg#. Chromium concentrations decrease rapidly over a small Mg# interval, from about 760 to 300 ppm. Nickel concentrations show a similar rapid decrease over a short Mg# interval. Most sills intruding the Edmund Group have higher Cr and lower Ni contents than other sills for a given Mg#, although the two samples with the highest Ni and Cr contents (GSWA 171710 and 152929) are 1070 Ma sills.

Fourteen trace elements (Be, Cu, Ga, Hf, Nb, Rb, Sn, Ta, Th, U, V, Y, Zn, and Zr) and the REE La and Yb are negatively correlated with Mg# (Figs 37–42). Although there is some scatter on most element versus

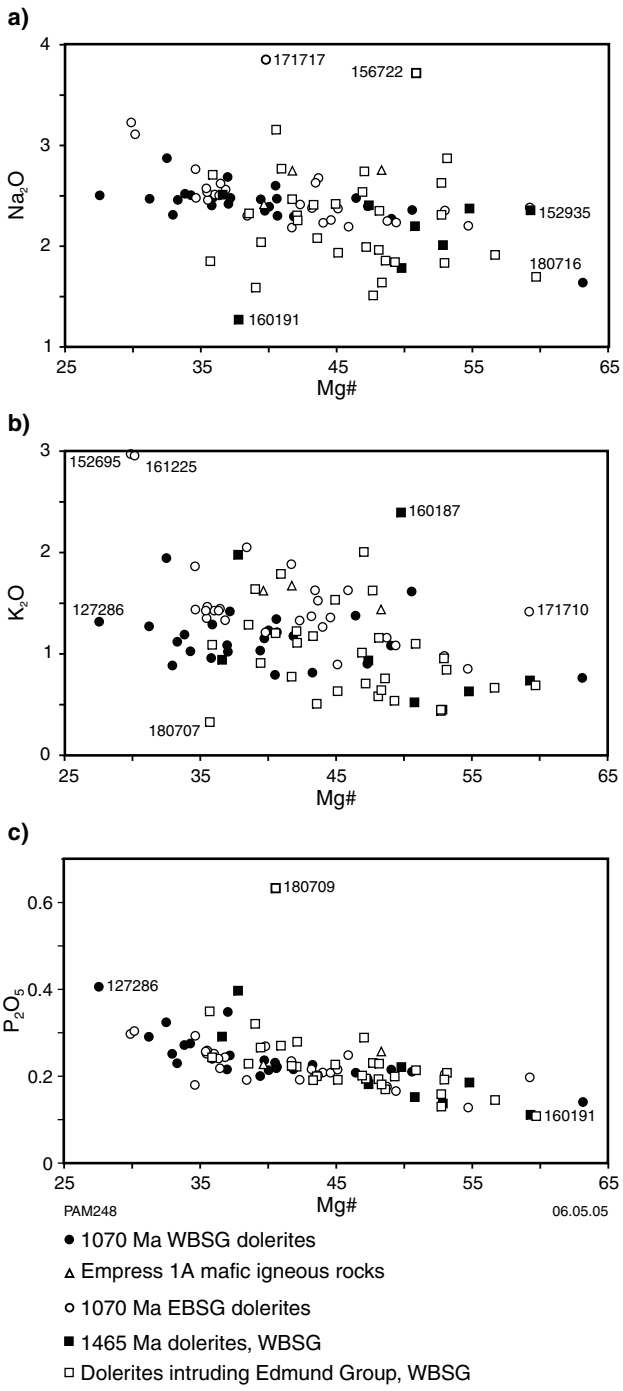

Figure 34. Bivariate plots showing: a) Na_2O versus Mg#; b) K_2O versus Mg#; c) P_2O_5 versus Mg#

Mg# plots, some samples have anomalously high or low concentrations of certain trace elements. The concentrations of Th, U, and Zr are generally lower for a given Mg# in the 1465 Ma western Bangemall Supergroup sills and in sills intruding the Edmund Group. Several 1070 Ma eastern Bangemall Supergroup sill samples have higher Rb, Sr, Th, U, and La contents than other samples at a given Mg#, and some of these samples form separate subparallel arrays to the main trends (e.g. La versus Mg#; Fig. 42a). Although some of these are LFSE, their

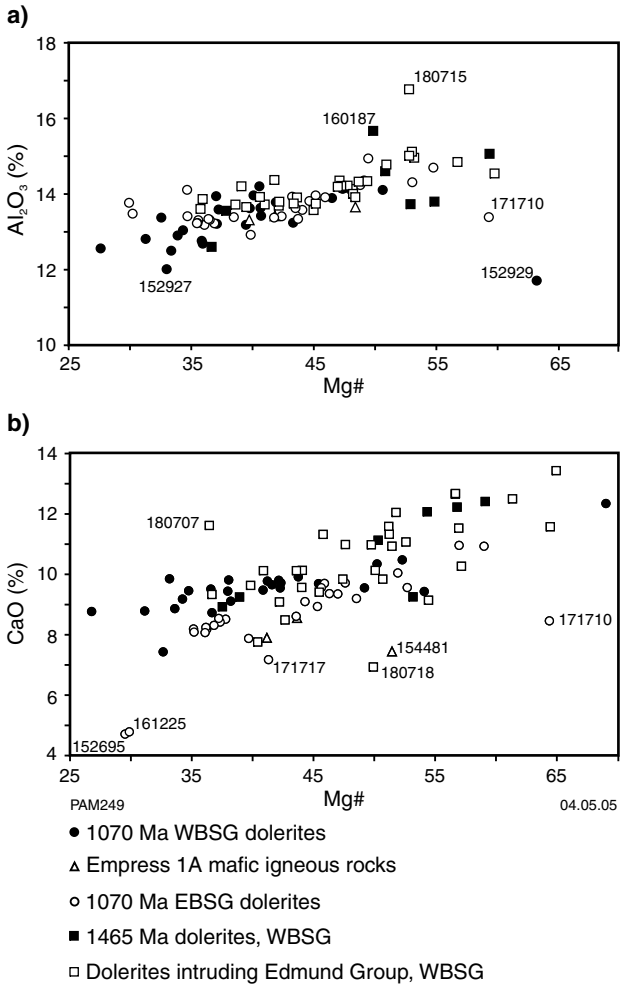

Figure 35. Bivariate plots showing: a) Al_2O_3 versus Mg#; b) CaO versus Mg#

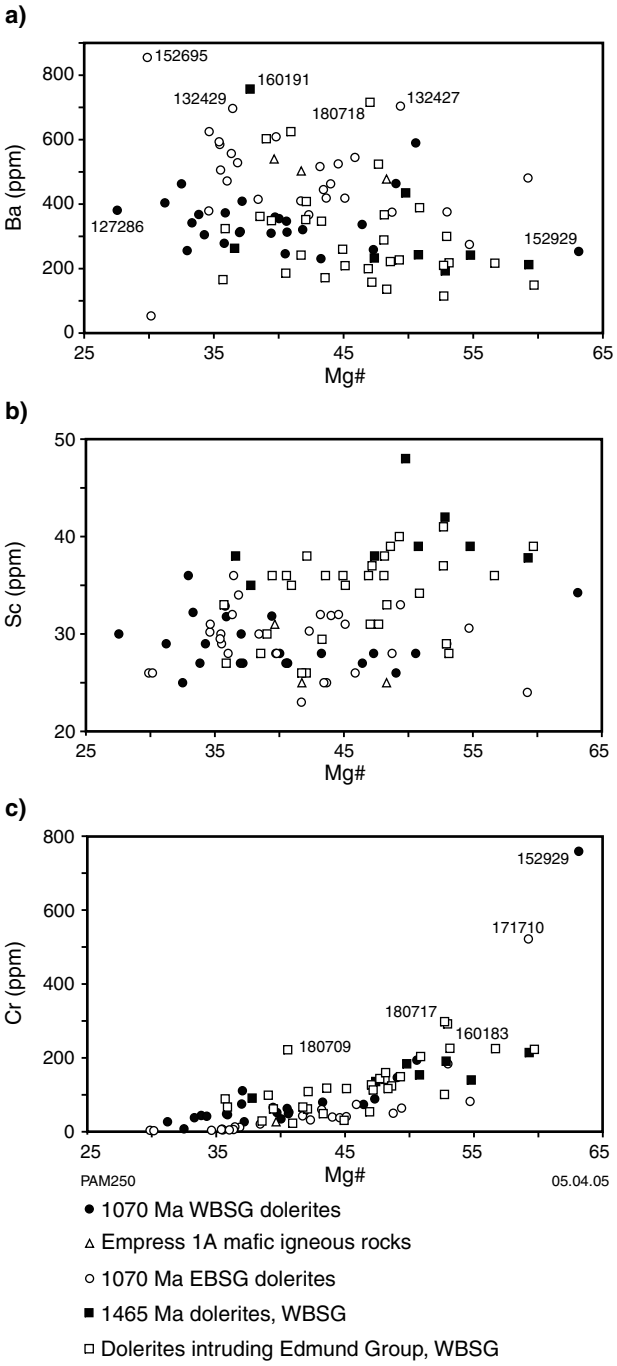

Figure 36. Bivariate plots showing: a) Ba versus Mg#; b) Sc versus Mg#; c) Cr versus Mg#

behaviour in relation to other less labile elements such as La and Th means that all of this variation cannot be attributed to alteration.

For a given Mg#, the 1465 Ma sills and most sills intruding the Edmund Group have lower contents of Cu, Ga, Sn, Th, and probably Rb, and higher contents of V. Gallium and Mg# show a stronger negative correlation for sills intruding the Edmund Group, and Th and U form steeper negative trends with Mg# for several 1070 Ma eastern Bangemall Supergroup samples (Figs 38a and 40a,b).

Discussion

Cursory examination of the dolerites in terms of their classification (Fig. 31a), and major and trace element variations, shows consistent differences in the composition of the different sill groupings. The 1465 Ma western Bangemall Supergroup sills and most of the sills intruding the Edmund Group sedimentary rocks are compositionally different to the 1070 Ma western Bangemall Supergroup sills and 1070 Ma eastern Bangemall Supergroup sills in that, in most cases, they have different absolute concentrations of Zr, Th, U, Cr, Ni, Mn, Cu, Ga, Sn, and Rb at a given Mg#. This separation is even more apparent if the five sill samples intruding the Edmund Group that plot with the 1070 Ma samples (Fig. 31a) are separated from the remaining sill samples that intrude the Edmund Group, as shown on Figure 38a. As many of these are non-labile elements, these differences cannot be explained by different degrees of post-magmatic alteration. Furthermore, as both groups have different concentrations of some elements at the same Mg#, the two groups cannot be linked by fractional crystallization of similar magma types, and were probably derived from fundamentally

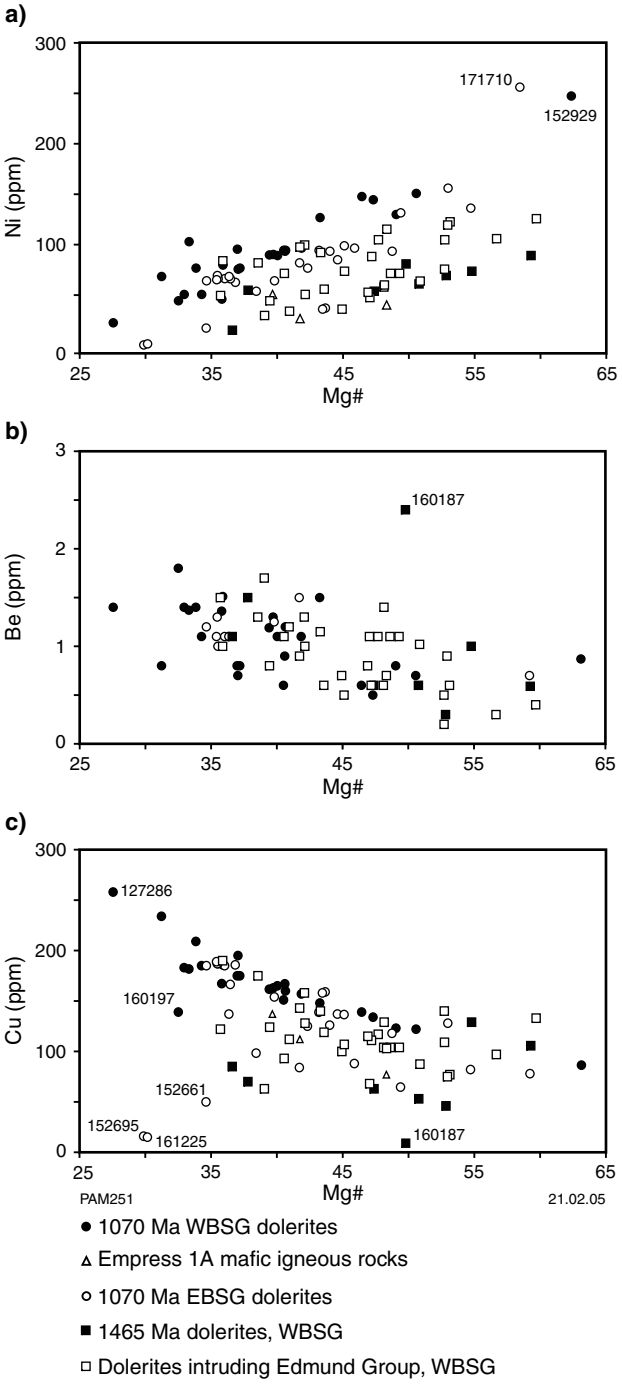

Figure 37. Bivariate plots showing: a) Ni versus Mg#; b) Be versus Mg#; c) Cu versus Mg#

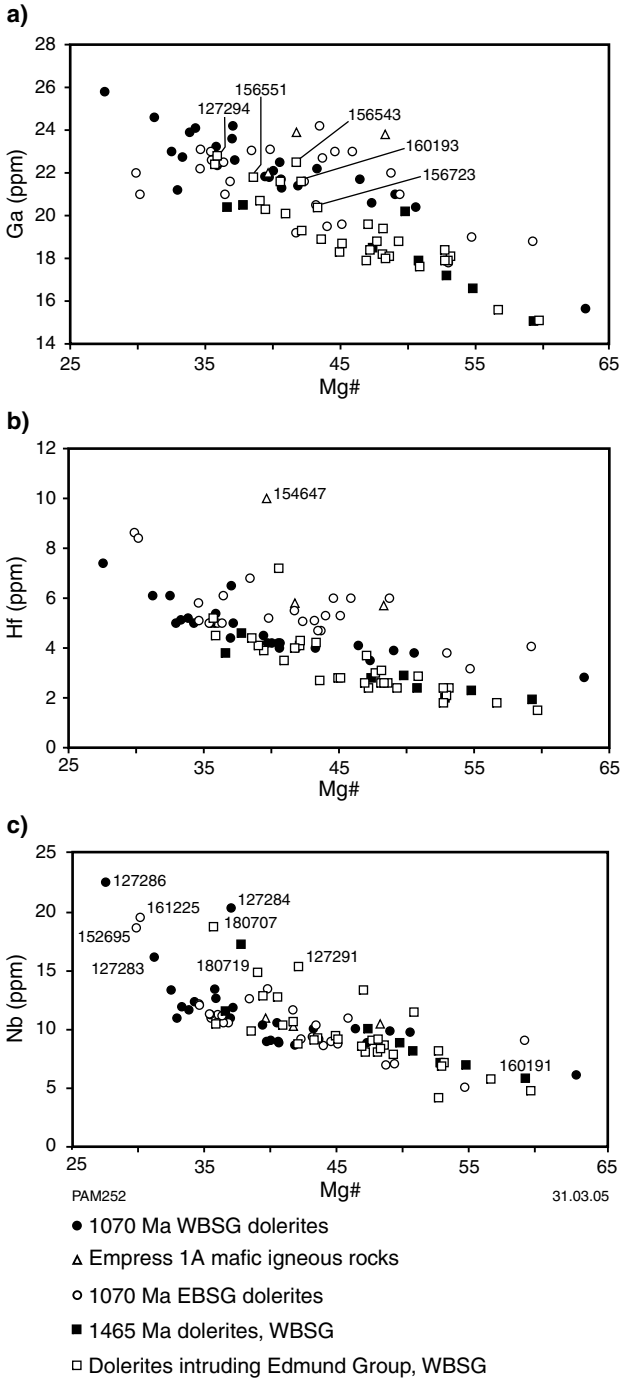

Figure 38. Bivariate plots showing: a) Ga versus Mg#. Numbered samples are sills intruding the Edmund Group that show 1070 Ma chemistry; b) Hf versus Mg#; c) Nb versus Mg#

different mantle sources. These differences in chemistry show firstly that the majority of sills intruding the Edmund Group sedimentary rocks belong to the 1465 Ma sill intrusion event, and secondly, it is possible to chemically separate sills from the older (1465 Ma) and younger (1070 Ma) intrusion events.

Some 1070 Ma eastern Bangemall Supergroup sills have higher SiO_2, LREE, and LFSE contents than other sills. Although some of the LFSE elements such as Rb are labile, and their concentrations could therefore be affected by post-magmatic alteration, the higher concentrations of other less labile LFSE such as La and Th at the same Mg# suggests that high LFSE in these sills is a magmatic feature. As sills with similar Mg# have different LFSE contents, relating sills by closed-system processes such as fractional crystallization is untenable. Despite these characteristics of the different sill groups, the general increase in most LFSE and LREE elements, and the decrease in compatible elements such as Cr and Ni with

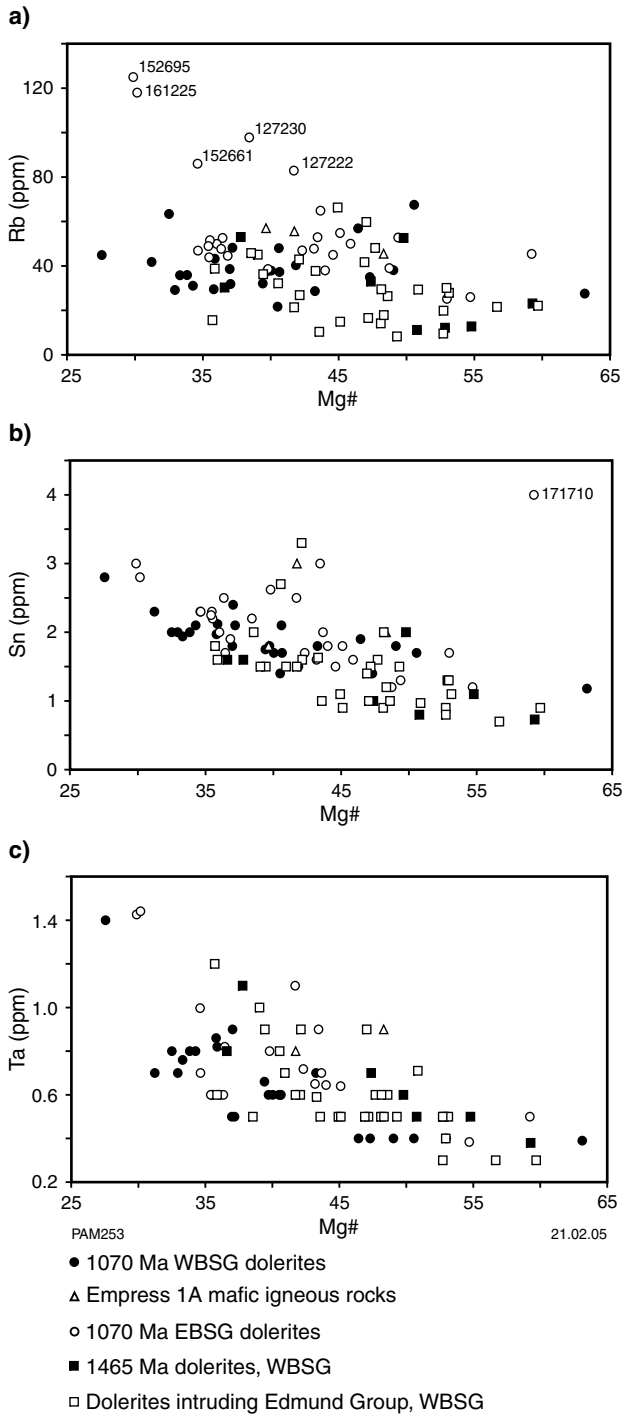

Figure 39. Bivariate plots showing: a) Rb versus Mg#; b) Sn versus Mg#; c) Ta versus Mg#

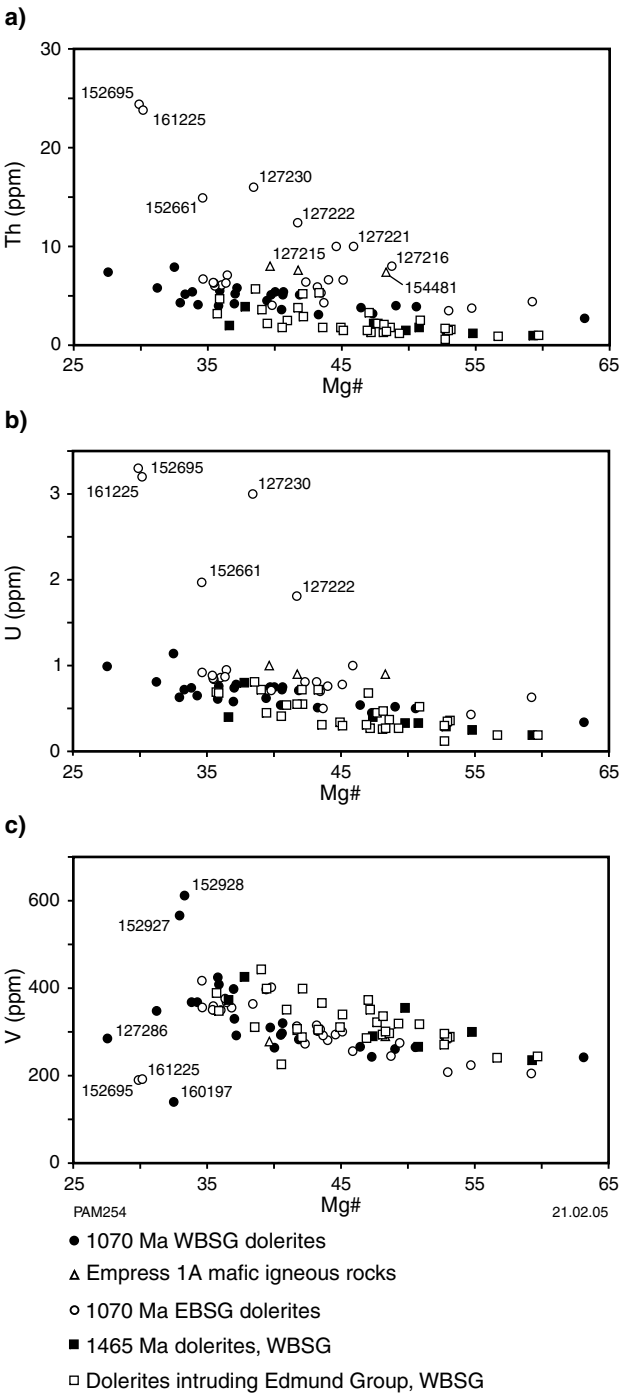

Figure 40. Bivariate plots showing: a) Th versus Mg#; b) U versus Mg#; c) V versus Mg#

decreasing Mg#, is consistent with some control by low-pressure fractional crystallization.

The ratio of trace elements that have bulk distribution coefficients (D) much less than 1 (such as Th, Nb, La, and Zr) shows little variation when the extent of either partial melting or fractional crystallization is changed (Rollinson, 1993). Careful selection of such incompatible elements means that any influence on element concentrations of post-magmatic alteration can be minimized, although some element ratios can be affected by crustal input to either the mantle source or the derived magma. To illustrate the use of such ratios, data have been plotted in terms of Th/Nb versus Mg# (Fig. 43), where Mg# monitors fractional crystallization, and D is much less than 1 for both Th and Nb. The 1465 Ma western Bangemall Supergroup sills and all but five analyses of sills intruding the Edmund Group show little variation in Th/Nb over the interval of 0.1 – 0.25 for a wide range in Mg#, although there is a weak overlap in Th/Nb with the 1070 Ma western

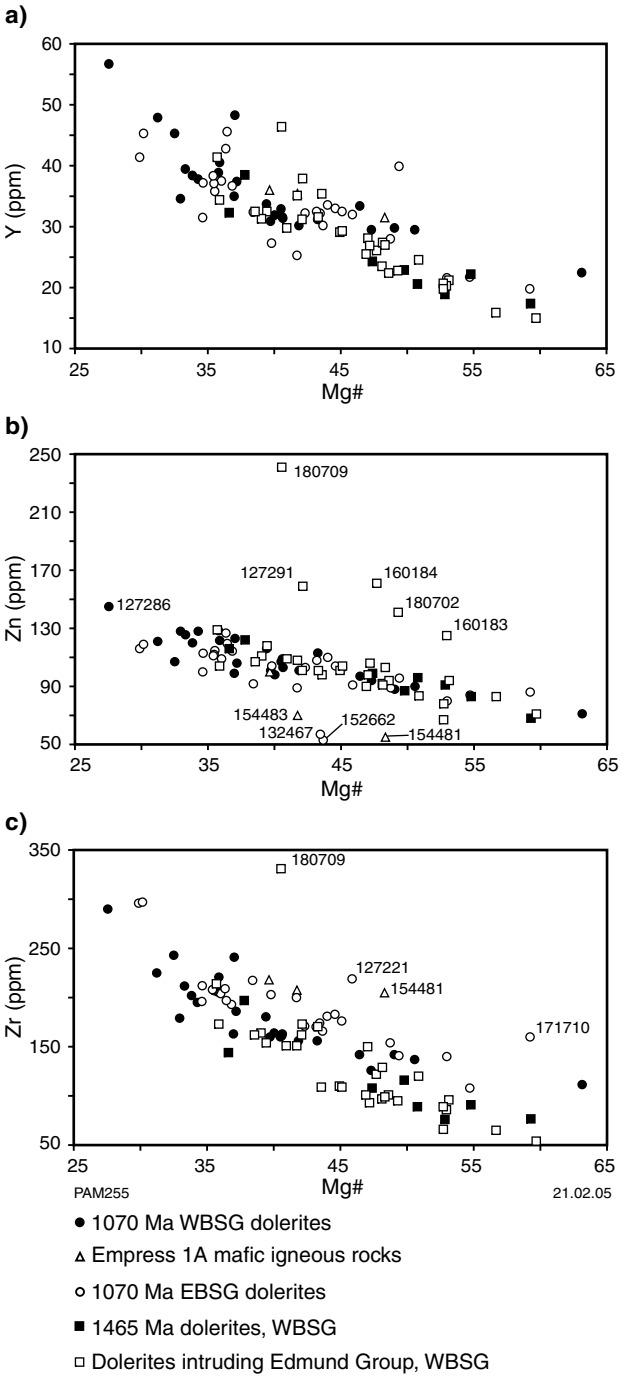

Figure 41. Bivariate plots showing: a) Y versus Mg#; b) Zn versus Mg#; c) Zr versus Mg#

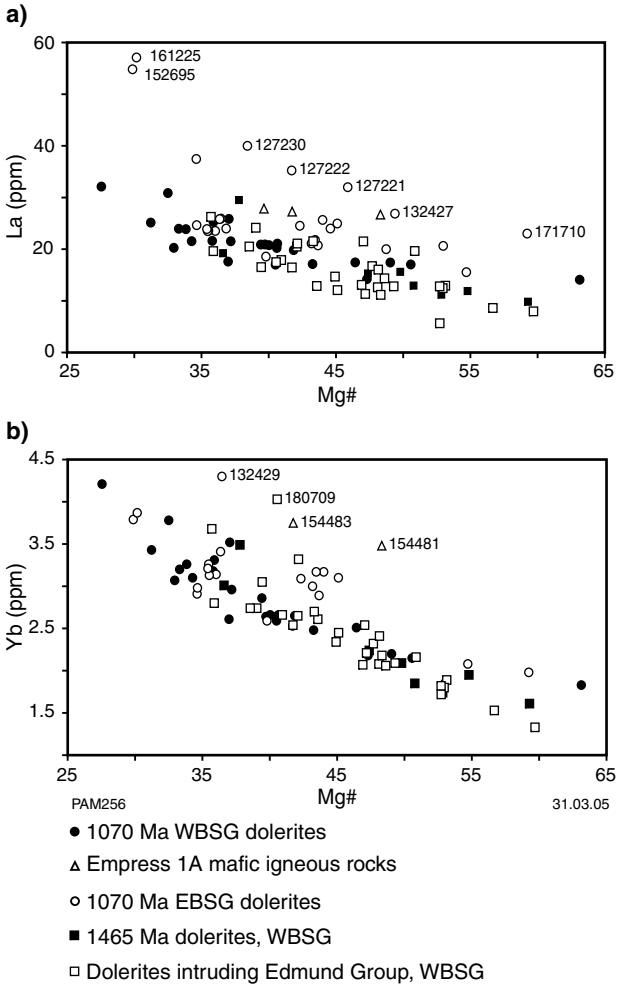

Figure 42. Bivariate plots showing: a) La versus Mg#; b) Yb versus Mg#

Bangemall Supergroup sills at about a Mg# of 35–40. Five samples from sills intruding the Edmund Group sedimentary rocks (GSWA 156551, 160193, 156723, 156543, and 127294) plot at higher Th/Nb with the 1070 Ma western Bangemall Supergroup sills. These are the same five samples that plot at higher Zr/P_2O_5 on Figure 31a and at higher Ga for a given Mg# on Figure 38a. This is consistent with major and trace element variations discussed above that indicate that most sills intruding the Edmund Group have similar chemistry to the 1465 Ma western Bangemall Supergroup sills.

The 1070 Ma western Bangemall Supergroup sills, five analyses of sills intruding the Edmund Group, most 1070 Ma eastern Bangemall Supergroup analyses, and the three analyses from the Empress 1A drillhole plot at higher Th/Nb levels (0.25 – 0.8) than the 1465 Ma dolerites and also show a spread in Mg#. A smaller group of eight 1070 Ma eastern Bangemall Supergroup samples (GSWA 152695, 161225, 152661, 127230, 127222, 127215, 127216, and 127221) plot at even higher Th/Nb levels (0.9 – 1.3); most of these samples also have higher concentrations of SiO_2 (Fig. 33a), and LFSE and LREE elements such as Rb, Th, U, and La (Figs 39a, 40a,c, and 42a). For ease of reference, these samples are informally termed the high-Th/Nb 1070 Ma eastern Bangemall Supergroup samples in the following discussion.

Although most sills are fractionated relative to primary mantle-derived liquid compositions (Frey et al., 1978), a few samples have high Mg#, and Ni and Cr contents approaching those of primary liquids. For example, 1070 Ma western Bangemall Supergroup sill sample GSWA 152929 has a Mg# of 63 (MgO = 9.74 %), 759 ppm Cr, and 245 ppm Ni. It is worth noting that this sample has a similar Th/Nb to more fractionated rocks (Fig. 43), which indicates that the Th/Nb ratio of the

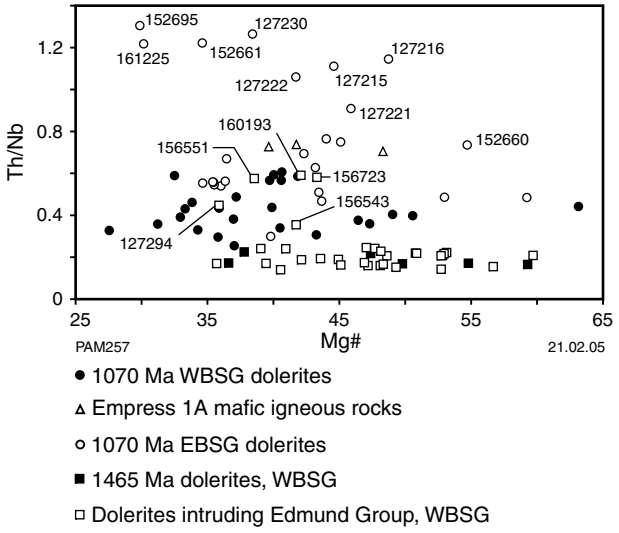

Figure 43. Bivariate plot showing Th/Nb versus Mg#. Note the separation, in terms of Th/Nb, of the 1465 Ma western Bangemall Supergroup sills, and most sills intruding the Edmund Group, from the 1070 Ma western Bangemall Supergroup and most eastern Bangemall Supergroup sills. Eight 1070 Ma eastern Bangemall Supergroup samples plot at higher Th/Nb than the other sills

1070 Ma western Bangemall Supergroup sills is inherited from the source. As is demonstrated below, the separate sill groupings also have distinctive REE characteristics indicative of their source.

Rare-earth element chemistry

Eight analyses from the 1465 Ma western Bangemall Supergroup sills (five samples from site 11 and three samples from site 21 of Wingate, 2002) form a tight REE grouping (Fig. 44a), although most analyses from site 11 have higher total REE contents than samples from site 21 (Table 3). The patterns are smooth, with a gradual decrease from LREE to HREE shown by an average $(La/Yb)_{CN}$ of 5 (range 4–6; where CN is chondrite normalized, using C1 chondrite values of Sun and McDonough, 1989) and a $(La)_{CN}$ of 70 (range 47–125). The LREE show more variation, with $(La/Sm)_{CN}$ ranging from 2.3 to 2.9 (average 2.5), compared to the HREE $(Gd/Yb)_{CN}$ range of 1.5 – 1.6. The samples have weakly developed positive Eu anomalies ($Eu/Eu^* = Eu_N/(Sm_N \times Gd_N)^{0.5}$; Taylor and McLennan, 1985) averaging 1.1 (range 1 – 1.4). The average composition of these 1465 Ma western Bangemall Supergroup sills (Fig. 44b) shows strong similarities to the average of the 26 sill samples intruding the Edmund Group that plot with the 1465 Ma sills in terms of Th/Nb versus Mg#, the values of which are given in Table 3, with similar values for $(Sm/Yb)_{CN}$, $(Gd/Yb)_{CN}$, $(La)_{CN}$, and Eu/Eu^*.

The average REE patterns for twenty-five 1070 Ma western Bangemall Supergroup sill analyses are shown in relation to the range of these samples (Fig. 45a), in addition to the average and range for eight 1465 Ma western Bangemall Supergroup sill samples. The range in $(La)_{CN}$ for the 1070 Ma western Bangemall Supergroup sills (59–136) is similar to that of the 1465 Ma sills and sills intruding the Edmund Group, as is the average $(La/Sm)_{CN}$ (2.5 compared with 2.2) and the range in $(La/Yb)_{CN}$ (4.5 – 5.3). However, the 1465 Ma sills have, on average, lower total REE, flatter HREE patterns ($(Gd/Yb)_{CN}$ of 1.52 compared with 1.85 for the 1070 Ma western Bangemall Supergroup sills), and a greater degree of LREE depletion ($(La)_{CN}$ of 62–66 compared to 89), with small positive Eu anomalies (Eu/Eu^* of 1.09 – 1.13) compared with a weak negative Eu/Eu^* (0.94) for the 1070 Ma western Bangemall Supergroup sills (Table 3). The five analyses from sills intruding the Edmund Group

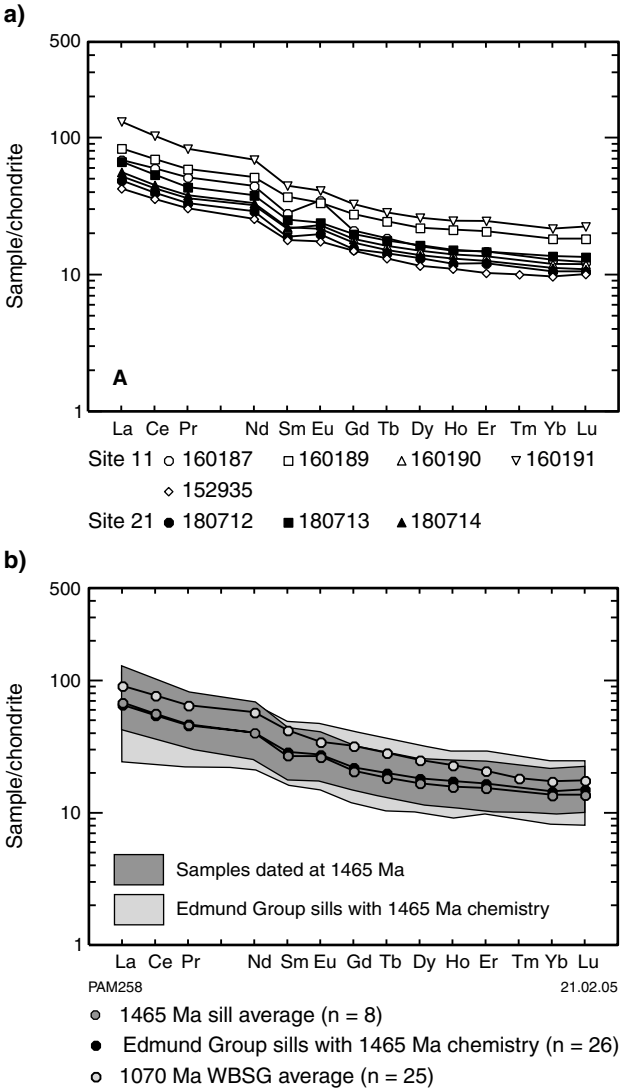

Figure 44. a) Chondrite-normalized REE for samples from sills 11 and 21 dated at 1465 Ma by Wingate (2002). Chondrite normalization factors are C1 chondrite values from Sun and McDonough (1989; table 1); b) chondrite-normalized REE patterns showing the average and range for sills dated at 1465 Ma from the western Bangemall Supergroup and sills intruding the Edmund Group that show 1465 Ma chemistry. Also shown is the 1070 Ma western Bangemall Supergroup sill average

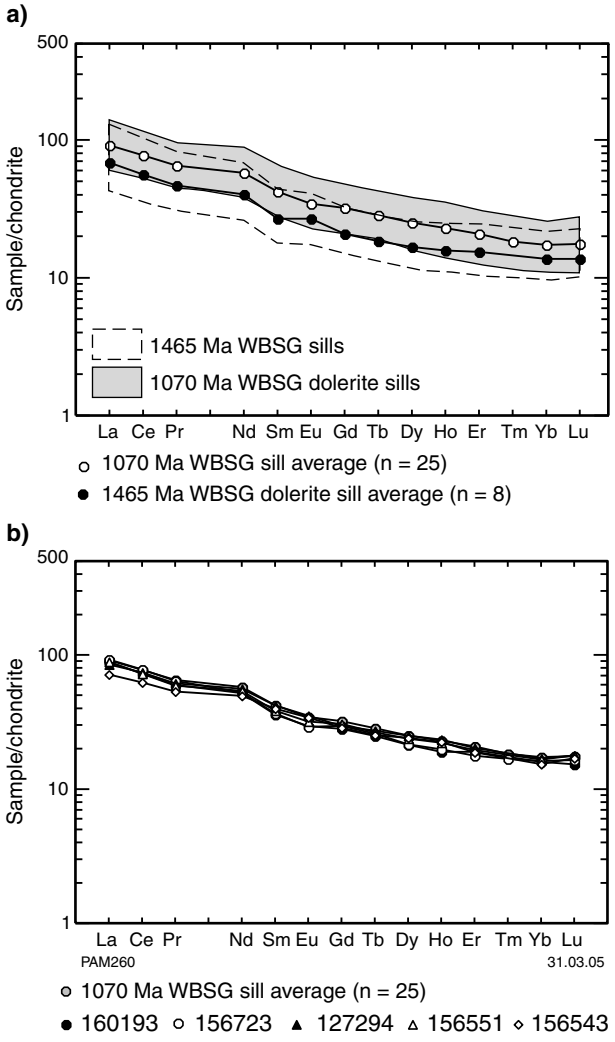

Figure 45. a) Chondrite-normalized REE patterns for the 1070 Ma western Bangemall Supergroup sill average and range, and the 1465 Ma western Bangemall Supergroup sill average and range; b) chondrite-normalized REE chemistry of five sills intruding the Edmund Group that show 1070 Ma chemistry compared to the average of the 1070 Ma western Bangemall Supergroup sills

that have the same Th/Nb versus Mg# characteristics as the 1070 Ma western Bangemall Supergroup sills have identical REE patterns to that of a 1070 Ma western Bangemall Supergroup sill average (Fig. 45b), providing further evidence that these five samples are from sills that were emplaced at 1070 Ma.

Average REE analyses for high- and low-Th/Nb 1070 Ma eastern Bangemall Supergroup sills are shown in Figure 46a, in addition to the range for low-Th/Nb sills. High-Th/Nb 1070 Ma eastern Bangemall Supergroup sill analyses have an average $(La)_{CN}$ of 159 compared with an average $(La)_{CN}$ of 97 for samples with lower Th/Nb values (Table 3). The high-Th/Nb 1070 Ma eastern Bangemall Supergroup samples have higher $(La/Yb)_{CN}$ (10) and $(La/Sm)_{CN}$ (3.4) compared with the lower Th/Nb group (6.5 and 2.6 respectively), and the degree of LREE enrichment is the main factor in separating the two groups. Both groups have similar chondrite-normalized HREE concentrations in terms of $(Gd/Yb)_{CN}$ of 1.92 and 1.85 respectively, and slight negative Eu/Eu^{*} of 0.87 (high-Th/Nb 1070 Ma eastern Bangemall Supergroup) and 0.92 (low-Th/Nb group). Also shown in Figure 46a is the average REE pattern for the 1070 Ma western Bangemall Supergroup sill analyses, which shows a stronger similarity in terms of REE chemistry with the low-Th/Nb sill average than with the high-Th/Nb sill average.

Complete REE data are available for two samples of 1058 Ma mafic igneous rocks from the Empress 1A drillhole (Fig. 46b). The REE patterns are similar to those for the 1070 Ma eastern Bangemall Supergroup low-Th/Nb sills.

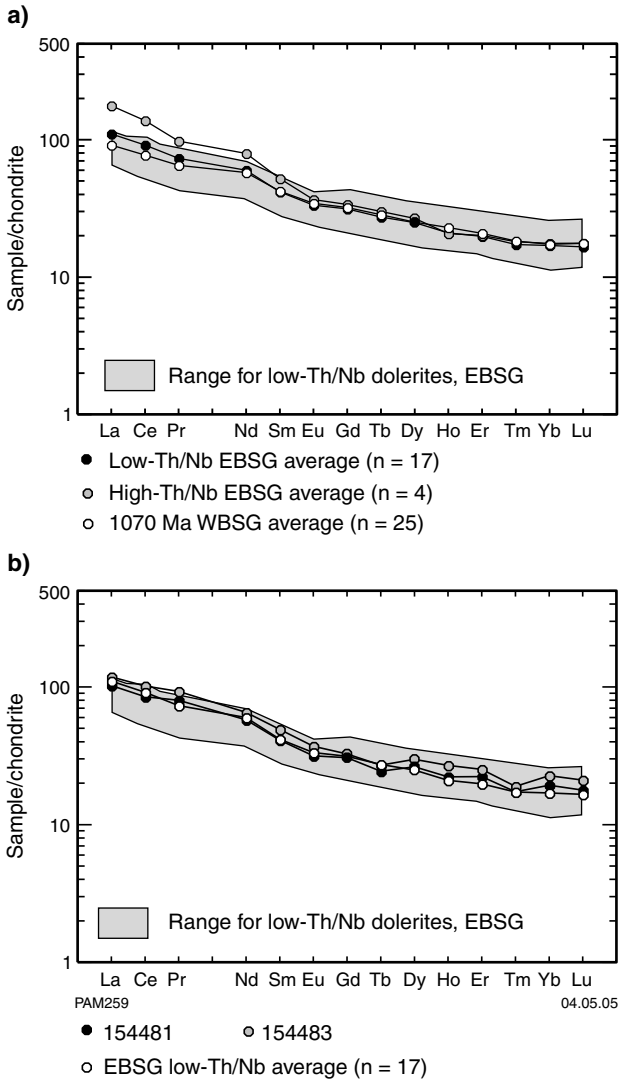

Figure 46. a) Chondrite-normalized REE patterns for average low-Th/Nb 1070 Ma eastern Bangemall Supergroup samples, high-Th/Nb samples, and the 1070 Ma western Bangemall Supergroup average. Also shown is the range of low-Th/Nb 1070 Ma eastern Bangemall Supergroup sill samples; b) chondrite-normalized REE patterns for samples from Empress 1A (GSWA 154481 and 154483) and the average and range for the 1070 Ma eastern Bangemall Supergroup low-Th/Nb sill samples

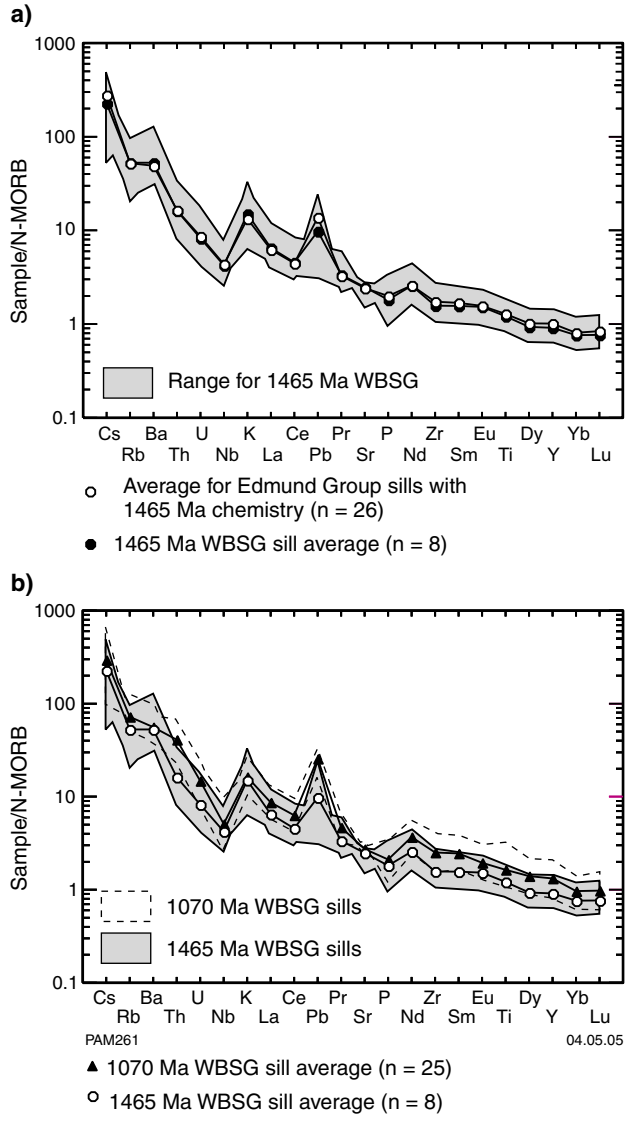

Figure 47. a) N-MORB-normalized patterns for the average and range of 1465 Ma samples from sills 11 and 21 (Wingate, 2002), and the average of sills with 1465 Ma chemistry intruding the Edmund Group. N-MORB normalization factors are from Sun and McDonough (1989; table 1); b) N-MORB-normalized patterns showing the average and range for the 1070 Ma western Bangemall Supergroup and the 1465 Ma western Bangemall Supergroup sills

N-MORB-normalized spider diagrams

The average composition for eight 1465 Ma western Bangemall Supergroup sills is shown relative to N-type mid-oceanic-ridge basalt (N-MORB) concentrations (Sun and McDonough, 1989) on Figure 47a, in addition to the range of N-MORB-normalized compositions for these rocks. The element order of these spider diagrams is largely based on the depletion pattern observed in N-MORB (Sun and McDonough, 1989). Concentrations show a gradual decrease from Cs to Lu, with well-developed negative Nb anomalies. Most samples have positive Pb anomalies and negative P anomalies relative to adjacent elements. The average composition shows a positive Ba anomaly relative to adjacent elements, but the scatter in Ba concentrations (Fig. 36a) means that individual samples can have both positive and negative Ba anomalies. Also shown is the average composition of 26 samples from sills intruding the Edmund Group that have 1465 Ma chemistry, which has an N-MORB-normalized pattern strongly coincident with the average pattern for the two sills (eight samples) dated at 1465 Ma.

Relative to the c. 1465 Ma western Bangemall Supergroup sills, the 1070 Ma western Bangemall Supergroup sills form a tighter grouping on N-MORB-normalized spider diagrams for the LFSE (Fig. 47b). In contrast to the 1465 Ma western Bangemall Supergroup sills, the 1070 Ma western Bangemall Supergroup sills have consistent positive Pb and negative P anomalies, although the variation in Ba concentrations leads to both positive and negative Ba anomalies for different samples. The average composition of the 1070 Ma western Bangemall Supergroup sills and the 1465 Ma western Bangemall Supergroup sills is also shown. The 1070 Ma western Bangemall Supergroup sill average has similar contents of some LFSE such as Ba and K, generally higher concentrations of all other elements, and a stronger Pb anomaly. Five analyses from dolerites intruding the Edmund Group that show c. 1070 Ma chemistry (Fig. 48a) show a strong overlap with the 1070 Ma western Bangemall Supergroup sill average, with the greatest variation between the two patterns being in the Cs–Th interval. Elements in this interval are relatively prone to remobilization due to alteration or metamorphism, which may account for these discrepancies.

The average composition of low-Th/Nb 1070 Ma eastern Bangemall Supergroup sills is similar to the 1070 Ma western Bangemall Supergroup sill average (Fig. 48b). Major differences between the two averages are in terms of LFSE concentrations such as Cs, Ba, and Rb. The high-Th/Nb group of sills has different LFSE characteristics compared to other 1070 Ma eastern Bangemall Supergroup samples, in that Ba is variably depleted relative to Cs and Th, and in three samples Cs is depleted relative to Rb (Fig. 48b). Overall, the high-Th/Nb group has higher N-MORB-normalized concentrations of most trace elements. Two samples (GSWA 154481 and 154483) from the Empress 1A drillhole (Fig. 49) are broadly similar to patterns for the 1070 Ma eastern Bangemall Supergroup low-Th/Nb Glenayle samples. There are no REE data for the third Empress 1A sample (GSWA 154476), but it has lower Rb, Ba, Th, and Sr contents that may be due to post-magmatic alteration. All three samples are compositionally similar to the 1070 Ma western Bangemall Supergroup samples.

Geochemistry of the Glenayle and Prenti Dolerites

Pirajno and Hocking (2002) have identified two dolerite types in the Glenayle area — the Glenayle Dolerite and a locally intrusive, finer grained phase, the Prenti Dolerite. The latter usually forms sills, but is occasionally observed

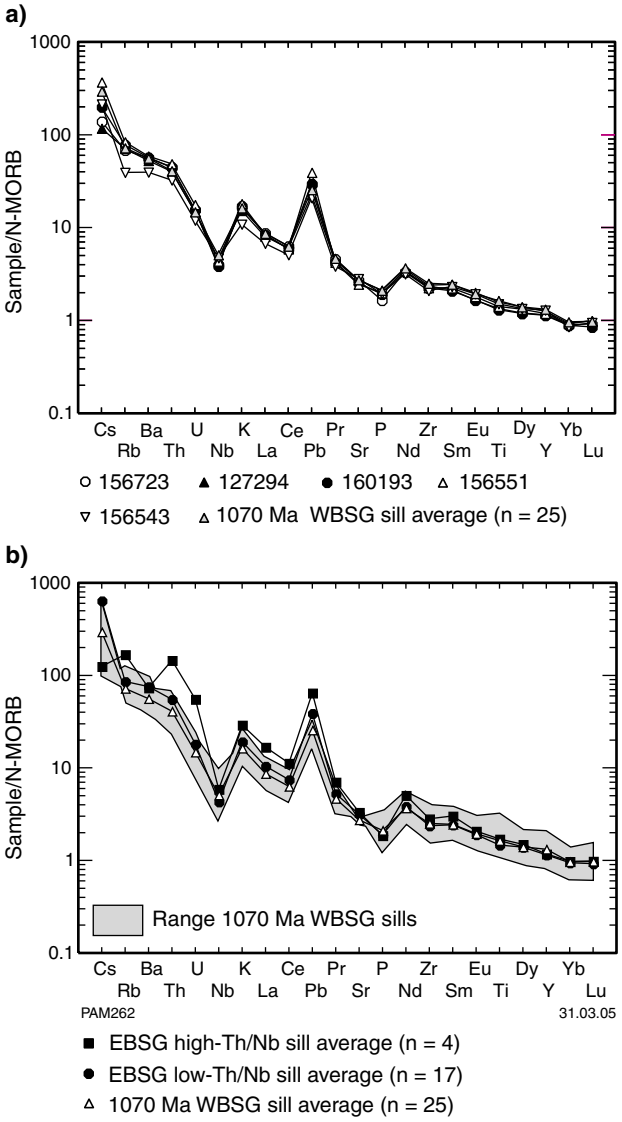

Figure 48. a) N-MORB-normalized patterns for five samples from sills intruding the Edmund Group showing 1070 Ma chemistry compared to the average of the 1070 Ma western Bangemall Supergroup sills; b) N-MORB-normalized patterns for the average high-Th/Nb 1070 Ma eastern Bangemall Supergroup sills, low-Th/Nb sills, and the range and average of the 1070 Ma western Bangemall Supergroup sills

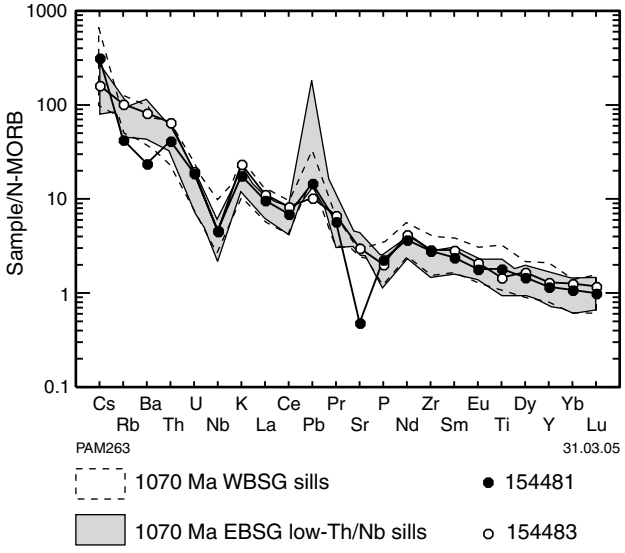

Figure 49. N-MORB-normalized patterns for samples from Empress 1A (GSWA 154481 and 154483) and the range for the 1070 Ma western Bangemall Supergroup and 1070 Ma low-Th/Nb eastern Bangemall Supergroup sills

as dykes. The petrography of these dolerite types has been discussed earlier in this Report and indicates that they can be differentiated in terms of texture (the Prenti Dolerite is finer grained and porphyritic) and mineralogy (the Fe–Ti oxides in the Prenti Dolerite give it a distinctive texture). Of the two dolerite types, the Glenayle Dolerite shows a wider compositional range, but both have similar average SiO_2 contents (Glenayle Dolerite 50.5%, Prenti Dolerite 51.9%) and Mg# of 37 and 44 respectively. They lie on common trends on incompatible element plots (Fig. 50a), with no clear separation in terms of element concentrations. Although they cannot be entirely separated in terms of Th/Nb versus Mg# (Fig. 50b), most Prenti Dolerite analyses have lower Th/Nb at a given Mg# compared to the Glenayle Dolerite. In terms of REE

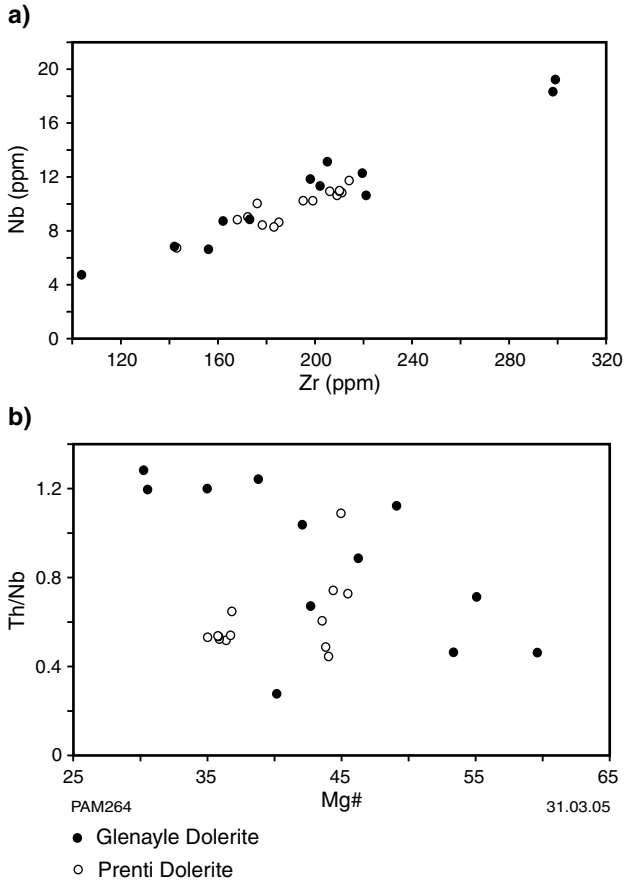

Figure 50. Bivariate plots for the Glenayle and Prenti Dolerites showing: a) Nb versus Zr; b) Th/Nb versus Mg#

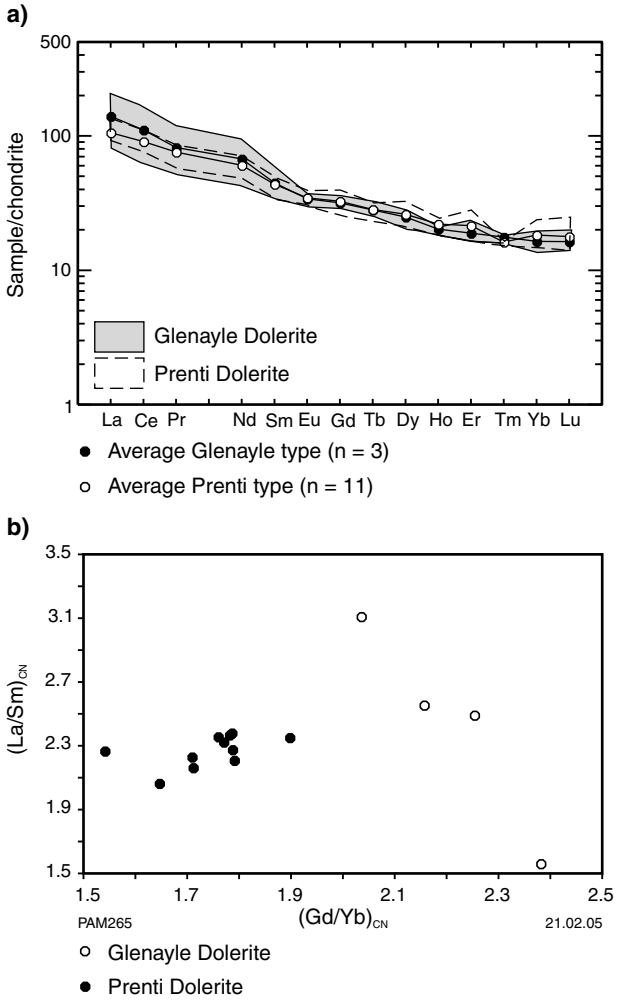

Figure 51. a) Chondrite-normalized REE patterns for average Glenayle and Prenti Dolerites. The range for each dolerite type is also shown; b) $(La/Sm)_{CN}$ versus $(Gd/Yb)_{CN}$ (where CN is chondrite normalized using factors from Sun and McDonough, 1989, table 1) for the Glenayle and Prenti Dolerites

(Fig. 51a), the two dolerite types show some overlap, although the Glenayle Dolerite has a greater range in REE (especially LREE) and slightly steeper REE patterns with an average $(La/Yb)_{CN}$ of 7.6 compared to the Prenti Dolerite value of 5.5. The average $(La)_{CN}$ for the Glenayle Dolerite is 113 compared to 96 for the Prenti Dolerite. Both dolerite types have weak negative Eu/Eu*; the average for the Glenayle Dolerite is 0.88 compared to 0.93 for the Prenti Dolerite. In terms of HREE, the Glenayle Dolerite has steeper HREE (average $(Gd/Yb)_{CN}$ = 2.2) compared to the Prenti Dolerite (1.8; Fig. 51b).

Incompatible element behaviour (Fig. 50a) shows that both dolerite types were derived from a similar mantle source. Between-sample variations in chemistry could reflect differences in the degree of partial melting coupled with variable amounts of fractional crystallization. Mafic rocks with flatter HREE patterns, such as the Prenti Dolerite (Fig. 51b), may reflect melting at a shallower depth, where garnet is not a residual phase. As the Prenti Dolerite locally intrudes the Glenayle Dolerite, it is possible that the Prenti Dolerite was derived from the shallower melting of the same source material as the Glenayle Dolerite. Another possibility is that the Glenayle Dolerite represents contamination by garnet-bearing lower crust, which would be consistent with $^{143}Nd/^{144}Nd$ data discussed in the following section.

Isotope chemistry

Eighteen samples have been analysed for $^{143}Nd/^{144}Nd$ and 16 of these have also been analysed for $^{87}Sr/^{86}Sr$ (Table 4). All analyses were carried out at Shimane University (Japan), following procedures discussed by Iizumi et al. (1994, 1995), except from GSWA 152666, which was analysed at the University of Melbourne under conditions discussed by Waight et al. (2000). Measured Nd isotope ratios were normalized to $^{146}Nd/^{144}Nd$ equal to 0.7219. The average and standard deviation for standards analysed with unknowns at Shimane University (Table 5) show a high level of precision.

Seven analyses of 1465 Ma western Bangemall Supergroup dolerite include two analyses from the sill at site 21 (GSWA 180712 and GSWA 180714) and two from the sill at site 11 (GSWA 160187 and GSWA 160190). The three other samples are from sills with 1465 Ma chemistry (GSWA 180701 (site 13), GSWA 127297 (near site 7), and GSWA 160183 (site 17)). Five samples are from 1070 Ma western Bangemall Supergroup sills, and one sample (GSWA 156723) that intrudes the Edmund Group and has 1070 Ma western Bangemall Supergroup chemistry. GSWA 152933 is a crosscutting dyke on Elliott Creek (1:100 000) that is tentatively included with the 1070 Ma sills, but could be part of the 755 Ma Mundine Well dyke swarm (Wingate and Giddings, 2000). Four samples are from the 1070 Ma eastern Bangemall Supergroup dolerites and comprise three samples of Glenayle Dolerite and one sample of the Prenti Dolerite (GSWA 152662).

Initial $^{143}Nd/^{144}Nd$ ratios (i.e. the $^{143}Nd/^{144}Nd$ at the time of crystallization, which in this study is either 1070 or 1465 Ma) can be expressed relative to a chondrite-uniform reservoir (CHUR) in epsilon notation (Faure, 1986). εNd(T) values (where T is the time of crystallization) for the 1465 Ma western Bangemall Supergroup samples show a similar range (-2.7 to -4.6), but are lower than the 1070 Ma western Bangemall Supergroup sill samples (0.4 to -2.4; Table 4). The 1070 Ma western Bangemall Supergroup sills show a wider range in εNd(T) and are more depleted (i.e. higher $^{143}Nd/^{144}Nd$) compared to those from the eastern Bangemall Supergroup (Glenayle Dolerite values of -6.0 to -6.5), although the Prenti Dolerite has a similar εNd(T) of -3.4. GSWA 152933 has a εNd(T) equal to 0.7.

As Sr is a LFSE, it may have undergone some post-magmatic redistribution, and $^{87}Sr/^{86}Sr$ may therefore not be primarily magmatic. However, εNd and $^{87}Sr/^{86}Sr$ show a negative correlation typical of igneous rocks that have undergone crustal contamination (Fig. 52). Analyses from both 1465 and 1070 Ma sills form a relatively flat array, in that there is a relatively wide variation in $^{87}Sr/^{86}Sr(T)$ (0.7050 – 0.7115) compared to εNd(T). Two analyses

Table 4. Isotope data for the Bangemall Supergroup sills

Sample no.	*Sm (ppm)*	*Nd (ppm)*	$^{147}Sm/^{144}Nd$	$^{143}Nd/^{144}Nd$ (m)	*2s*	$^{143}Nd/^{144}Nd$ (i)	εNd	T_{CHUR}	$^{87}Sr/^{86}Sr$ (m)	*2s*	*Sr (ppm)*	*Rb (ppm)*	$^{87}Rb/^{86}Sr$	$^{87}Sr/^{86}Sr$ (i)
152695	10.19	49.44	0.124	0.511823	0.000009	0.510952	-6.0	1 706	0.734500	0.000009	229	125	1.580	0.710317
152666	5.06	23.1	0.132	0.511873	0.000029	0.510947	-6.1	1 793	0.712801	0.000009	336	27	0.233	0.709241
152661	7.62	35.07	0.131	0.511844	0.000009	0.510926	-6.5	1 831	0.722939	0.000010	313	86	0.795	0.710767
152662	6	24.5	0.147	0.512118	0.000010	0.511083	-3.4	1 605	0.720080	0.000009	329.7	64.9	0.569	0.711359
156723	5.51	24.11	0.138	0.512100	0.000023	0.511134	-2.4	1 385	0.713916	0.000009	241.1	37.78	0.453	0.706974
152928	6.75	28.58	0.142	0.512220	0.000012	0.511222	-0.7	1 167	0.712477	0.000009	237.91	35.8	0.435	0.705811
152927	6.5	26.58	0.147	0.512309	0.000012	0.511275	0.4	1 013	0.710897	0.000009	221.16	30.32	0.396	0.704824
152933	6.65	27.71	0.144	0.512305	0.000009	0.511291	0.7	971	0.711198	0.000018	218.37	31.53	0.418	0.704801
160185	6.81	28.59	0.143	0.512199	0.000011	0.511192	-1.3	1 254	0.712855	0.000009	236.9	35.9	0.439	0.706141
160195	5.63	24.53	0.138	0.512104	0.000010	0.511134	-2.4	1 388	0.713962	0.000009	223.3	37.3	0.483	0.706562
180706	5.06	23.64	0.129	0.512178	0.000019	0.511273	0.3	1 033	0.714808	0.000010	227.2	40.3	0.513	0.706950
127297	5.33	22.09	0.145	0.511969	0.000014	0.510571	-3.4	1 975	0.715109	0.000011	253.1	36.3	0.415	0.706385
160183	3.06	14.13	0.130	0.511803	0.000014	0.510548	-3.8	1 912	–	–	–	–	–	–
160187	4.1	19.86	0.124	0.511706	0.000007	0.510509	-4.6	1 955	0.732255	0.000009	129	52.6	1.179	0.707453
160190	3.17	14.39	0.133	0.511848	0.000011	0.510571	-3.4	1 873	–	–	–	–	–	–
180701	4.1	18.46	0.134	0.511805	0.000019	0.510518	-4.4	2 008	0.712490	0.000009	281.2	29.5	0.304	0.706109
180712	2.8	13.17	0.128	0.511838	0.000009	0.510606	-2.7	1 769	0.709213	0.000009	227	12.2	0.156	0.705944
180714	3.3	15.12	0.131	0.511809	0.000011	0.510544	-3.9	1 928	0.708952	0.000010	236.3	11.2	0.137	0.706069

NOTES:
2s two standard deviations of the mean
(m) measured ratio
(i) initial ratio
T_{CHUR} model age

1070 Ma eastern Bangemall Supergroup
152695, 152666, 152661 — Glenayle Dolerite
152662 — Prenti Dolerite

1070 Ma western Bangemall Supergroup
156723, 152928, 152927, 152933 (crosscutting dyke of the ?Mundine Well dyke swarm)
160185 (site 8)
160195 (site 1)
180706 (site 10)

1465 Ma western Bangemall Supergroup
127297
160183 (site 17)
160187 and 160190 (site 11)
180701 (site 13)
180712 and 180714 (site 21)

Table 5. Isotope analyses of the reference materials determined at Shimane University

Standard	*$^{87}Sr/^{86}Sr$*	*±(2s)*	*Standard*	*$^{143}Nd/^{144}Nd$*	*±(2s)*
NBS987	0.710250	0.000008	La Jolla	0.511849	0.000009
NBS987	0.710228	0.000009	La Jolla	0.511832	0.000009
NBS987	0.710256	0.000008	La Jolla	0.511834	0.000008
NBS987	0.710242	0.000008	La Jolla	0.511859	0.000008
NBS987	0.710266	0.000008	La Jolla	0.511876	0.000006
NBS987	0.710232	0.000009	**Average**	0.511850	
NBS987	0.710215	0.000009	Standard deviation	0.000018	
Average	0.710241				
Standard deviation	0.000018				

NOTE: 2s is two standard deviations of the mean

(crosscutting dyke GSWA 152933 and the western Bangemall Supergroup 1070 Ma sill sample GSWA 152927) plot close to bulk silicate earth (BSE; Zindler and Hart, 1986), whereas the remaining data plot in the flood-basalt field between BSE and enriched mantle component EM II. Rollinson (1993) noted that the low εNd and elevated $^{87}Sr/^{86}Sr$ of EM II is typical of upper crustal compositions. He argued that its isotopic composition can be explained by recycling of continental crust into the mantle through subduction.

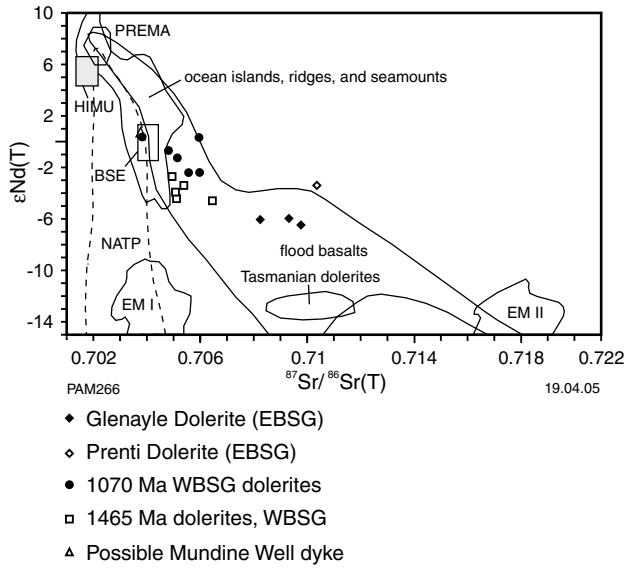

Figure 52. εNd(T) versus $^{87}Sr/^{86}Sr(T)$ for the 1070 Ma western Bangemall Supergroup sill samples, 1070 Ma eastern Bangemall Supergroup sill samples (Glenayle and Prenti Dolerites), 1465 Ma western Bangemall Supergroup sill samples, and crosscutting dyke GSWA 152933. Fields for PREMA (prevalent mantle), HIMU (mantle enriched in Th and U relative to Pb), BSE (bulk silicate Earth), EM I and EM II (enriched mantle components), flood basalts, and NATP (North Atlantic Tertiary Province) are from Zindler and Hart (1986). The field for the Tasmanian dolerites is from Hergt et al. (1991). εNd(T) has been calculated using present-day CHUR values of $^{143}Nd/^{144}Nd$ equals 0.512638 and $^{147}Sm/^{144}Nd$ equals 0.1967

Three broad sill groupings can be identified (Fig. 53). The 1070 Ma western Bangemall Supergroup sills and GSWA 152933 are isotopically the most depleted, in that they have the highest εNd and the lowest $^{87}Sr/^{86}Sr(T)$ (0.7048 – 0.7069). The 1465 Ma western Bangemall Supergroup sills have a similar range in $^{87}Sr/^{86}Sr(T)$ values (0.7059 – 0.7075), but have lower εNd values than the 1070 Ma western Bangemall Supergroup sills. The 1070 Ma eastern Bangemall Supergroup sills are the most radiogenic in terms of $^{87}Sr/^{86}Sr$ (0.7092 – 0.7108) and have the lowest εNd, apart from the one Prenti Dolerite sample.

If the negative correlation between $^{143}Nd/^{144}Nd$ and $^{87}Sr/^{86}Sr$ reflects crustal contamination, there should also be a negative correlation between εNd and SiO_2 and also εNd and $(La/Sm)_{CN}$, and a positive correlation between εNd and Mg#. Four of the five 1070 Ma western Bangemall Supergroup sills show a negative correlation between εNd and both SiO_2 and $(La/Sm)_{CN}$ (Fig. 54a,b), as opposed to the 1465 Ma western Bangemall Supergroup sills, which

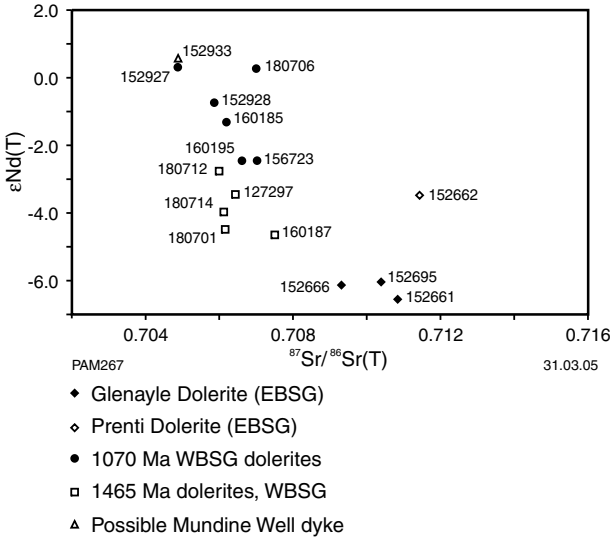

Figure 53. εNd(T) versus $^{87}Sr/^{86}Sr(T)$ for the Bangemall Supergroup sill samples. εNd(T) has been calculated using present-day CHUR values of $^{143}Nd/^{144}Nd$ equals 0.512638 and $^{147}Sm/^{144}Nd$ equals 0.1967

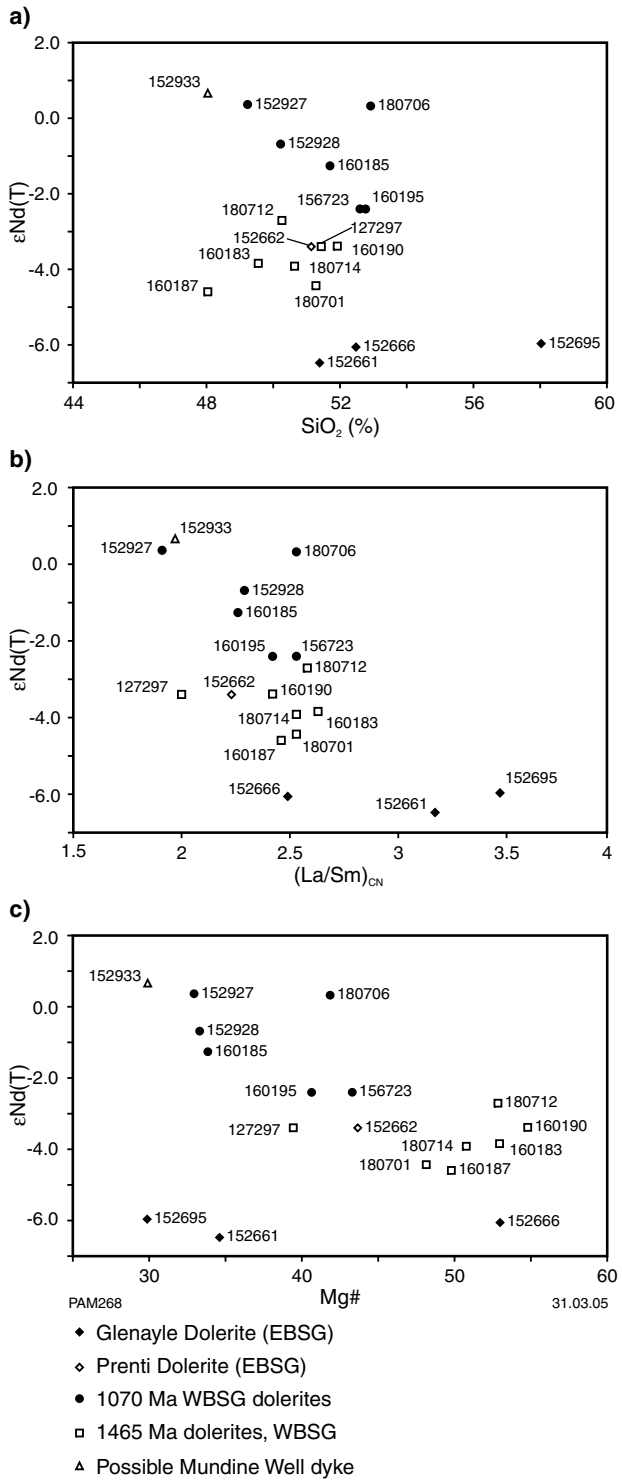

Figure 54. a) εNd versus SiO_2; b) εNd versus $(La/Sm)_{CN}$ where CN is chondrite normalized using values from Sun and McDonough (1989; table 1); c) εNd versus Mg#. εNd(T) has been calculated using present-day CHUR values of $^{143}Nd/^{144}Nd$ equals 0.512638 and $^{147}Sm/^{144}Nd$ equals 0.1967

show a range in εNd, but little correlation with either SiO_2 or $(La/Sm)_{CN}$. In contrast, the three Glenayle Dolerite samples show a range in both SiO_2 and $(La/Sm)_{CN}$, but little change in εNd, although two of these analyses have similar SiO_2 contents. A plot of εNd versus Mg# (Fig. 54c) shows that the 1070 Ma western Bangemall Supergroup sills have increasingly negative εNd with increasing Mg#, which is the opposite trend of that expected if εNd variations were controlled by crustal contamination. In contrast, the western Bangemall Supergroup 1465 Ma sills show a weak positive correlation that is consistent with crustal contamination.

Crustal contamination can also be examined using εNd versus 1/Nd relations, because crustal rocks have low εNd (i.e. high $^{143}Nd/^{144}Nd$) and high Nd contents (Rudnick and Fountain, 1995; Windrim and McCulloch, 1986). The 1070 Ma western Bangemall Supergroup and 1465 Ma western Bangemall Supergroup samples were plotted in terms of $^{143}Nd/^{144}Nd$ and 1/Nd (Fig. 55), as well as possible crustal contaminants that show a range in $^{143}Nd/^{144}Nd$ and Nd contents. Chosen contaminants encompassed rocks that

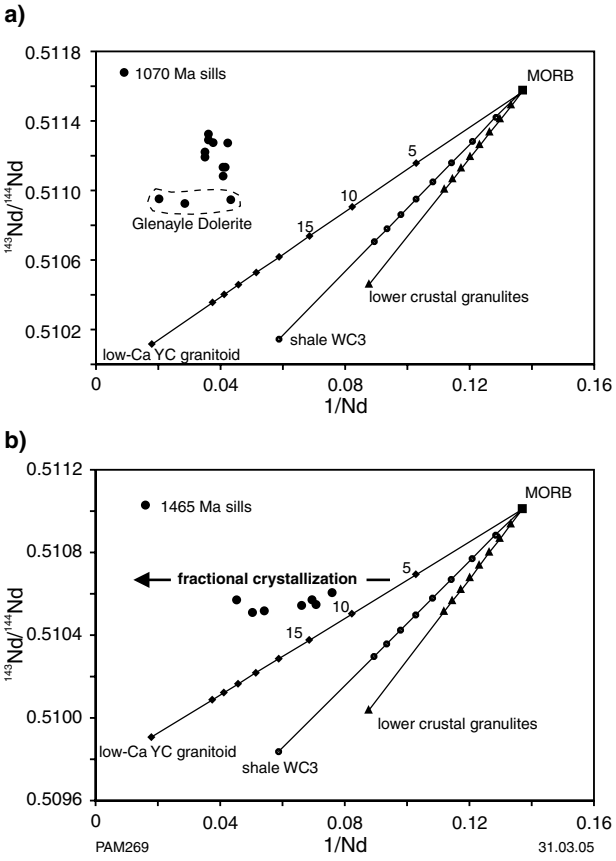

Figure 55. Simple mixing between N-MORB (Sun and McDonough, 1989; Rollinson, 1993, table 6.6) and three possible crustal compositions of lower crustal granulite average (Strangways Complex; Windrim and McCulloch, 1986), Archaean shale WC3 (Allegré and Rousseau, 1984), and low-Ca Yilgarn Craton granitoid average (Cassidy, K. F., 2002, written comm.; Champion, D. C., 2003, written comm.) in terms of $^{143}Nd/^{144}Nd$ and 1/Nd. Numbers are % addition of contaminant for: a) 1070 Ma western Bangemall Supergroup and eastern Bangemall Supergroup; b) 1465 Ma western Bangemall Supergroup. The likely fractional crystallization vector assumes Nd behaves incompatibly during fractional crystallization

are spatially associated with the Bangemall Supergroup, including a low-Ca Yilgarn Craton granitoid average (Cassidy, K. F., 2002, written comm.; Champion, D. C., 2003, written comm.) and a Pilbara Craton Archaean shale (WC3; Allegré and Rousseau, 1984). Another contaminant considered was an example of possible lower crustal composition that was a mafic granulite average from the Strangways Complex of Central Australia (Windrim and McCulloch, 1986). Mixing trajectories between these contaminants and N-MORB (Sun and McDonough, 1989; Rollinson, 1993, table 6.6) do not intersect either the 1070 Ma western Bangemall Supergroup sills or the 1465 Ma western Bangemall Supergroup sills, although the latter plot close to the mixing line between the Yilgarn Craton low-Ca granitoid and N-MORB at about 8–10% addition of contaminant. These mixing trajectories essentially model bulk assimilation, and do not take into account, for example, the effects of fractional crystallization that would shift compositions to lower 1/Nd, but not affect $^{143}Nd/^{144}Nd$. The range in 1/Nd of 0.04 – 0.07 shown by the 1465 Ma western Bangemall Supergroup sills would require about 50% fractional crystallization, assuming that D(Nd) is equal to zero. The three Glenayle sill samples show a wide range in $^{87}Sr/^{86}Sr$ but little change in $^{143}Nd/^{144}Nd$, which is a similar pattern to the 1465 Ma sills (Fig. 54b). Thus, the three Glenayle sill samples could also reflect contamination followed by fractional crystallization.

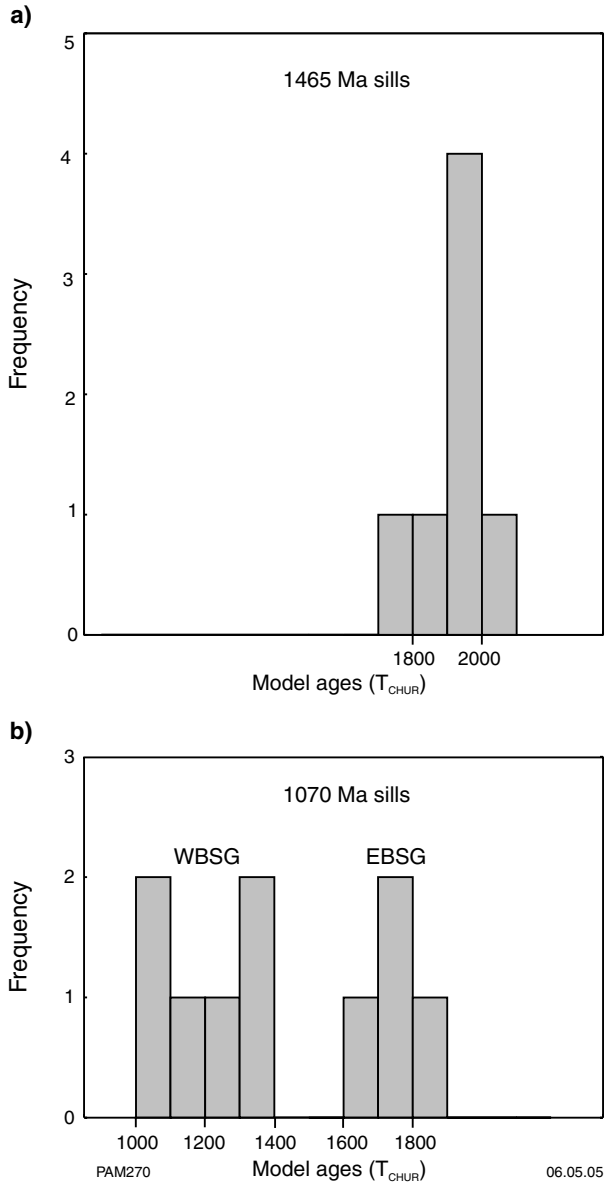

Figure 56. Histograms of model ages (T_{CHUR}) for: a) 1465 Ma western Bangemall Supergroup sill samples; b) 1070 Ma sill samples

Sheppard et al. (2004) have discussed the age and chemistry of Palaeoproterozoic granitic rocks of the Dalgaringa Supersuite, which form part of the southern Gascoyne Complex, adjacent to (and possibly underlying part of) the western Bangemall Supergroup. Sheppard et al. (2004) have argued that the Dalgaringa Supersuite represents an Andean-type batholith generated above a northwest-dipping subduction zone. The SHRIMP U–Pb zircon ages of these rocks span 2005–1970 Ma. Model ages calculated relative to CHUR (T_{CHUR}) record the age at which magma separated from the mantle source and acquired a different Sm/Nd, assuming that the Earth's primitive mantle had a chondritic isotope composition at the time of its formation (Faure, 1986; Allegré and Rousseau, 1984). T_{CHUR} ages for the 1465 Ma sills span the range 2008–1769 Ma (Fig. 56a), and overlap with SHRIMP U–Pb zircon ages for the Dalgaringa Supersuite granitic rocks.

In contrast, T_{CHUR} ages for the 1070 Ma western Bangemall Supergroup sills are notably younger (Fig. 56b), ranging between 1388 and 1013 Ma, and overlapping with crystallization ages. GSWA 152933 has a younger model age of 971 Ma.

Model ages of 1831–1706 Ma for the Glenayle Dolerite sill samples are younger than ages for both the Dalgaringa Supersuite and the 1990 ± 6 Ma age reported by Nelson (2001) for the quartz–feldspar porphyry of the Imbin Inlier that lies on the southern margin of the 1070 Ma dolerites in the Glenayle area.

Relationship of sill age, palaeomagnetism, and geochemistry in the western Bangemall Supergroup

Wingate (2002) carried out palaeomagnetic determinations on dolerite and siliciclastic sedimentary rock samples from 25 sites in the western Bangemall Supergroup, many of which have been discussed in this Report. He used these data to assign dolerite sills to one of the two intrusion events (1465 or 1070 Ma) by combining palaeomagnetic characteristics and SHRIMP U–Pb zircon and baddeleyite geochronology. Wingate (2002) identified two types of magnetic behaviour, termed type A and type B. Type A, a stable magnetization component identified in samples from 15 of the 25 sites (Wingate, 2002; figs 3 and 4), was interpreted as primary thermoremnant

magnetization acquired at the time of sill cooling. Based on palaeomagnetic data and geological relations, Wingate (2002) argued that 'the presence of A-type magnetizations can be used to identify sills belonging to the young suite' (i.e. the 1070 Ma western Bangemall Supergroup sills). Type-B magnetization was present in samples from 20 sites. Wingate (2002) suggested that it was carried by maghemite, and the erratic directions represented by this magnetization type were indicative of an overprint. Wingate (2002) noted that although the two sills dated at 1465 Ma, from sites 11 and 21, both yielded type-B magnetization, 'the presence of a B-type remanence does not indicate that a sill belongs to the older suite' (i.e the 1465 Ma western Bangemall Supergroup sills). Based on palaeomagnetism and geological relations, and the high proportion of sills with type-A magnetization, Wingate (2002) suggested that the 1070 Ma event was more widespread throughout the western Bangemall Supergroup, with sills intruding both the Collier and Edmund Groups. He suggested that the older (c. 1465 Ma) sills were restricted to the Edmund Group. Wingate (2002) cited field evidence to support a common intrusion age for sills with either type-A or type-AB magnetization. He noted that the sill at site 12 (Wingate, 2002; fig. 4) showed type-A magnetization, and the along-strike extension of this sill at site 13 showed both A- and B-type magnetization.

Earlier discussion on separation of the 1465 and 1070 Ma sill intrusion events, in terms of their chemistry, has emphasized consistent compositional differences between sills of the two groups, especially in terms of incompatible element ratios, absolute element concentrations at similar degrees of fractionation, and differences in both LREE and HREE as shown in Figure 57. This figure shows the differences in chemistry of the sill groupings, with annotations indicating the different palaeomagnetic characteristics. The three sills dated at 1070 Ma in the western Bangemall Supergroup (at sites 1, 7, and 10) cluster with sills intruding the Collier Group sedimentary rocks at higher $(Gd/Yb)_{CN}$. Also in this group is an analysis of a sample from site 2 (GSWA 160193) that, although intruding the Edmund Group, has 1070 Ma chemistry. Amongst this group, samples show both type-A and combined AB magnetization. Plotting at lower $(Gd/Yb)_{CN}$ are samples showing type-B magnetization from sites 11 and 21, and the remainder of the samples showing combined AB magnetization. This group does not contain any samples with type-A magnetization only.

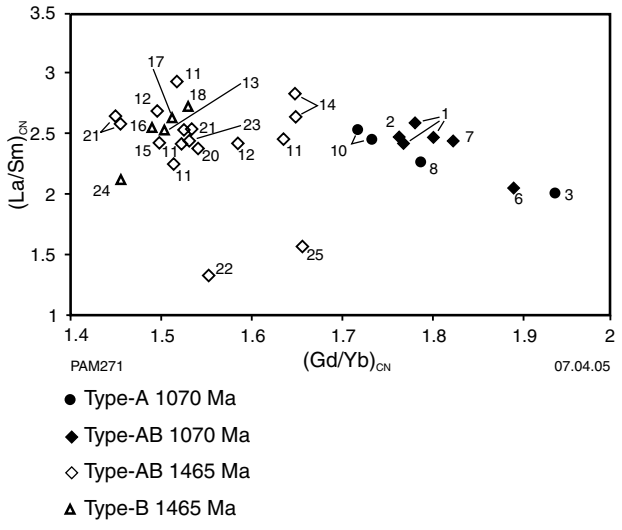

Figure 57. $(La/Sm)_{CN}$ versus $(Gd/Yb)_{CN}$ (where CN is chondrite normalized using factors from Sun and McDonough, 1989; table 1) for 1465 and 1070 Ma western Bangemall Supergroup sill samples according to palaeomagnetic signatures A, B, or AB (Wingate, 2002). Numbers next to symbols indicate sample sites of Wingate (2002)

Three observations can be made in relation to sill chemistry and palaeomagnetism. Consistent with Wingate's (2002) assertion, all samples showing type-A magnetization belong to the 1070 Ma intrusion event. However, in contrast to Wingate's (2002) assertion, sill samples showing both type-A and and type-B magnetization are found in both sill groups. Therefore, only sills with type-A magnetization alone can be assigned to the 1070 Ma event. Although the dataset is small, the two sills belonging to the 1465 Ma intrusion event have only type-B magnetization and, although speculative, it could be that the presence of this magnetization type alone is characteristic of the 1465 Ma event. In support of this is the observation that the seven sills intruding the Edmund Group that have only type-B magnetization (at sites 13, 16, 17, 18, 23, 24, and 22; i.e. excluding the dated sills at sites 11 and 21) all show 1465 Ma chemistry.

Comparison of 1070 Ma sills of the western Bangemall Basin with dykes of the Mundine Well dyke swarm

A series of northeast-trending dolerite dykes, which were referred to as the Mundine Well dyke swarm (MDS) by Hickman and Lipple (1978), intrude the Archaean and Proterozoic rocks of the Gascoyne Complex, Hamersley and Ashburton Basins, Bangemall Supergroup, and Pilbara Craton. These unmetamorphosed dykes represent the last recorded igneous event in the Pilbara Craton (Wingate and Giddings, 2000). SHRIMP U–Pb zircon and baddeleyite geochronology for four samples that intrude the the Bangemall Supergroup, Ashburton Basin and Gascoyne Complex, and the granite–greenstones of the Pilbara Craton yielded an age of 755 ± 3 Ma (Wingate and Giddings, 2000). This age is within analytical error of a K–Ar age of 748 ± 8 Ma for petrographically similar dykes intruding the Northampton Complex as reported by Embleton and Schmidt (1985).

The consistent northeasterly orientation of the MDS, and its occurrence as dykes rather than sills, should allow for clear separation of the MDS and the 1465 and 1070 Ma western Bangemall Supergroup sills. However, assuming that the Mundine Well dykes are mantle derived,

their chemistry may shed some light on the evolution of the mantle source beneath the Bangemall Supergroup. Seven Mundine Well dyke analyses (Sheppard, S., 2003, written comm.) have been plotted in relationship to the 1070 Ma western Bangemall Supergroup sills in Figure 58. Both dolerite dyke sets have similar degrees of LREE enrichment (Mundine Well dykes average $(La)_{CN}$ equal to 83, as compared to the 1070 Ma western Bangemall Supergroup $(La)_{CN}$ equal to 89), similar Eu/Eu^* (average Mundine Well dyke value of 0.95 compared to 0.94), but the Mundine Well dyke REE patterns are slightly flatter with an average $(La/Yb)_{CN}$ equal to 6, compared to $(La/Yb)_{CN}$ equal to 5.3 for the 1070 Ma western Bangemall Supergroup sills. Dyke GSWA 152933 has almost identical REE chemistry to sample GSWA 178715. The Mundine Well dykes are also, on average, less fractionated in that they have higher average Mg# (53), Ni (122 ppm), and Cr (198 ppm) compared to the 1070 Ma western Bangemall Supergroup 1070 sills with corresponding values of 39, 99 ppm, and 95 ppm respectively. In terms of N-MORB-normalized chemistry (Fig. 58b), most Mundine Well dyke analyses are similar and show the same morphology as the 1070 Ma western Bangemall Supergroup dolerite sills. An exception is GSWA 178762, which has a more pronounced negative Ba anomaly and a stronger positive Pb spike; it is also more LREE enriched than the other samples (Fig. 58a).

In this case, chemistry cannot separate the MDS dykes from the 1070 Ma sills, which implies that both are derived from a compositionally similar mantle source. This is also consistent with the small amount of available isotope data that shows that the one analysis of a crosscutting dyke (GSWA 152933) plots close to the 1070 Ma western Bangemall Supergroup sill data, but has a younger model age of 971 Ma.

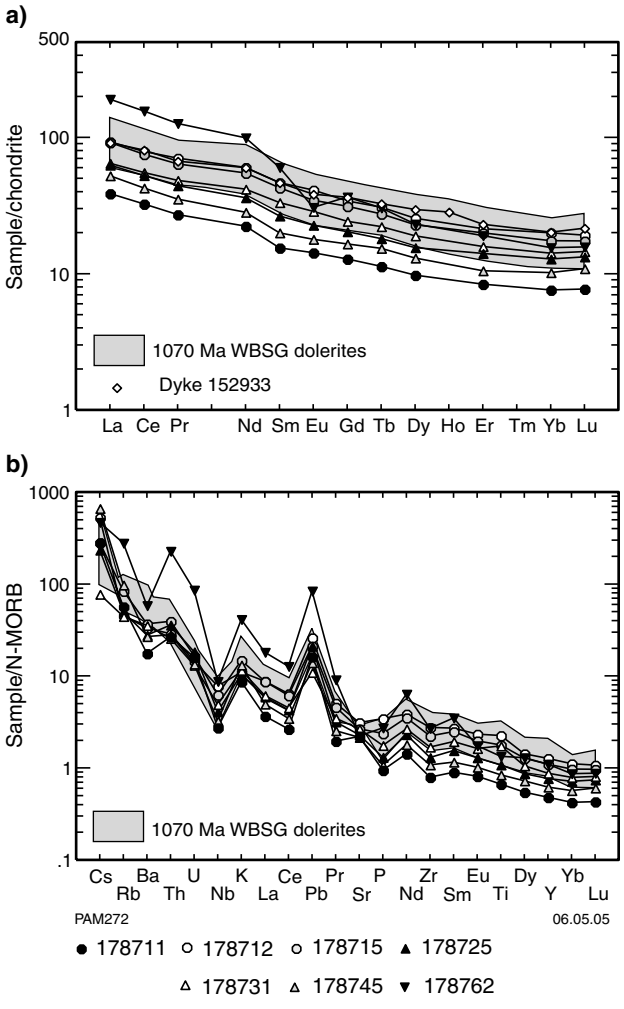

Figure 58. a) Chondrite-normalized REE patterns for seven Mundine Well dolerite dykes (Sheppard, S., 2003, written comm.) compared to the range for the 1070 Ma western Bangemall Supergroup sill samples and dyke GSWA 152933; b) N-MORB-normalized patterns for seven Mundine Well dolerite dykes compared to the range for the 1070 Ma western Bangemall Supergroup sill samples

Controls on sill chemistry

There are several contributory factors to sill chemistry. These include source composition (modal mineralogy), the extent to which the source is melted, the nature and extent of fractionating mineral phases, whether the source or the resulting magma has been contaminated, and the nature of the contaminant. In assessing the relative importance of these components when dealing with volcanic rocks, it is often assumed that the composition approximates to that of the magma, especially for weakly crystalline rocks. However, a more complicated situation exists for holocrystalline rocks such as dolerites, where the chemistry can reflect both the removal and accumulation of liquidus phases. This is further evaluated in the following discussion.

For all Bangemall Supergroup sills, the decrease in concentration of Cr and Ni with decreasing Mg#, and the corresponding increase in concentrations of incompatible elements such as Hf, Th, Y, Zr, and La, is indicative of some fractional crystallization control. The sharp decrease in both Cr and Ni concentrations over a small Mg# interval suggests crystallization of phases with high mineral/melt partition coefficients for both elements. In Figure 59a, vectors for the fractionation of olivine and clinopyroxene are shown for Ni versus Mg#, using mineral compositions from Cox et al. (1979; appendix 5) and mineral/melt distribution coefficients from Rollinson (1993; table 4.1). Removal of both olivine and clinopyroxene produces the observed decrease in Ni concentration with decreasing Mg#, but removal of a smaller amount of olivine is required relative to clinopyroxene; for example, at Mg# of about 51 and Ni about 40 ppm, approximately 10% olivine has been removed compared to about 30% clinopyroxene. The olivine vector for 10–15% olivine removal roughly parallels the trend for both the 1465 and 1070 Ma western Bangemall Supergroup sills over the interval Mg# of 40–50, and early olivine removal seems, therefore, a viable mechanism to explain the behaviour of Ni. The decrease in Ni concentration is inconsistent with the removal of a sulfide phase because Cu increases in concentration with decreasing Mg#, rather than decreasing as would be the case if sulfide was removed. Olivine and

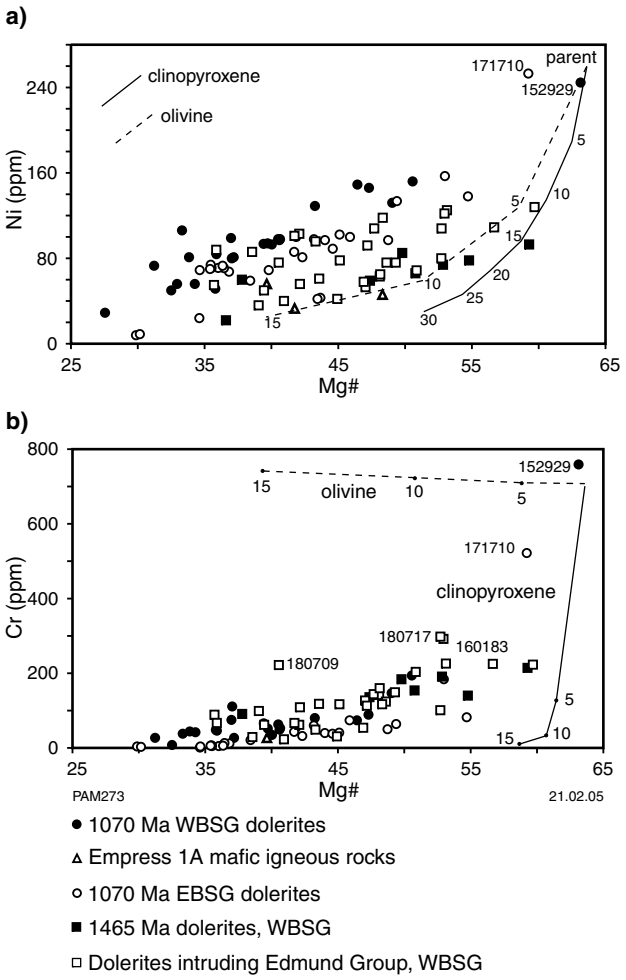

Figure 59. Bivariate plots showing: a) Ni versus Mg#; b) Cr versus Mg#. Calculated fractionation vectors for clinopyroxene (solid line) and olivine (broken line) assume a parent composition with Ni of 260 ppm and Mg# of 63. Mineral compositions are from Cox et al. (1979; appendix 5), and mineral/melt distribution coefficients are from Rollinson (1993; table 4.1). Numbers are % of mineral removed

clinopyroxene fractionation vectors for Cr versus Mg# (Fig. 59b) show that removal of only 5% clinopyroxene produces a significant decrease in the Cr content of the magma over a small Mg# interval. In contrast, removal of olivine produces a radical decrease in Mg#, but a slight increase in Cr content. It must be emphasized that in this type of modelling the calculated fractionation vectors are highly sensitive to the choice of mineral/melt distribution coefficients, which show a wide range for some minerals and elements, especially for mineral/melt distribution coefficients much greater than one (Rollinson, 1993). However, setting this aside, the early fractionation of clinopyroxene and olivine is consistent with the behaviour of both Ni and Cr.

Clinopyroxene and plagioclase, in roughly equal proportions, are the major constituents of both the 1465 and 1070 Ma dolerites, and it reasonable to assume that the removal and addition of these phases can affect the sill chemistry. In evaluating the relative importance of these phases in this context, it is important to choose trace elements that are sensitive to the addition or removal of one phase but not the other. Both Sc and Sr have different mineral/melt distribution coefficients for plagioclase and clinopyroxene in basaltic liquids (Rollinson, 1993; table 4.1), in that Sc is preferentially partitioned into clinopyroxene (but not plagioclase) and Sr is partitioned into plagioclase (but not clinopyroxene).

In terms of Sc/Sr versus Sc (Fig. 60a), analyses fall into two broad groups, albeit with some overlap. The 1070 Ma western Bangemall Supergroup sills, 1070 Ma eastern Bangemall Supergroup sills, and the two samples from the Empress 1A drillhole have lower Sc/Sr and Sc contents than the 1465 Ma western Bangemall Supergroup sills. Sills with 1465 Ma chemistry that intrude the Edmund Group span both fields. Vectors for the removal or accumulation of plagioclase and clinopyroxene are diametrically opposite and subparallel to the trend shown by the sill analyses. Vectors for the removal of olivine and magnetite would plot subparallel to the Sc axis, as D(Sc/L) ol, D(Sc/L) mt, D(Sr/L) ol, and D(Sr/L) mt (where, for example, D(Sc/L) ol is the mineral/melt (mt) distribution coefficient for Sc between olivine and the liquid) are all near zero, meaning that both Sc and Sr behave incompatibly. One interpretation of this plot is that the chemistry of the sills is largely controlled by either the addition or removal of both clinopyroxene and plagioclase. However, the separation of the two sill groupings in terms of both Sc/Sr and Sc could mean that the 1070 Ma western Bangemall Supergroup sills were derived from a magma source in which clinopyroxene has been retained in the source, but plagioclase has been partitioned into the liquid (i.e. low Sc/Sr and Sc), whereas the 1465 Ma western Bangemall Supergroup sills were derived from a source with less residual clinopyroxene. Whether removal or addition of plagioclase is important in relation to source mineralogy can be further evaluated by examining Sc/Sr in relation to Eu/Eu^* (Fig. 60b). Plagioclase removal should produce liquids with a negative Eu/Eu^*, whereas plagioclase accumulation should result in Eu/Eu^* greater than one. Similarly, Sc/Sr should decrease with plagioclase accumulation and increase with plagioclase removal. Although there is some scatter in the data (Fig. 60b), the sill analyses prescribe a trend that is almost at right angles to the predicted vectors for either plagioclase accumulation or removal. This suggests that the 1465 and 1070 Ma sill chemistry is controlled by source mineralogy and probably different degrees of partial melting, as well as by low-pressure fractional crystallization.

In addition to clinopyroxene, garnet has a mineral/melt distribution coefficient of 8.5 for Sc, but a value of 0.012 for Sr (Rollinson, 1993; table 4.1). It is well established that with a greater retention of garnet in the mantle source, the liquids resulting from partial melting have increasingly depleted HREE patterns, as shown by higher $(Gd/Yb)_{CN}$ (Rollinson, 1993). The 1465 Ma western Bangemall Supergroup sills and sills with 1465 Ma chemistry intruding the Edmund Group have higher Sc/Sr and lower $(Gd/Yb)_{CN}$ than the 1070 Ma sills (Fig. 60c), which is consistent with a lower proportion of retained garnet in the source for the 1465 Ma sills.

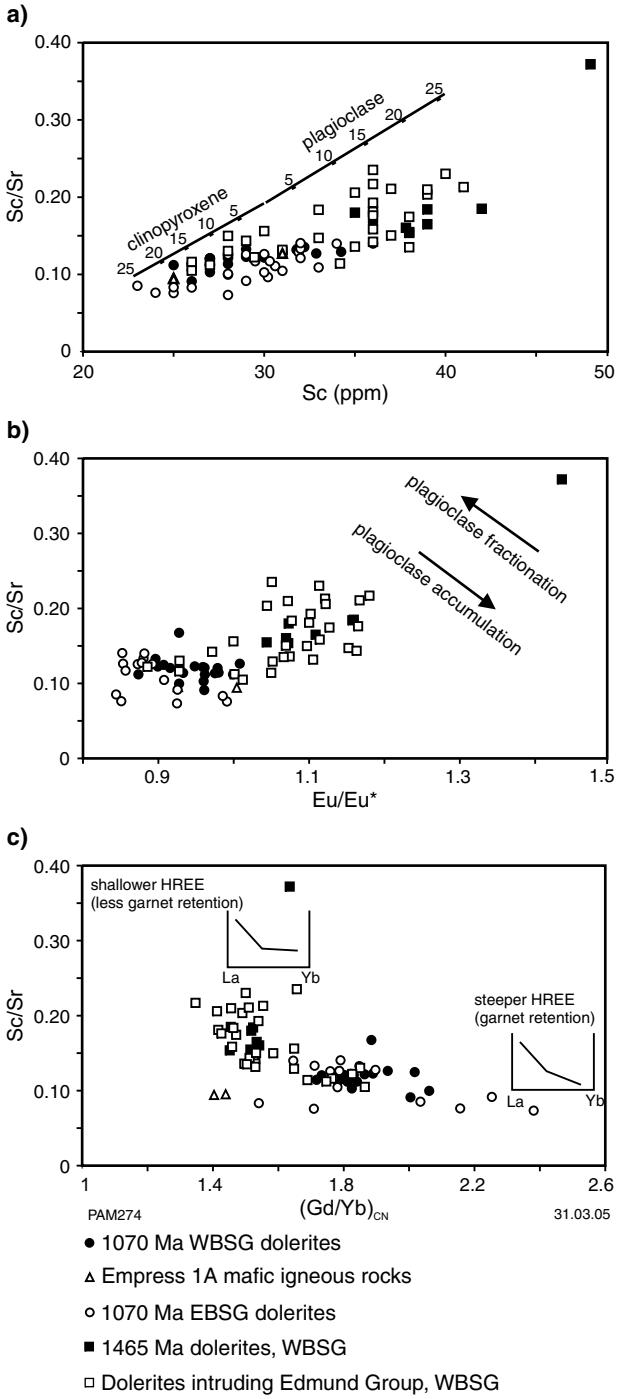

Figure 60. Bivariate plots showing: a) Sc/Sr versus Sc for the Bangemall Supergroup sill samples. Fractionation vectors for clinopyroxene and plagioclase have been calculated using mineral/melt distribution coefficients from Rollinson (1993; table 4.1). Numbers are % removal of the respective mineral phase; b) Sc/Sr versus Eu/Eu*. Vectors for plagioclase fractionation and accumulation are indicative only; c) Sc/Sr versus $(Gd/Yb)_{CN}$ where CN is chondrite normalized using values from Sun and McDonough (1989; table 1). Inset diagrams show the effect of variable garnet retention on REE patterns

Comparison of Warakurna LIP rocks with coeval LIPs

Two large igneous provinces that are roughly coeval with the Warakurna LIP are mafic flows and sills of the Keweenawan Event in North America, and basalt flows and related intrusive rocks of the Umkondo Group of Zimbabwe. A comparison of the chemistry of these LIPs with that of the Warakurna LIP and the 1465 Ma western Bangemall Supergroup sills illustrates the likely diversity in LIP composition.

Flows and sills of the Keweenawan Event are part of the Midcontinent Rift System (MRS) described by Ernst and Buchan (1997). Although the age of the MRS magmatism spans 1109–1087 Ma, most of the volcanic rocks, many of which make up the Keweenawan Event, were erupted over a short time interval from 1098 to 1094 Ma (Davis and Paces, 1990; Nicholson et al., 1992). The volcanic rocks span a wide compositional range that includes tholeiitic to transitional alkalic basalts, variably Si-saturated tholeiitic basalts, and minor rhyolite. The intrusive rocks comprise gabbro complexes (including the Duluth Complex), and tholeiitic dykes and sills, the orientation of which is controlled by pre-existing rifts (Nicholson et al., 1992).

Basalt and dolerite of the Umkondo Group of eastern Zimbabwe (Munyanyiwa, 1999) have been dated at 1078 ± 143 Ma by whole-rock and mineral Rb–Sr isochrons (Allsopp et al., 1989), whereas Wingate (2001) has provided a SHRIMP U–Pb baddeleyite age for the Weld Spring Dolerite sill of 1066 ± 14 Ma on Trainor (Fig. 20). The Umkondo Group comprises shallow-marine sedimentary rocks intruded by dolerite sills, with subordinate basaltic flows (Munyanyiwa, 1999).

Geochemical data for the Keweenawan Event rocks comprise basalt, dolerite, and gabbro analyses from the Geochemical Earth Reference Model (GERM) website <http://www.earthref.org/GERM/index.html?main.htm>, and data for the Umkondo basalt flows and dolerite sills are from Munyanyiwa (1999). A series of average values from these two datasets and for the 1465 and 1070 Ma western Bangemall Supergroup sills are shown in Table 6. Compared to the Keweenawan basalts, gabbros, and dolerites, the Umkondo dolerites and basalts have higher SiO_2, and lower Cr, Ni, and TiO_2; MgO and Mg# are similar. The 1070 Ma western Bangemall Supergroup sills have an average SiO_2 content that lies between the two groups, but average TiO_2 is higher, and MgO, Mg#, Cr, and Ni are lower, indicating a more fractionated nature. The 1465 Ma western Bangemall Supergroup sills have SiO_2 and TiO_2 contents that lie between the Umkondo and Keweenawan averages, and although MgO, Mg#, and Cr contents are similar to the Umkondo average values, the average Ni value is notably lower.

The REE patterns for Umkondo, Keweenawan, and the 1465 and 1070 Ma western Bangemall Supergroup sills are shown in Figure 61a, with some of the REE parameters summarized in Table 6. The Keweenawan rocks have, on average, flatter REE patterns and are less LREE enriched compared to the Umkondo dolerites, with

Table 6. Average data for the Keweenawan basalts, dolerites and gabbros, Umkondo dolerites, and 1070 and 1465 Ma western Bangemall Supergroup dolerites

	Keweenawan (n=149)	*Umkondo* (n=34)	*1070 Ma western Bangemall Supergroup* (n=22)	*1465 Ma western Bangemall Supergroup* (n=8)
SiO_2 (%)	48.0	53.1	51.0	49.5
TiO_2 (%)	1.84	0.97	2.0	1.5
MgO (%)	6.0	6.4	4.9	6.0
Mg#	51	50	40	47
Cr (ppm)	205	154	95	149
Ni (ppm)	145	112	98	63
$(La)_{CN}$	67	84	89	70
$(La/Yb)_{CN}$	4.3	6.6	5.3	5
Eu/Eu*	0.95	0.82	0.95	1.14

NOTE: n number of samples analysed

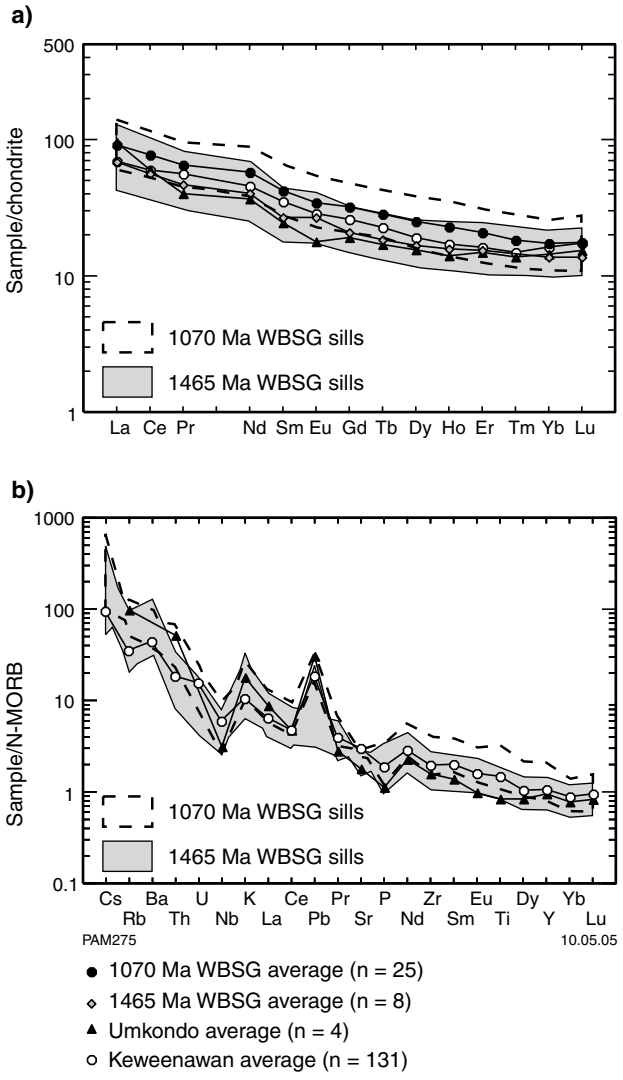

the average Keweenawan pattern closely following that for the 1465 Ma western Bangemall Supergroup sills. The 1070 Ma western Bangemall Supergroup sills show a similar degree of LREE enrichment to the Umkondo rocks, but the overall REE content is higher, and the pattern slightly flatter as shown by $(La/Yb)_{CN}$); Umkondo dolerites have the lowest REE contents of the four groups. Apart from the 1465 Ma western Bangemall Supergroup sills, all groups have Eu/Eu^* values less than one.

N-MORB-normalized spider diagram patterns for both the Umkondo dolerites and the Keweenawan rocks are broadly similar, and follow the pattern shown by the 1465 Ma western Bangemall Supergroup sills (Fig. 61b). The average Umkondo pattern has the most well-developed negative Nb anomaly and positive Pb anomaly.

Puffer (2001) examined the chemistry of ten large continental flood-basalt (CFB) provinces, and divided them into two types based on HFSE distribution: plume continental-flood basalts (P-CFB) and arc-like continental flood basalts (A-CFB). He argued that the compositional diversity of P-CFB reflected the interaction of the plume head with various mantle components, and included

Figure 61. a) Chondrite-normalized REE patterns for average Keweenawan basalts, dolerites, and gabbros and Umkondo dolerites. Also shown are the average and range for 1070 Ma western Bangemall Supergroup and 1465 Ma western Bangemall Supergroup dolerites; b) N-MORB-normalized patterns for average Keweenawan basalts, dolerites, and gabbros and Umkondo dolerites. Also shown are ranges for 1070 and 1465 Ma western Bangemall Supergroup dolerites

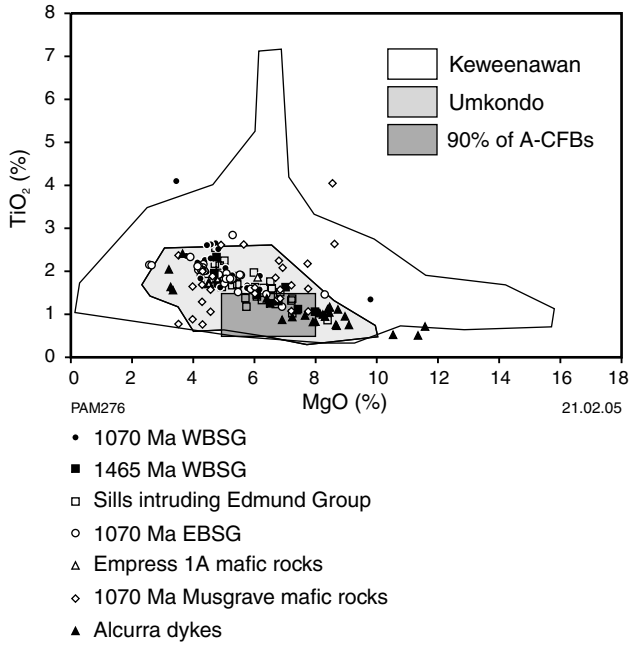

Figure 62. Bivariate plot showing TiO_2 versus MgO for the Bangemall Supergroup dolerites, 1070 Ma mafic rocks of the Musgrave Complex, and the Alcurra dykes. Fields for the Keweenawan and Umkondo mafic igneous rocks are also shown. 90% of arc-like continental flood basalts (A-CFB) plot in the dark-grey box according to Puffer (2001)

eruption products from the plume tail. In contrast, A-CFB represent the melting of arc or back-arc regions that had become isolated beneath continental lithospheric plates. Of interest is that, despite this division, silicate earth-normalized spider diagrams for data from the ten provinces show negative HFSE relative to adjacent LFSE (e.g. Nb relative to Th and K). Furthermore, both A-CFB and P-CFB can be found in a single province (e.g. the Deccan Traps). This overlap in the two CFB types, and the compositional diversity of P-CFB, has been shown by Puffer (2001) in terms of TiO_2 versus MgO (Fig. 62). This diagram clearly shows the compositional diversity of the Keweenawan rocks (P-CFB and A-CFB) relative to the restricted compositional range for the Umkondo rocks. Also shown are data for the Warakurna LIP samples, including the 1070 Ma western Bangemall Supergroup and eastern Bangemall Supergroup sills, mafic volcanic rocks and coeval sills from the Musgrave Complex (Glikson et al., 1996; this Report), and the Alcurra dyke data from the Northern Territory (Edgoose, C. J., 2002, written comm.). All these data plot in a relatively restricted range that shows overlap with the A-CFB field.

Klewin and Berg (1991) discussed the petrology of picrites, basalts, and basaltic andesites of the 5 km-thick Mamainse Point Formation, one of the best exposed successions of the Keweenawan succession. Their conclusions that these rocks represented the combination of melting at different depths, periodic replenishment of magma chambers, and fractional crystallization are consistent with the wide composition range (Fig. 62). They also suggested that evolution of the rift system in part controlled magma composition; initial fracturing allowed the passage of largely unfractionated magma to the surface, whereas later, slower rifting led to the development of crustal magma chambers that underwent periodic replenishment and fractionation. Munyanyiwa (1999) has suggested that certain REE ratios (e.g. Ce/Yb) and LREE/HFSE ratios (e.g. La/Nb) are typical of many continental flood-basalt provinces, and emphasized the depletion of HFSE, such as Nb, in relation to LFSE and LREE on normalized diagrams.

N-MORB-normalized spider diagrams (e.g. Fig. 48b) and TiO_2 versus MgO relations (Fig. 62) illustrate that rocks from the Warakurna LIP and the 1465 Ma western Bangemall Supergroup dolerites show geochemical characteristics indicative of a subduction-modified mantle source, which is also seen in the Central Atlantic, Lesotho, and Siberian continental flood-basalt provinces (Puffer, 2001). The spread of Warakurna LIP and Umkondo data from the A-CFB box on Figure 62 is consistent with input from other processes such as crustal contamination and fractional crystallization. It is interesting to note, however, that of the ten CFB provinces examined by Puffer (2001), three show A-CFB characteristics and the remaining seven a more diverse chemistry typical of P-CFBs.

Regional relations of 1070 Ma Bangemall Supergroup sills and the Warakurna LIP

Mafic rocks of approximately the same age as the 1070 Ma sills in the Bangemall Supergroup are found elsewhere in Western Australia, and in parts of South Australia and the Northern Territory, and form the basis for Wingate et al.'s (2004) Warakurna LIP. The regional setting of these rocks is discussed more fully in the following section, which emphasizes the tectonic implications of the Warakurna LIP, and only details dealing with comparative chemistry are discussed in this section.

In the western part of the Musgrave Complex, gabbroic dykes and bimodal (basalt–rhyolite) volcanic rocks forming part of the Giles intrusions (Glikson et al., 1996; Sheraton and Sun, 1997) have SHRIMP U–Pb zircon ages clustering near 1070 Ma. Although there are a large amount of analytical data for these and other Giles intrusive rocks (Glikson et al., 1996), these analyses were carried out by XRF, which means that the data for key elements such as Th, Nb, and the REE show poor precision at low levels and cannot be directly compared with data for the Bangemall Supergroup sills produced in this study. Two gabbro sills from the Giles intrusions have been reanalysed by Geoscience Australia, and these data are compared with the 1070 Ma Bangemall Supergroup sill data. Zhao and McCulloch (1993a,b) have reported c. 1070 Ma ages for the Stuart and Kulgera Dyke Swarms in the eastern part of the Musgrave Complex, and dykes of similar age (the Alcurra dykes) have also been reported from parts of the Northern Territory by Edgoose et al. (1993), Scrimgeour et al. (1999), and Close et al. (2003). The average

composition of five Alcurra dykes (Edgoose, C. J., 2003, written comm.) is discussed here. Cowley (1991) has reported on the extent and composition of c. 1050 Ma amygdaloidal basalt flows of the Beda Volcanics in South Australia that were dated at about 1050 Ma by the Rb–Sr isochron method. The average of 40 Beda Volcanics analyses are discussed here.

Relative to the Bangemall Supergroup sills, the two Musgrave dykes are unfractionated, with Mg# near 59, Ni of 205 and 247 ppm, and Cr of 267 and 384 ppm. Both the Alcurra and Beda averages are more fractionated relative to the Musgrave dykes, with lower Mg# (Beda = 52, Alcurra = 31), Ni (Beda = 88 ppm, Alcurra = 72 ppm), and Cr (Beda = 110 ppm, Alcurra = 152 ppm). These data are shown in addition to the least fractionated examples of both the 1070 Ma western Bangemall Supergroup (GSWA 152929) and eastern Bangemall Supergroup (GSWA 171710) sills (i.e. highest Mg#, Ni, and Cr) on Figure 63a. Although there are differences in the absolute concentrations of some elements, the N-MORB-normalized patterns are fundamentally similar in that Nb and P_2O_5 are depleted relative to neighbouring elements, and LFSE and Pb are enriched relative to adjacent elements. The concentrations of REE are broadly similar. Figure 63b shows the average 1070 Ma sill compositions for the western and eastern Bangemall Supergroup in addition to the Beda Volcanics and Alcurra dyke averages and the northeastern Japan arc average. The Alcurra and Beda averages show some aberrant behaviour for some LFSE (e.g. Cs, U, Pb; Fig. 63b), which probably reflects post-magmatic alteration, but overall they have similar patterns to the Bangemall Supergroup sills. Shown for comparison with the 1465 Ma western Bangemall Supergroup, 1070 Ma western Bangemall Supergroup, and 1070 Ma eastern Bangemall Supergroup averages on Figure 63c is a typical arc-tholeiite average (northeastern Japan arc data from Shibata and Nakamura,

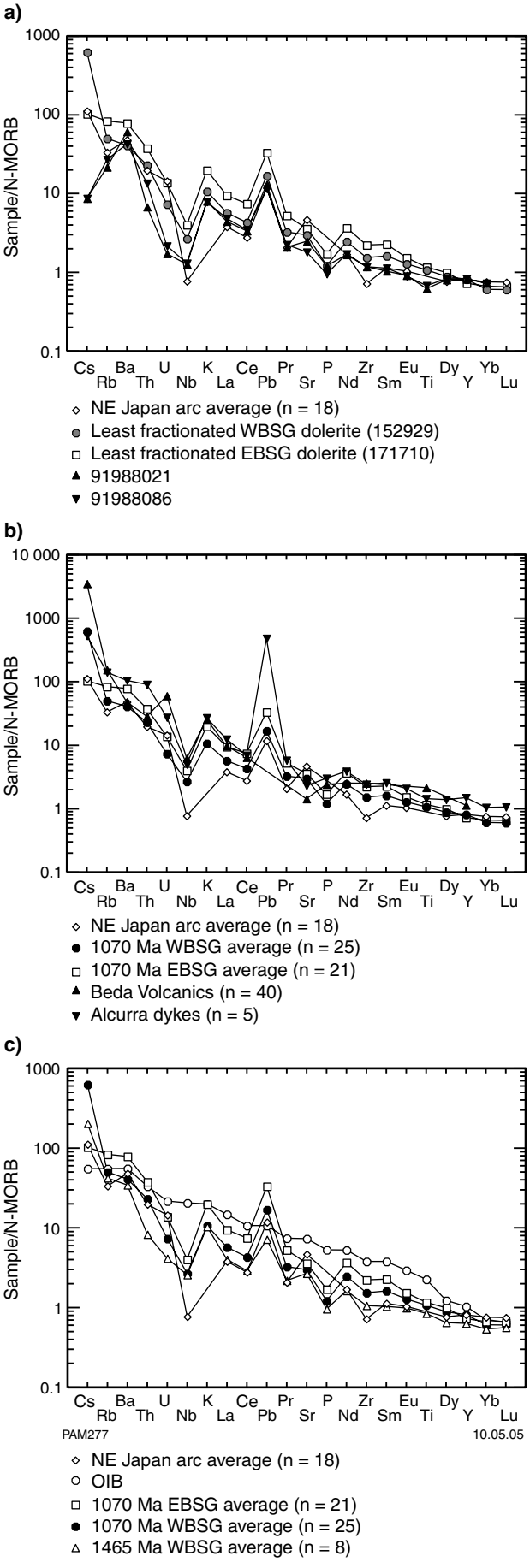

Figure 63. a) N-MORB-normalized patterns for the least fractionated 1070 Ma western Bangemall Supergroup sill sample (GSWA 152929), least fractionated 1070 Ma eastern Bangemall Supergroup sill sample (GSWA 171710), and two type-A dolerite sills (91988021 and 91988086) from the Giles intrusions (Musgrave Complex) initially analysed by Glikson et al. (1996) and reanalysed at Geoscience Australia for this study. Also shown is the average of 18 arc basaltic rocks from the northeastern Japan arc (Shibata and Nakamura, 1997); b) N-MORB-normalized patterns for the average of 1070 Ma western Bangemall Supergroup sill samples, 1070 Ma eastern Bangemall Supergroup sill samples, the Beda Volcanics of South Australia (Cowley, 1991), the Alcurra dykes (Edgoose, C. J., 2003, written comm.), and the northeastern Japan arc basaltic rock average (Shibata and Nakamura, 1997); c) N-MORB-normalized patterns for the average compositions of 1070 Ma western Bangemall Supergroup sill samples, 1070 Ma eastern Bangemall Supergroup sill samples, 1465 Ma western Bangemall Supergroup sill samples, northeastern Japan arc average basaltic rocks (Shibata and Nakamura, 1997), and ocean island basalt (OIB; Sun and McDonough, 1989)

1997) and a typical ocean island basalt (OIB) from Sun and McDonough (1989). The patterns for the Warakurna LIP rocks in Western Australia, South Australia, and the Northern Territory show strong similarities to the arc tholeiite pattern in terms of HFSE depletion (Nb and Zr) and the relative LFSE enrichment (especially the positive Pb anomaly). OIBs typically lack the HFSE depletion (Sun and McDonough, 1989).

Glikson et al. (1996) and Zhao and McCulloch (1993a,b) have also argued that the Giles intrusions and the Stuart and Kulgera Dyke Swarms were derived from a subduction-modified mantle source, with melting initiated by impingement of a mantle plume. As discussed in **Regional and global geodynamics context: a 1070 Ma mantle plume in Rodinia?**, the Bangemall Supergroup sills were emplaced during periods of divergence, and there is no suggestion that these rocks were emplaced at a convergent margin. Supporting evidence for subduction modification of the source for the Bangemall Supergroup sills is provided by Nd model ages (discussed previously); those calculated for the 1465 Ma western Bangemall Supergroup sills show some overlap with the Dalgaringa Supersuite granitic rocks that Sheppard et al. (2004) have argued were emplaced above a north-dipping subduction zone during the Palaeoproterozoic.

There are some isotopic data available for the Warakurna LIP rocks that can shed further light on the mantle source for these rocks. Figure 64 shows εNd(T) for the 1070 and 1465 Ma sills of the Warakurna LIP in addition to εNd(T) data for the broadly coeval rocks of the Giles intrusions (Musgrave Complex; Glikson et al., 1996), and the Kulgera and Stuart Dyke Swarms (Zhao and McCulloch, 1993a). For the Giles intrusions, these include one type-A dyke and three Tollu Group samples comprising one analysis of the Mummawarrawarra Basalt and two analyses of the Smoke Hills Felsic Volcanics. The dyke analysis (εNd = 2.64) does not overlap with data from the 1070 Ma western Bangemall Supergroup or eastern Bangemall Supergroup dolerite sills, but the three analyses from the Tollu Group, which span the interval εNd equals -1.09 – 0.92, overlap with the Warakurna LIP data. Some of the εNd data for the Stuart dykes overlap with Glenayle area dolerite values, whereas the Kulgera dyke analyses are less radiogenic and form a strong overlap with the 1070 Ma western Bangemall Supergroup sill data. Zhao and McCulloch (1993a) have argued that the Nd isotope data show that the Stuart dykes were derived from a more enriched source than the Kulgera dykes. The strong overlap in εNd for the Stuart dykes and the 1070 Ma eastern Bangemall Supergroup (Glenayle) sills indicates that they may have been derived from similar (enriched) sources, which is consistent with the trace element evidence for contamination of some Glenayle samples discussed previously. Similarly, the overlap in εNd of the Kulgera dykes, Musgrave intrusive and extrusive rocks, and the 1070 Ma western Bangemall Supergroup samples is consistent with an isotopically similar source that is depleted relative to the Stuart dykes and the 1070 Ma eastern Bangemall Supergroup source.

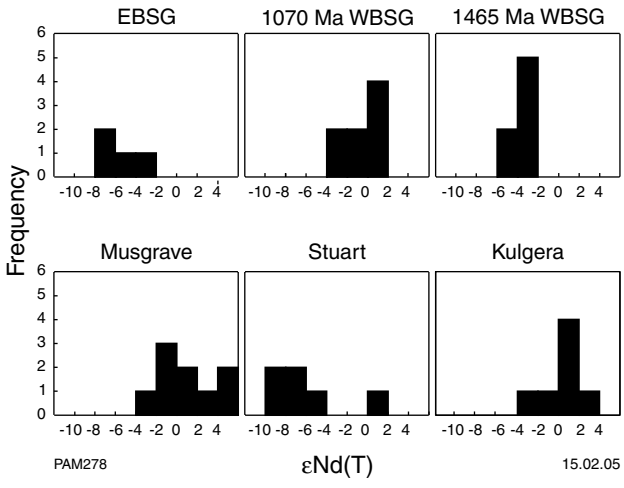

Figure 64. Frequency histogram of εNd(T) for mafic igneous Bangemall Supergroup rocks (this study), 1070 Ma Musgrave Complex igneous rocks (Glikson et al., 1996), and the Stuart and Kulgera dykes (Zhao and McCulloch, 1993a). εNd(T) has been calculated using present-day CHUR values of $^{143}Nd/^{144}Nd$ equals 0.512638 and $^{147}Sm/^{144}Nd$ equals 0.1967

Regional and global geodynamics context: a 1070 Ma mantle plume in Rodinia?

Introduction

Intraplate tectono-magmatic phenomena, including the emplacement of layered intrusions, sill complexes, giant dyke swarms, anorogenic (hotspot) volcanism, oceanic plateaus, rifting processes, basin formation, and geomorphological features such as uplift, have been attributed to the ascent of mantle plumes that rise either from the 660 km discontinuity or from the core–mantle boundary and impinge onto the lithosphere (Schubert et al., 2001; Davies, 1999; Courtillot et al., 2003). The mantle plume hypothesis is a theory that attempts to explain the vast extent of coeval igneous provinces and anomalous thermal anomalies in convecting mantle. The plume theory is consistent with experimental studies and seismic tomography (Schubert et al., 2001; Montelli et al., 2004). In addition, the assembly of supercontinents and their subsequent breakup are inferred to relate to the reorganization of the deep mantle-convection system (Ziegler, 1993) and the arrival of mantle plumes or superplumes (Pirajno, 2000 and references therein; Dalziel et al., 2000). Mantle plume activity leading to the breakup of supercontinents results in regional tensional stresses and the development of rift basins, as well as the emplacement of LIPs (White and McKenzie, 1995; Coffin and Eldholm, 1992, 1994; Courtillot et al., 1999; Corti et al., 2003). Examples of links between mantle plumes and the geodynamics of supercontinent assembly and breakup have been discussed in Condie (2001), Dalziel et al. (2000), and Li et al. (1999, 2003). Barley and Groves (1992) and Barley et al. (1997, 1998) proposed a relationship of mantle plumes to supercontinent aggregation and dispersal, and the distribution of ore

deposits through geological time. In summary, the arrival of mantle plume(s) is considered to be the driving force for the rifting of a supercontinent and the associated breakup magmatism. However, the plume theory is not unchallenged. Alternative models have been proposed whereby intraplate magmatism (or a hotspot) would be related either to plate stresses that cause fracturing and volcanism, or to shallow mantle convection (Anderson, 1994; King and Anderson, 1998; Sheth, 1999; <http://www.mantleplumes.org>).

Wingate et al. (2004) reported on the 1070 Ma Warakurna LIP, which includes the sill complexes of the western and eastern Bangemall Supergroup, the mafic–ultramafic Giles intrusions and associated felsic intrusive and extrusive rocks, and the Alcurra Dyke Swarm. The Warakurna LIP extends in an approximately east–west direction for about 2400 km; its width is uncertain, but based on present evidence it could be up to 800 km wide and cover a total area of approximately 1.5 million km^2 (Wingate et al., 2004). The authors of this Report propose that the emplacement of the Warakurna LIP was the result of the impingement of a mantle plume at about 1070 Ma at the meeting point of the West Australian, South Australian, and North Australian cratonic blocks of Myers et al. (1996). This is schematically shown as the northwest to south Paterson–Gawler trend, the northeast Albany–Fraser trend and the west-northwest Capricorn trend (Figs 65a and 66b; see also the reconstructions in Wingate and Evans, 2003; Karlstrom et al., 2001; Piper, 2000).

A number of features have been recognized in the Warakurna LIP that suggest the involvement of a mantle plume. These include the large areal extent and volume of the coeval western and eastern Bangemall Supergroup sills and the Giles layered intrusions (for which a mantle plume link was proposed by Glikson et al., 1996); bimodal magmatism (the Tollu Group volcanic and granitic rocks; Glikson et al., 1996; Scrimgeour et al., 1999); and the overall continental tholeiitic composition of the mafic rocks, and the geochemical parameters, including the REE patterns (see **Major and trace element variations; Rare-earth element chemistry**). One of the diagnostic features of mantle plume magmatism is the presence of high-temperature lavas (picrites and komatiites; Kerr et al., 2000), but these are lacking probably due to the low level of exposure of the Warakurna LIP. In addition, the impingement of a mantle plume at the base of the lithosphere and emplacement of LIPs results in thermal and dynamic uplift of the crust, thereby displacing seawater and modifying sea levels. Domal uplifts can exceed 2 km (Rainbird and Ernst, 2001) and affect patterns of sedimentation. Subsidence follows due to thermal decay and results in the inception of intracontinental basins. Assuming that the focus of the Warakurna LIP was in the Musgrave region (Giles intrusions), then it is likely that the Centralian Superbasin (Walter et al., 1995) could have formed as a large sag resulting from crustal thinning over a mantle plume (Lindsay, 2002; Pirajno, 2004b).

A Rodinia link?

The age of the Warakurna LIP is close to the timing for the assembly of the Rodinia supercontinent (Pisaversky et al., 2003a,b). Reconstructions of the Late Mesoproterozoic Rodinia supercontinent are essentially based on the matching of Proterozoic orogenic belts that exhibit similar geology and geochronology, and on palaeomagnetic data. Orogenic belts that have isotopic ages of c. 1300–1100 Ma are correlated with the Grenville Orogen, and together form an intracontinental collisional and accretionary orogenic zone nearly 20 000 km long (Hoffman, 1991). This orogenic zone includes the Albany–Fraser and Paterson Orogens in Australia, the eastern margin of the Dharwar Craton (Eastern Ghats, India), Sri Lanka, Madagascar, the northern margin of East Antarctica, the margins of the Kalahari province (Namaqua–Natal Orogen), the eastern side of the Congo Craton, the southern margins of Laurentia (Grenville Orogen proper), and the northern margin of Amazonia (the Rio Branco, Parecis, Sierra Pampeana, Patagonia, and Pre-Cordillera orogenic zones). Concomitant with, or after collision, rifting occurred in a number of places, in a direction almost perpendicular to the collision line. An example of this is the Midcontinent Rift System in North America, which is of Rodinian age (c. 1100 Ma). The Grenvillian collisions culminated at about 1000 Ma and resulted in the joining of continental blocks to form the Rodinia supercontinent (Windley, 1995).

Various Rodinia configurations have been proposed, based on palaeomagnetic data (Moores, 1991; Powell et al., 1993; Unrug, 1996, 1997; Li and Powell, 2001). More recently, attention has focused on Australia–Laurentia reconstructions within the Rodinia supercontinent, for which the integration of geochronological and palaeomagnetic data permit at least three possible configurations, namely: Southwest United States – East Antarctic or SWEAT (Moores, 1991; Dalziel, 1991; Hoffman, 1991), Australia–Western United States or AUSWUS (Karlstrom et al., 1999; Burrett and Berry, 2000), and Australia–Mexico or AUSMEX (Wingate et al., 2002; Pisarevsky et al., 2003b). Figures 65b and 67 show two Rodinia reconstructions, one from Unrug (1996; 1997) and the other based on the AUSMEX configuration from Wingate et al. (2002) and Pisarevsky (2003a,b). On these figures are plotted extension zones, rift structures, and associated LIPs within the age range of 1100–1000 Ma that include the Warakurna LIP in Australia (Wingate et al., 2004), the Umkondo LIP in the Kalahari Craton (Hanson et al., 1998), and the Keweenawan LIP in the previously mentioned Midcontinent Rift System in North America (Okajangas et al., 2001). There are other mafic igneous provinces, not shown on Figures 65b and 67, which are within the same age range, such as the Southwestern USA diabase province (1090–1060 Ma), the Laanila–Kautokeino event in the Fennoscandian shield, and the Bahia dyke swarms in Brazil (1100–1000 Ma; possibly linked to plume arrival and breakup of the Congo – São Francisco Craton; Ernst and Buchan, 2001).

As mentioned above, the assembly of the Rodinia supercontinent is thought to have taken place at about 1100 Ma and to have involved collisional tectonics. The breakup is assumed to have begun at about 800–750 Ma (Pisarevsky et al., 2003a,b and references cited therein). The latest palaeomagnetic data suggest that the

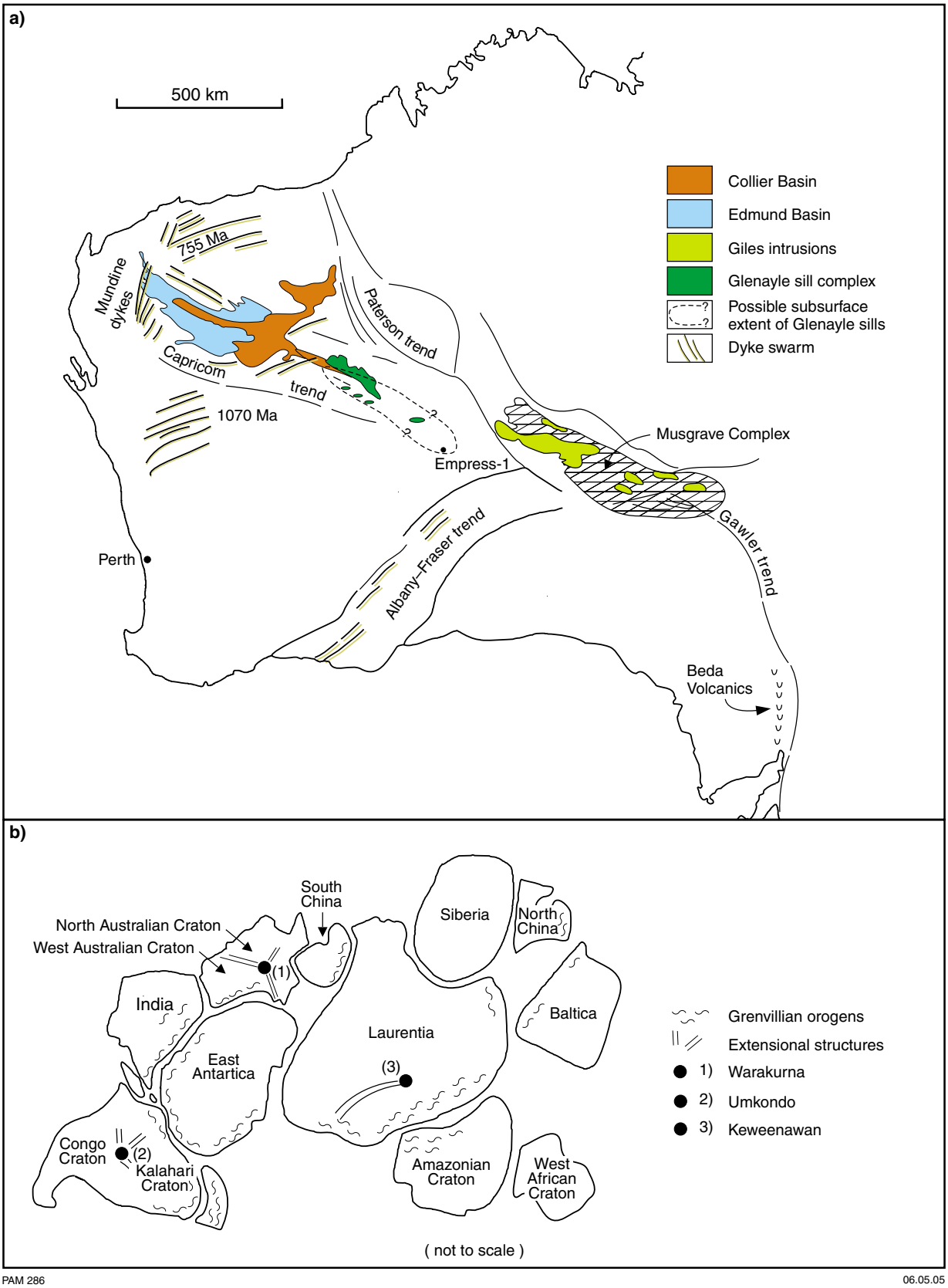

Figure 65. a) Distribution of the Glenayle sill complex and Giles intrusions, and major structures at the meeting point of the west-northwest Capricorn trend, northeast Albany–Fraser trend and northwest to south Paterson–Gawler trend; b) Position of the Warakurna LIP on a possible failed rift structure between the North and West Australian Cratons, the Midcontinent Rift System (Keweenawan LIP) in Laurentia, and the Umkondo LIP in the Congo Craton, on a Rodinia assembly at c. 1000 Ma (after Unrug, 1996)

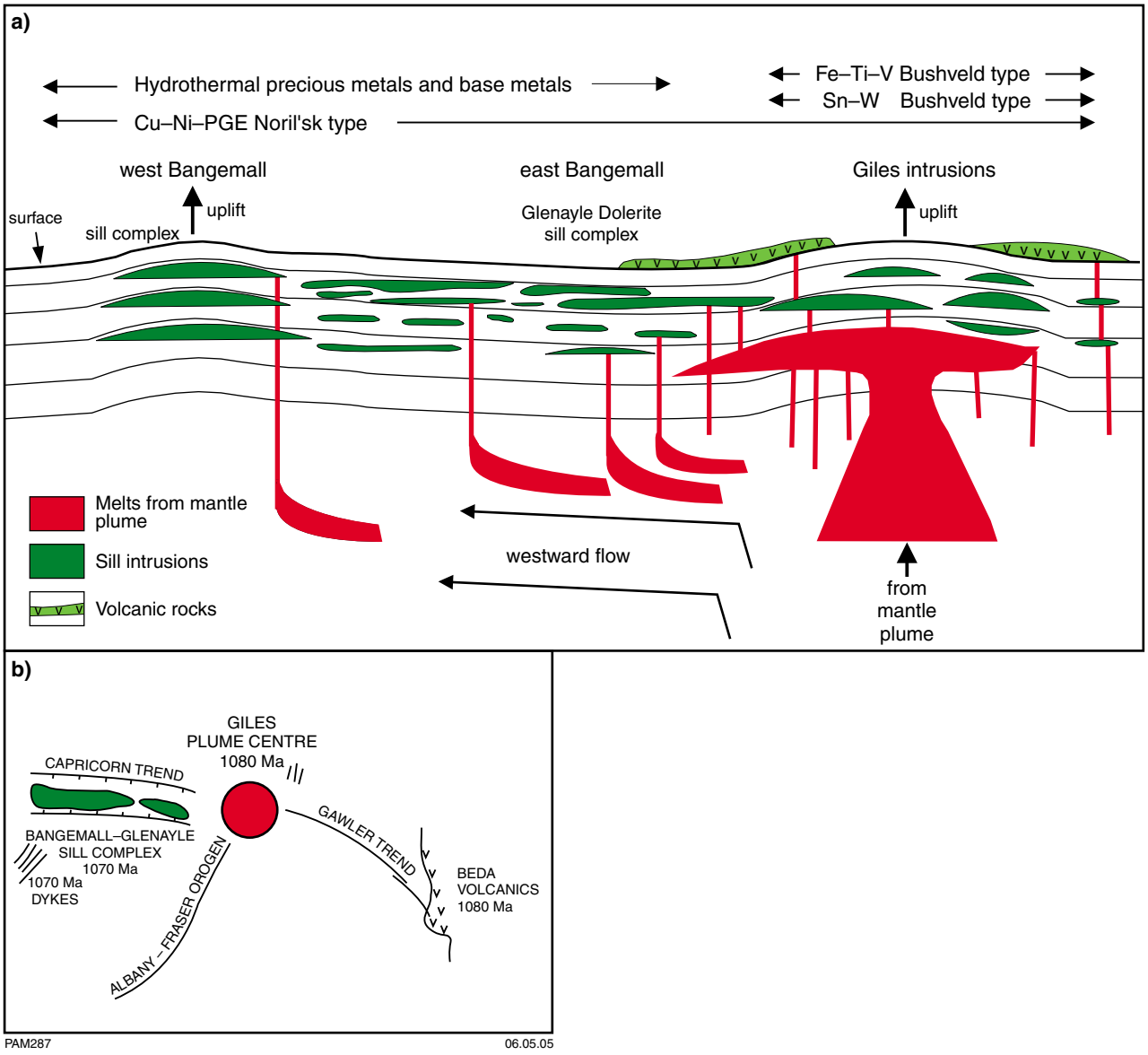

Figure 66. a) Schematic longitudinal section (not to scale) depicting a working model illustrating the regional architecture of the Warakurna LIP that is characterized by a series of sill complexes (western and eastern Bangemall Supergroup). It has been formed by the westward flow from a plume head, above which are the layered Giles intrusions of the Musgrave Complex. In places, basaltic melts originating from these underlying intrusions erupted at the surface forming lava fields, the remnants of which are now represented by volcanic rocks of the Tollu Group. Also shown is the distribution of potential magmatic and hydrothermal deposits in the Warakurna LIP; b) schematic diagram of the postulated structures that may define a failed rift system that extends from the plume head (Giles intrusions) westward (Bangemall Supergroup sill complexes) to the southeast towards the coeval Beda Volcanics and to the southwest along the margin of the Albany–Fraser Orogen

Australia–Laurentia configuration is likely to have been in accordance with the AUSMEX hypothesis (Fig. 67) in which the Kalahari Craton, with the Umkondo LIP, was located to the west of Australia and the Keeweenawan LIP to the east (Pisarevsky et al., 2003a). In the AUSMEX configuration, Pisarevsky et al. (2003a) have proposed that the Kalahari – East Antarctica plates (Dronning Maud Land Craton) collided with the Australia–Mawson Craton between 1100 and 1000 Ma. As the emplacement of continental LIPs requires extension and rifting, there may be an apparent contradiction because the geodynamics of the Rodinia assembly at about 1000 Ma involved collisional tectonics and therefore compressional stresses. This apparent contradiction could be explained with one of three possibilities: that the collision zones (e.g. Grenvillian orogenic belts) were associated with 'behind-collision' extension, in a fashion similar to back-arc rifting; the reorganization of plate boundaries and kinematics following major collisions, with subsequent build-up of extensional stresses; or plume-modified orogeny in which collision tectonics and plume-related magmatic events are interrelated. With the available evidence and the

Figure 67. Distribution of the Warakurna (1), Umkondo (2), and Keweenawan (3) LIPs on a 1070 Ma Rodinia reconstruction (modified from Pisarevsky (2003a,b)

uncertainty of the Rodinia reconstructions, it is difficult to assess which of the three possibilities is correct.

The Warakurna, Umkondo, and Keweenawan LIPs were formed through decompression melting following the impingement of mantle plumes that were active in the early stages of the Rodinia assembly at about 1000 Ma. These plumes may have contributed to the weakening and thinning of the lithosphere that led to the breakup of the supercontinent at 800–750 Ma, with reactivation or continuing activity of at least one mantle plume beneath south-central Australia at about 800 Ma (Gawler Craton and Gairdner Dyke Swarm; Zhao et al., 1994; Wingate et al., 1998). This also suggests that global plate geodynamics may have a bearing on the rise of mantle plumes (passive model; Bott, 1995), as opposed to cases in which the impingement of mantle plumes onto the lithosphere is a primary cause for extension and rifting (active model; Bott, 1995; Ruppel, 1995) as is the case for the Afar Triangle in the East African Rift System (Le Pichon and Francheteau, 1978; Tesfaye et al., 2003).

Whether there were separate mantle-plume events for the emplacement of the Warakurna, Umkondo, and Keweenawan LIPs and the other large mafic provinces mentioned above, or whether these were the result of a superplume event, remains to be established. There is, however, evidence of a superplume event responsible for the Permian–Triassic flood basalts (Siberian, Emeishan, and other similar age volcanic provinces in Asia) that affected a huge area in central-northern Asia of about 4000 × 3000 km (Nikishin et al., 2002). Similarly, the Karoo–Ferrar LIP extends for about 4000 km from East Antarctica to South America. It is therefore possible that the emplacement of the Warakurna – Umkondo – Keweenawan LIPs, if the AUSMEX configuration is accepted, may have been the result of a superplume event at about 1100–1070 Ma.

The mineralization potential of the Warakurna LIP

The recognition of the Warakurna LIP in west-central Australia, and its assumed relationship with mantle plume activity, has important implications for the mineral potential of the region. There are three main groups of ore deposits that can be linked, either directly or indirectly, to mantle plumes: primary magmatic, magmatic-

hydrothermal and hydrothermal ore deposits (Pirajno, 2000, 2004a,b).

Primary magmatic-ore deposits

There are two principal types of magmatic mineral deposits that are associated with extensional tectonics and mantle plumes: mafic–ultramafic-related Cu–Ni–PGE sulfides and mafic-related Fe–Ti–V oxides.

Mafic–ultramafic-related Cu–Ni–PGE sulfides

Magmatic sulfide Cu–Ni–PGE deposits are found in differentiated layered mafic–ultramafic intrusions. Layered intrusions are commonly found in intracontinental rifts and are related to flood basalts. Typically, layered intrusive complexes comprise dunite, peridotite, pyroxenite, norite, troctolite, and gabbro. Sulfides, both massive and disseminated, tend to form lenses near the base of the layered complex or in the footwall below the main intrusion. Deposit styles comprise massive sulfides, sulfide-matrix breccias, interstitial sulfide networks, and disseminated sulfides. Sulfide veins and dissemination commonly penetrate the footwall rocks. Ore elements include Ni, Cu, PGE, Co, Se, Te, and Au. The more common ore minerals include pentlandite, chalcopyrite, cubanite, millerite, pyrrhotite, various PGE minerals, and pyrite. The depositional process involves multiple injections of melt into the upper crust in tensional environments associated with rifting. Contamination of the magma is an important factor in order to attain the sulfur saturation that is necessary to cause precipitation of sulfides.

Examples of mafic–ultramafic-related Cu–Ni–PGE deposits are the well-known Noril'sk and Talnakh intrusions of the Siberian Traps (Naldrett, 1992; Duzhikov et al., 1992; Naldrett and Lightfoot, 1993; Naldrett et al., 1995; Arndt et al., 2003). In these deposits, detailed chemostratigraphy and computer modelling have demonstrated that the addition of about 23% tonalitic crust and minor gabbro (2.5%) to the Mokulaevsky magma can be used to explain the chemistry of the Nadezhdinsky unit, which is characterized by higher SiO_2 and Ce/Yb that are indicative of some crustal contamination (Lightfoot et al., 1990). A feature of the Nadezhdinsky unit is that it is relatively depleted in chalcophile elements (e.g. Cu) and PGEs, with correspondingly higher Cu/Zr, La/Sm, and SiO_2 (Lightfoot and Hawkesworth, 1997). The model proposed is that ingestion of even small amounts of crustal material can cause a sufficiently large decrease in the liquidus temperature to promote precipitation of sulfides and PGEs, thus producing a parent magma relatively depleted in chalcophile elements. Although there is some debate about the sulfur budget, Lightfoot and Hawkesworth (1997) have argued that the assimilant need not be sulfur rich — the key aspect is a reduction in the liquidus temperature.

Mafic-related Fe–Ti–V oxides

Magmatic deposits of Ti–Fe(–V) oxides consist of layers and lenses containing massive, disseminated titanomagnetite or vanadium magnetite, with minor amounts of ilmenite and chromite, in differentiated gabbroic intrusions. The host rocks are mainly norite, gabbro–norite, and troctolite. The mineralized layers are usually present near or at the tops of the intrusions. Mafic–ultramafic pipes may be associated with the intrusions. The principal ore mineral is titanomagnetite and/or vanadium magnetite. Associated minerals are ilmenite, hematite, spinel, and sulfide minerals such as pyrite, pyrrhotite, and chalcopyrite. The Fe- and Ti-oxide phases form by crystal settling or filter pressing during crystallization of the gabbroic magmas and result in layers and segregations. Examples of this type of mineralization can be found in the 2.8 Ga Windimurra Complex in Western Australia (Mathison and Ahmat, 1996), and the vanadiferous magnetite layers in the Upper Zone (gabbro) of the 2.05 Ga Bushveld Complex in South Africa (Eales and Cawthorn, 1996). Vanadiferous and titaniferous magnetite layers are present in gabbro units of the Giles intrusions (Daniels, 1974).

Magmatic-hydrothermal ore deposits

Intracontinental anorogenic and alkaline magmatism is commonly associated with large igneous provinces (e.g. Deccan, Paraná–Etendeka, Karoo; Pirajno, 2000, 2004a).

Anorogenic granitoids host or are associated with a great variety of ore deposits that include magmatic and hydrothermal types and combinations of the two (Pirajno, 1992). Anorogenic magmas are enriched in incompatible elements (e.g. Ti, P, Y, Nb, K, Th, U, F, Ba, and REE) and produce peraluminous and peralkaline granitoids that commonly contain greisen or late-magmatic subsolidus Sn, W, Zn, Cu, U, and Nb mineralization (Pirajno, 1992, 1994). The giant Olympic Dam Cu–Au–U–REE–Fe deposit in South Australia is genetically related to a 1.6 Ga anorogenic granite (Roxby Downs Granite; Reynolds, 2001), and is part of a recently recognized class of hydrothermal iron oxide–copper–gold deposits (Hitzman et al., 1992). Another giant deposit of the same class is the REE–Nb–Fe Bayan Obo deposit in Inner Mongolia, which is also genetically related to anorogenic magmatism in a rift setting (Drew et al., 1990).

Intracontinental alkaline magmatism usually takes place during the early phases of rifting events in which direct links are assumed with melt generation by mantle plume upwellings beneath thinned lithosphere. Anorogenic alkaline complexes and carbonatites are present in many LIPs (e.g. Deccan Traps, Siberian Traps, Paraná–Etendeka, Keweenawan). The Late Jurassic – Early Cretaceous Damaraland alkaline igneous province in Namibia is linked to the Tristan da Cunha plume in the South Atlantic Ocean, from which the Paraná–Etendeka flood basalts were generated (Pirajno, 1994; Pirajno et al., 2000; Trumbull et al., 2000). The alkaline rocks of the province may be the result of lithospheric melting in response to the thermal perturbation caused by this plume (Ewart et al., 1998). Ore deposits that are associated with alkaline magmatism include magmatic-hydrothermal Sn–W, REE, U, Mo, Cu, Fe, and P (Pirajno, 1992, 1994).

Giant hydrothermal systems linked to mantle plumes and LIPs

Hydrothermal ore deposits can be formed as a result of heat transfer due to the emplacement of voluminous mafic melts into the crust. This heat energy is capable of activating giant hydrothermal systems, typically in rift settings, and resulting in a wide range of hydrothermal ore deposits (Pirajno, 2000, 2004b). The high heat flow associated with the Yellowstone hot spot (western USA) gave rise to circulation of hydrothermal fluids that may have been responsible for the famed Carlin-style Au deposits in Nevada (Oppliger et al., 1997).

The exploration potential of the Warakurna LIP in Western Australia

Without taking into account the coeval Beda Volcanics on the margin of the Gawler Craton in South Australia (Cowley, 1991), the Warakurna LIP extends over a vast region from the Musgrave Complex to the western Bangemall Supergroup, a distance of approximately 2400 km. On the basis of the summary of ore deposit types reviewed above, the exploration potential of the Warakurna LIP can be considered in terms of primary magmatic ores in mafic–ultramafic layered complexes, sill complexes (Noril'sk type), anorogenic complexes, and hydrothermal deposits.

Layered intrusions and sill complexes

The Giles intrusions comprise a series of mafic–ultramafic layered rocks (Daniels, 1974; Glikson et al., 1996) that contain Ni–Cu–PGE sulfides (e.g. the Babel and Nebo prospects; Baker and Waugh, 2003). The area also contains nickel laterite deposits (Goode, 2002; Acclaim Exploration NL, 2003).

The Giles intrusions were emplaced at about 1080 Ma, forming a series of intrusive sill-like and sheet-like bodies that extend roughly for 550 km along an east–west trend, with an aggregate north–south extent of over 100 km, from Western Australia into South Australia and the southwestern corner of the Northern Territory. The Giles intrusions were emplaced at several crustal levels (Fig. 66a). Aspects of the geology of the Giles intrusions have been discussed by Goode and Krieg (1967), Nesbitt et al. (1970), Daniels (1974), Gray and Goode (1989), Myers (1990), Major and Connor (1993), and Glikson et al. (1996). The Giles intrusions comprise almost the full range of intrusive mafic and ultramafic rocks such as gabbro, anorthosite, troctolite, norite, clino- and orthopyroxenite, and peridotite.

The sill complexes of the western and eastern Bangemall Supergroup have received little or no exploration attention. Morris et al. (2003) considered the exploration potential of sections of the Glenayle Dolerite for Ni–Cu and PGE mineralization on the basis of regolith geochemistry, field mapping, and geophysical data. These authors correlated the presence of a large, positive gravity high with the Weld Spring Dolerite Member of the Glenayle Dolerite, which has been interpreted as a laccolith about 36 km across and 3 km thick. Using an additive index approach and element associations, Morris et al. (2003) were able to show that regolith materials in the same area contain elevated chalcophile index (As + Sb + Bi +Mo + Ag +Sn + W + Se) values and Cr contents. These results suggest the possibility of Noril'sk-type Ni–Cu–PGE mineralization. Data from the Noril'sk–Talnakh area (Lightfoot et al.,1990) have been plotted in terms of Cu versus Th/Nb (Fig. 68a), which illustrates the contamination argument and the effect on chalcophile element concentrations. The Nadezhdinsky lavas have higher Th/Nb and lower Cu contents due to contamination by tonalitic crust (Lightfoot et al., 1990). Sill analyses from the Bangemall Supergroup (Fig. 68b) show that the 1465 Ma western Bangemall Supergroup

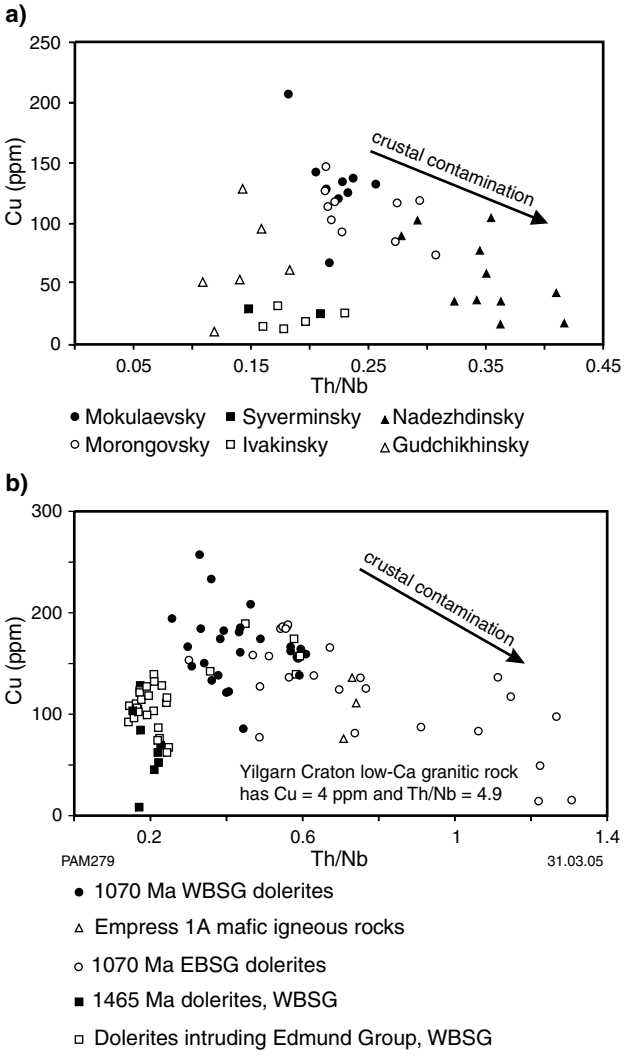

Figure 68. Bivariate plots showing: a) Cu versus Th/Nb for samples of various lava units from the Noril'sk area (Lightfoot et al., 1990). The vector shows the likely direction of crustal contamination towards the Nadezhdinsky lavas; b) Cu versus Th/Nb for the Bangemall Supergroup sill samples

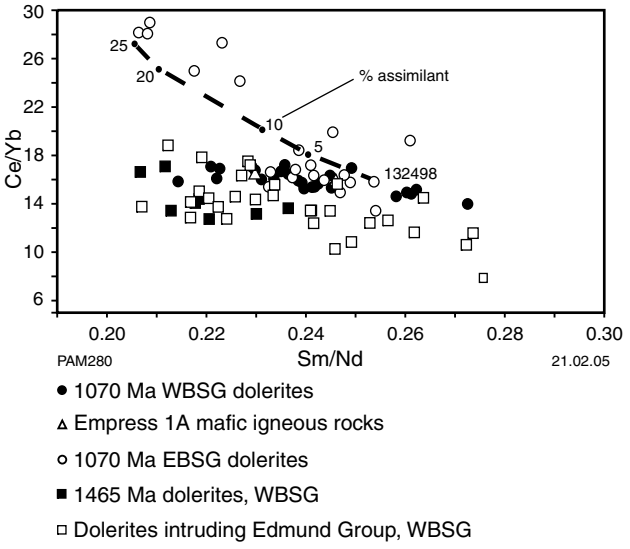

Figure 69. Bivariate plot showing Ce/Yb versus Sm/Nd for the Bangemall Supergroup sills. The vector has been calculated assuming combined assimilation and fractional crystallization (De Paolo, 1981; using parameters shown in Table 7) between GSWA 132498 and Yilgarn Craton low-Ca granitic rock. Numbers are percent fractionation, which is twice the rate of assimilation

sills show little variation in Th/Nb, and Cu concentrations mostly range between 50 and 150 ppm. The 1070 Ma western Bangemall Supergroup sills show some scatter in Cu concentrations, and wider variations in Th/Nb. The most extreme variations are shown in the 1070 Ma eastern Bangemall Supergroup sills, where Cu decreases and Th/Nb correspondingly increases. There is a clear analogy with the data for the Noril'sk–Talnakh area for the low- and high-Th/Nb sills found in the Glenayle area.

This argument can be further extended by examining the extent to which crustal contamination can account for the chemistry of the high-Th/Nb eastern Bangemall Supergroup sills. Bangemall Supergroup data have been plotted in terms of Ce/Yb versus Sm/Nd (Fig. 69). On this diagram, Ce/Yb should increase and Sm/Nd should decrease with increasing crustal contamination. Most crustal rocks have Ce/Yb less than 25 (Rudnick and Fountain, 1995; Taylor and McLennan, 1985), which rules them out as possible contaminants for the 1070 Ma eastern Bangemall Supergroup sills. However, the Yilgarn Craton low-Ca granitoid average has high Ce (140 ppm), low Yb (1.1 ppm), and correspondingly high Ce/Yb (127.3), as well as low Sm/Nd (0.12). Assimilation/fractional crystallization (De Paolo, 1981) modelling, using the parameters in Table 7, shows that assimilation of about 8–15% Yilgarn Craton low-Ca granitoid, assuming an assimilation/fractionation ratio of 0.5 and a crystal extract of 50% clinopyroxene and 50% plagioclase, produces a trend that broadly parallels that of the 1070 Ma eastern Bangemall Supergroup high-Th/Nb sills. The assimilation/fractionation ratio of 0.5 reasonably assumes twice as much fractionation as assimilation, and the 50:50 ratio of plagioclase to clinopyroxene crystal extract is consistent with the petrography of dolerites. Modelling, as discussed earlier, indicates a small role for olivine crystallization, which is not considered here. The limited amount of isotope data available are consistent with a crustal contamination model, in that the Glenayle Dolerite sill samples GSWA 152695 and 152661 have high Th/Nb and $^{87}Sr/^{86}Sr$, but low $^{143}Nd/^{144}Nd$.

As mentioned above, a combination of detailed geological mapping, regolith geochemistry, and geophysical data (aeromagnetic and gravity) can provide useful vectors for magmatic sulfide deposits. The western Bangemall Supergroup with its thick mafic sill sequence would be a prime exploration target for Ni–Cu–PGE sulfides. Figure 66a shows an idealized longitudinal cross section extending from the western Bangemall Supergroup to the Musgrave Complex in the east. This is a model that schematically illustrates the overall geometry of the sill complexes, the Giles mafic–ultramafic intrusions and their allied extrusive rocks, and the spatial relationship to possible ore deposits.

Anorogenic magmatism associated with the emplacement of the Giles intrusions

The Giles layered intrusions are associated in space and time with felsic intrusive and extrusive rocks (Bentley

Table 7. Parameters used in assimilation/fractional crystallization modelling

	Ce (ppm)	*Yb (ppm)*	*Ce/Yb*	*Sm (ppm)*	*Nd (ppm)*	*Sm/Nd*
GSWA 132498	54.3	3.41	15.9	7.54	29.75	0.25
YC low-Ca granitoid	140	1.1	127.3	5.2	43	0.12
Mineral/melt distribution coefficients[(a)]						
Clinopyroxene	0.15	0.62	–	0.5	0.31	–
Plagioclase	0.12	0.067	–	0.067	0.081	–
Bulk distribution coefficient	0.135	0.3435	–	0.2835	0.1955	–

SOURCES: De Paolo (1981)
(a) Rollinson (1993, table 4.1)

NOTES: YC Yilgarn Craton
Ratio assimilant:crystals = 0.5

Supergroup) in addition to various types of 1.09 – 1.06 Ga within-plate granitic rocks such as the Angatja Granite, the 1.07 Ga Hull Granite Suite, and a 1.07 Ga rapakivi granite (Scrimgeour et al., 1999; Close et al., 2003). The origin of these granites has been attributed to either crustal melting due to the intrusion of mafic–ultramafic melts or a combination of crustal assimilation and fractional crystallization (Sun et al., 1996). This association is very important because the relationship of these felsic rocks with the Giles mafic–ultramafic intrusions may be similar to that of the Layered Suite of the Bushveld Complex and the Lebowa Granite Suite and the extrusive felsites of the Rooiberg Group in South Africa (Pirajno (2000) and references therein). These felsic rocks are genetically, spatially, and temporally associated with the Bushveld Complex, and are well endowed with a wide range of hydrothermal ore deposits ranging from greisen-style and breccia pipes with Sn–W to epithermal- and mesothermal-lode Au (Pirajno, 2000). Similar types of ore deposits could exist in the Musgrave region in Australia.

Giant hydrothermal systems

The Edmund and Collier Basins developed in an intracratonic setting over the site of the Capricorn Orogen between c. 1640 and 1000 Ma (Martin et al., 1999; Martin and Thorne, 2000, 2001). The geodynamic evolution of the Edmund and Collier Basins is poorly known, but it is possible that the history of these basins began with either the reactivation of basement faults as a result of far-field stresses, or intracontinental rifting along a zone of pre-existing structural weakness, possibly determined by the buried suture between the Pilbara and Yilgarn Cratons. This would be the same zone of structural weakness exploited by the flow of mantle plume material from the assumed plume head beneath the Giles intrusions (see Fig. 66a). This lateral flow would have resulted in the intrusion into the Edmund and Collier Groups of the numerous dolerite sills and dykes of tholeiitic composition that now form the western and eastern Bangemall Supergroup sill complexes.

Mineralization in the Edmund and Collier Basins has been reviewed by Marston (1979), Muhling and Brakel (1985), and Cooper et al. (1998). Structurally controlled mineralization, including base-metal and precious-metal hydrothermal veins and lodes of Cu, Pb–Zn–Ag, and Au is common (Pirajno, 2004b, figure 6). The buried Abra stratabound Pb–Cu–Ba(–Ag–Au–W) deposit (Collins and McDonald, 1994), located within an easterly trending rift basin, exhibits hydrothermal alteration assemblages and patterns that suggest that this deposit may be of the iron oxide–copper–gold class referred to above, and a mantle plume relationship has been suggested for this deposit (Pirajno, 2000, 2004a).

Pirajno (2004b), in reviewing the metallogeny in the Capricorn Orogen, proposed that the origin of the structurally controlled hydrothermal vein and lode deposits in the Edmund and Collier Basins is linked to the large-scale circulation of fluids heated by the emplacement of the western and eastern Bangemall Supergroup sill complexes. The mantle plume hypothesis considerably enhances the prospectivity of the Edmund and Collier Basins, not only for Noril'sk-type Cu–Ni–PGE sulfide mineralization, but also for Olympic Dam-style iron oxide–copper–gold and for bonanza-type lode deposits.

Discussion

A simplified version of the major structural trends in central-western Australia and around the region of the Warakurna LIP and Giles mafic–ultramafic intrusions is shown in Figure 66b. If a mantle plume impinged onto the lithosphere at c. 1070 Ma beneath the present-day Musgrave Complex, then this region represents a hotspot junction where a failed rift system was formed at the meeting point of the North Australian, South Australian, and West Australian Cratons (a type of r–r–r rift system as discussed in Burke and Dewey, 1973) as shown in Figures 65 and 66b. A large proportion of these rift structures are now buried beneath the Officer and Eucla Basins, with the Musgrave and Bangemall regions being exposed through later uplifts such as the 560–520 Ma Petermann Orogeny and the 1000 Ma Edmundian Orogeny. The mineral resources of this vast region remain by and large unknown, yet by analogy with rift-related tectonic settings elsewhere, such as the Limpopo–Sabi province in South Africa and the Damara Orogen in Namibia (Pirajno, 1998, 2000), and the Midcontinent Rift System in North America (Nicholson et al., 1992), the Bangemall–Musgrave area should be a prime exploration target for an extensive range of ore deposit types.

Conclusions

This Report has focused on resolving whether the Bangemall Supergroup sills could be chemically fingerprinted, whether feeder systems could be identified, whether chemistry could help in identifying the relative contributions of mantle and crust to sill composition, and whether palaeomagnetism was a robust dating tool. The recognition that isolated occurrences of mafic igneous rocks found over a distance of about 1300 km in Western Australia are part of the same igneous event is the cumulative result of detailed regional mapping (with subsequent stratigraphic revision), the application of SHRIMP U–Pb zircon and baddeleyite geochronology to the direct dating of sills and detrital zircon from country rocks, and the discovery that a number of mafic sills showed the same palaeomagnetic declination.

The average composition of different sill groupings is shown in Table 3. The majority of Bangemall Supergroup sills are fractionated in terms of Mg#, Ni, and Cr contents, and show a limited range in SiO_2. Although sills of different age lie on similar element versus Mg# trends for some elements, the 1465 and 1070 Ma sills in the western Bangemall Supergroup have different concentrations of Zr, Th, U, Cr, Ni, Mn, Cu, Ga, Sn, and Rb at similar Mg#, and different incompatible-element ratios (e.g. Th/Nb and Zr/P_2O_5). As these ratios are constant over a wide Mg# range, it is likely that they are indicative of the mantle source. The 1465 and 1070 Ma sills are also different in terms of REE chemistry. The older sills have lower total

REE contents, flatter REE patterns, greater degrees of LREE depletion, and small positive Eu/Eu^* compared to small negative Eu/Eu^* for the 1070 Ma sills.

According to available geochronology, the sills intruding the Edmund Group could belong to either the 1465 or 1070 Ma events. Of 31 analyses from these sills, all but five have similar chemistry to the 1465 Ma western Bangemall Supergroup sills. As sills intruding the Collier Group all belong to the 1070 Ma event, this suggests a close temporal relationship between sill emplacement and sedimentation — old sedimentary rocks are largely intruded by old sills and young sedimentary rocks by young sills.

Most 1070 Ma eastern Bangemall Supergroup sills, and mafic igneous rocks from the Empress 1A drillhole, have identical chemistry to the 1070 Ma western Bangemall Supergroup sill samples, suggesting that, at that time, a compositionally uniform mantle source existed beneath the Bangemall Supergroup. Some 1070 Ma eastern Bangemall Supergroup sill samples have notably higher LREE, LFSE, and SiO_2, as well as elevated incompatible-element ratios such as Th/Nb. As samples with varying degrees of LREE and LFSE enrichment are found close together, there is a case for localized crustal contamination. Assimilation/fractional crystallization modelling shows that sills with higher LFSE, LREE, and SiO_2 contents can be explained by about 10% contamination by Yilgarn Craton granitic rock, coupled with about 20% fractional crystallization of clinopyroxene and plagioclase. For these sills, Cu decreases with increasing Th/Nb, and this localized contamination may also promote the loss of a sulfide phase (c.f. Noril'sk model), thus offering the potential for magmatic-hosted massive sulfide mineralization.

The homogeneity of the 1070 Ma rocks over a strike length of about 1300 km argues for a compositionally uniform magma source. Apart from geophysical evidence supporting a laccolith-shaped feeder system approximately 36×3 km in the Glenayle area, roots to the sill complexes have not been detected.

The poor correlation of εNd for the 1465 Ma western Bangemall Supergroup with either SiO_2 or La/Sm is not consistent with crustal contamination. Although the 1070 Ma western Bangemall Supergroup analyses show some negative correlation between εNd and both SiO_2 and La/Sm, a negative correlation between εNd and Mg# relationship does not support such contamination. The few data for the 1070 Ma eastern Bangemall Supergroup sills show little variation in εNd despite a wide variation in SiO_2. Nd model ages for the 1465 Ma western Bangemall Supergroup sills overlap with dates for the subduction-related Dalgaranga Supersuite granitic rocks of the Gascoyne Complex. It is possible that the slightly confused crustal contamination signature results from melting of a source modified by crustal material during Palaeoproterozoic subduction. The subduction modification of the mantle source for the Bangemall Supergroup sills is also consistent with the depletion in HFSE relative to LFSE and LREE, as shown on the N-MORB-normalized spider diagrams. Although there are variations in absolute concentrations, these REE and spider diagram patterns are similar to those for the 1070 Ma dykes from the Musgrave Complex (Giles intrusions; Glikson et al., 1996) and the Alcurra, Stuart Pass, and Kulgera dykes of the Northern Territory (Zhao and McCulloch, 1993a,b), where the petrogenesis has been attributed to melting of a subduction-modified mantle source, with the necessary heat provided by a mantle plume.

Rigorous evaluation of the relative contributions of mantle and crust to sill chemistry is difficult, in that the sills have undergone both accumulation and fractionation of liquidus phases. Simple fractionation modelling shows that the decrease in Cr and Ni contents at higher Mg# is consistent with fractionation of olivine and clinopyroxene, whereas loss or accumulation of clinopyroxene and plagioclase can account for element variations in sills with a lower Mg#. Small differences in REE chemistry (particularly HREE) indicate that the 1465 and 1070 Ma magmas were derived by melting at different depths. It is likely that the 1465 Ma sills were derived by melting at shallower depths than the 1070 Ma sills.

Chemical grouping of the 1465 and 1070 Ma sills in the western Bangemall Supergroup shows that Wingate's (2002) assertions dealing with the use of palaeomagnetism as a dating tool requires some qualification. Sill chemical fingerprinting shows that type-A magnetization was acquired by the 1070 Ma sills, and type-B magnetization may be an indicator of the 1465 Ma sills, but combined A and B magnetization is not indicative of either 1465 or 1070 Ma sills.

A feature of the 1070 Ma sills in the Bangemall Supergroup is their overall chemical homogeneity over several hundred kilometres. In the course of field mapping in both the western and eastern Bangemall Supergroups, no evidence has been detected for feeder systems for these sills, and only the gravity modelling suggests a possible feeder in the Glenayle area (Morris et al., 2003). Without further information, it is inconclusive whether sills were locally emplaced or result from long-distance magma transport, similar to that postulated for giant dyke swarms (Ernst and Buchan, 1997).

Some of the sills intruding the Bangemall Supergroup show features indicative of emplacement into weakly consolidated sediments, such as plastically deformed country rock xenoliths, fluidization features, and variolitic sill margins. Martin (2003) has discussed some of these features in relation to a sill that crosscuts both the Edmund and Collier Groups, suggesting that there is little time gap between deposition of the two groups, since part of the Coodardo Formation (the uppermost part of the Edmund Group) may be part of the Collier Group. The close temporal relationship between sill emplacement and sedimentation is also shown by sills being confined to the basin, although dykes of similar age have been dated beyond the basin margins (Wingate et al., 2004; Myers et al., 1996), and that the majority of sills intruding the Edmund Group are 1465 Ma sills, and the Collier Group is intruded by 1070 Ma sills. Rapid emplacement of voluminous magma into crustal magma chambers, where it underwent low-pressure fractionation before intrusion, would have caused accelerated uplift of the overlying crust and rapid deposition of sediment. Martin (2003) has argued for high rates of sedimentation and subsidence

during the deposition of the Collier Group sedimentary rocks, which he has linked to the emplacement of the dolerite sills.

The Bangemall Supergroup sill complexes, together with the mafic–ultramafic Giles layered intrusions and associated silicic rocks, belong to the Warakurna LIP, which was emplaced at around 1070 Ma, perhaps at a triple junction (Fig. 66b). Westward lateral flow of plume material from a plume head in the region of the Musgrave Complex exploited a zone of crustal weakness defined by the Capricorn Orogen, resulting in the emplacement of the Bangemall Supergroup sill complexes. The timing of the emplacement of the Warakurna LIP is very close to the timing of other large mafic igneous provinces in the world, such as the Umkondo LIP in southern Africa, the Keweenawan LIP, and the Southwestern USA diabase province in North America. Taken together, these igneous events may reflect the activity of a superplume at around 1100–1000 Ma.

Western Australia is a highly prospective region. Growth in mineral production, however, is attributable to a limited number of specific deposit types, whereas other deposit styles for which there should be very good analogues in Western Australia, on the basis of geological conditions, are anomalously underrepresented. Notable is the apparent absence of Noril'sk-type mineralization.

The Warakurna LIP has the potential for magmatic, magmatic-hydrothermal, and hydrothermal mineral deposits. The Bangemall Supergroup extends for about 1300 km and is considered to be highly prospective for Noril'sk-type Ni–PGE deposits in the sill complexes, for hydrothermal vein deposits, and also possibly for Olympic Dam-style anorogenic ore systems.

References

ACCLAIM EXPLORATION NL, 2003, Annual Report: Acclaim Exploration NL, 44p.

ALLEGRÉ, C. J., and ROUSSEAU, D., 1984, The growth of the continent through geological time studied by Nd isotope analyses of shales: Earth and Planetary Science Letters, v. 67, p. 19–34.

ALLSOPP, H. L., KRAMERS, J. D., JONES, D. L., and ERLANK, A. J., 1989, The age of the Umkondo Group, eastern Zimbabwe, and implications for palaeomagnetic correlations: South African Journal of Geology, v. 92, p. 11–19.

ANDERSON, D. L., 1994, Superplumes or supercontinents?: Geology, v. 22, p. 39–42.

ANDERSON, D. L., ZHANG, Y.-S., and TANIMOTO, T., 1992, Plume heads, continental lithosphere, flood basalts and tomography, *in* Magmatism and causes of continental break-up *edited by* B. C. STOREY, T. ALABASTER, and R. J. PANKHURST: The Geological Society of London, Special Publication, v. 68, p. 99–124.

ARDNT, N. T., CZAMANSKE, G. K., WALKER, R. J., CHAUVEL, C., and FEDORENKO, V. A., 2003, Geochemistry and origin of the intrusive hosts of the Noril'sk–Talnakh Cu–Ni–PGE sulfide deposits: Economic Geology, v. 98, p. 495–515.

BAKER, P. M., and WAUGH, R. S., 2003, The role of surface geochemistry in the discovery of the Babel and Nebo magmatic nickel–PGE deposits: Association of Exploration Geochemists; IGES 2003, Dublin, Ireland, Programme and Abstracts, p. 60.

BARLEY, M. E., and GROVES, D. I., 1992, Supercontinent cycles and the distribution of metal deposits through time: Geology, v. 20, p. 291–294.

BARLEY, M. E., KRAPEZ, B., GROVES, D. I., and KERRICH, R., 1998, The late Archaean bonanza: metallogenic and environmental consequences of the interaction between mantle plumes, lithospheric tectonics and global cyclicity: Precambrian Research, v. 91, p. 65–90.

BARLEY, M. E., PICKARD, A. L., and SYLVESTER, P. J., 1997, Emplacement of a large igneous province as a possible cause of banded iron formation 2.45 billion years ago: Nature, v. 385, p. 55–58.

BOTT, M. H. P., 1995, Mechanism of rifting: geodynamic modelling of continental rift systems, *in* Continental rifts: evolution, structure, tectonics *edited by* K. H. OLSEN: Development in Geotectonics, v. 25, p. 27–43.

BURKE, K., and DEWEY, J. F., 1973, Plume-generated triple junctions: key indicators in applying plate tectonics to old rocks: Journal of Geology, v. 81, p. 406–433.

BURRETT, C., and BERRY, R., 2000, Proterozoic Australia – Western United States (AUSWUS) fit between Laurentia and Australia: Geology, v. 28, p. 103–106.

CARLSEN, G. M., and GREY, K., 1998, GSWA Empress 1A and the petroleum evaluation of the western Officer Basin: Western Australia Geological Survey, Annual Review 1997–98, p. 119–126.

CAWOOD, P., and TYLER, I. M., 2004, Assembling and reactivating the Proterozoic Capricorn Orogen: lithotectonic elements, orogenies, and significance: Precambrian Research, v. 128, p. 201–218.

CHEVALIER, L., and WOODFORD, A., 1999, Morpho-tectonics and mechanism of emplacement of the dolerite rings and sills of the western Karoo, South Africa: South African Journal of Geology, v. 102, p. 43–54.

CHUCK, R. G., 1984, The sedimentary and tectonic evolution of the Bangemall Basin, Western Australia and implications for mineral exploration: Western Australian Mining and Petroleum Institute (WAMPRI), Report 6, 129p.

CLOSE, D. F., EDGOOSE, C. J., and SCRIMGEOUR, I. R., 2003, Hull and Bloods Range, Northern Territory: Northern Territory Geological Survey, 1:100 000 Geological Map Series Explanatory Notes, 46p.

COFFIN, M. F., and ELDHOLM, O., 1992, Volcanism and continental breakup: a global compilation of large igneous provinces, *in* Magmatism and causes of continental break-up *edited by* B. C. STOREY, T. ALABASTER, and R. J. PANKHURST: The Geological Society of London, Special Publication, v. 68, p. 17–30.

COFFIN, M. F., and ELDHOLM, O., 1993, Scratching the surface: estimating dimensions of large igneous provinces: Geology, v. 21, p. 515–518.

COFFIN, M. F., and ELDHOLM, O., 1994, Large igneous provinces: crustal structure, dimensions and external consequences: Reviews in Geophysics, v. 32, p. 1–36.

COLLINS, P. L. F., and McDONALD, I. R., 1994, A Proterozoic sediment-hosted polymetallic epithermal deposit at Abra in the Jillawarra sub-basin of the central Bangemall Basin, Western Australia: Geological Society of Australia, Abstracts, v. 37, p. 68–69.

COMPSTON, W., 1974, The Table Hill Volcanics of the Officer Basin: Precambrian or Palaeozoic?: Geological Society of Australia, Journal, v. 21, p. 403–411.

COMPSTON, W., and ARRIENS, P. A., 1968, The Precambrian geochronology of Australia: Canadian Journal of Earth Sciences, v. 5, p. 561–583.

CONDIE, K. C., 2001, Continental growth during the formation of Rodinia at 1.35–0.9 Ga: Gondwana Research, v. 4 p. 5–16.

COOPER, R. W., LANGFORD, R. L., and PIRAJNO, F., 1998, Mineral occurrences and exploration potential of the Bangemall Basin: Western Australia Geological Survey, Report 64, 42p.

COPP, I. A., MARTIN, D. McB., THORNE, A. M., and BAGAS, L., 1999, Ullawarra, W.A. Sheet 2151: Western Australia Geological Survey, 1:100 000 Geological Series.

CORTI, G., BONINI, M., CONTICELLI, S., INNOCENTI, F., MANETTI, P., and SOKOUTIS, D., 2003, Analogue modelling of continental extension: a review focused on the relations between the patterns of deformation and the presence of magmas: Earth Science Reviews, v. 63, p. 169–247.

COURTILLOT, V., DAVAILLE, A., BESSE, J., and STOCK, J., 2003, Three distinct types of hotspots in the Earth's mantle: Earth and Planetary Science Letters, v. 205, p. 295–308.

COURTILLOT, V., JAUPART, C., MANIGHETTI, I., TAPPONIER, P., and BESSE, J., 1999, On causal links between flood basalts and continental breakup: Earth and Planetary Science Letters, v. 166, p. 177–195.

COWLEY, W. M., 1991, Beda Volcanics and Backy Point Formation of the Eastern Gawler Craton: Department of Mines and Energy, South Australia, Report BK No. 90/16.

COX, K. G., BELL, J. D., and PANKHURST, R. J., 1979, The interpretation of igneous rocks: London, George Allen and Unwin, 450p.

DALZIEL, I. W. D., 1991, Pacific margins of Laurentia and East Antarctica – Australia as a conjugate rift pair: evidence and implications for an Eocambrian supercontinent: Geology, v. 19, p. 598–601.

DALZIEL, I. W. D., LAWVER, L. A., and MURPHY, J. B., 2000, Plumes, orogenesis and supercontinental fragmentation: Earth and Planetary Science Letters, v. 178, p. 1–11.

DANIELS, J. L., 1968, Edmund, W.A. Sheet SF 50-14: Western Australia Geological Survey, 1:250 000 Geological Series.

DANIELS, J. L., 1969, Edmund, W.A.: Western Australia Geological Survey, 1:250 000 Geological Series Explanatory Notes, 20p.

DANIELS, J. L., 1974, The geology of the Blackstone region, Western Australia: Western Australia Geological Survey, Bulletin 123, 257p.

DAVIES, G. F., 1999, Dynamic Earth: plates, plumes and mantle convection: Cambridge, Cambridge University Press.

DAVIS, D. W., and PACES, J. B., 1990, Time resolution of geologic events on the Keweenaw Peninsula and implications for development of the Midcontinent Rift System: Earth and Planetary Science Letters, v. 97, p. 54–64.

DE PAOLO, D. J., 1981, Trace element and isotopic effects of combined wallrock assimilation and fractional crystallisation: Earth and Planetary Science Letters, v. 53, p. 189–202.

DREW, L. J., MENG, Q., and SUN, W.,1990, The Bayan Obo iron–rare earth–niobium deposits, Inner Mongolia, China: Lithos, v. 26, p. 43 and 65.

DUZHIKOV, O. A., DISTLER, V. V., STRUNIN, B. M., MKRTYCHAYN, A. K., SHERMAN, M. L., SLUZHENIKIN, S. S., and LURYE, A. M., (editors), 1992, Geology and metallogeny of sulfide deposits, Noril'sk region, USSR: Society of Economic Geologists, Special Publication, no. 1.

EALES, H. V., and CAWTHORN, R. G., 1996, The Bushveld Complex, *in* Layered intrusions *edited by* R. G. CAWTHORN: Amsterdam, Elsevier, p. 181–230.

EDGOOSE, C. J., CAMACHO, A., WAKELIN-KING, G. A., and SIMONS, B. A., 1993, Kulgera, N.T., Sheet SG 53-5: Northern Territory Geological Survey, 1:250 000 Geological Map Series Explanatory Notes, 46p.

EGGINS, S. M., WOODHEAD, J. D., KINSLEY, L. P. J., MORTIMER, G. E., SYLVESTER, P., McCULLOCH, M. T., HERGT, J. M., and HANDLER, M. R., 1997, A simple method for the precise determination of ≥40 trace elements in geological samples by ICPMS using enriched isotope internal standardisation: Chemical Geology, v. 134, p. 311–326.

EMBLETON, B. J. J., and SCHMIDT, P. W., 1985, Age and significance of magnetisations in dolerite dykes from the Northampton Block, Western Australia: Australian Journal of Earth Sciences, v. 32, p. 279–286.

ERNST, R. E., and BUCHAN, K. L., 1997, Giant radiating dyke swarms: their use in identifying pre-Mesozoic large igneous provinces and mantle plumes, *in* Large igneous provinces, continental, oceanic, and planetary flood volcanism *edited by* J. J. MAHONEY and M. F. COFFIN: American Geophysical Union, Geophysical Monograph 100, p. 297–333.

ERNST, R. E., and BUCHAN, K. L., 2001, Large mafic magmatic events throughout time and links to mantle-plume heads, *in* Mantle plumes: their identification through time *edited by* R. E. ERNST and K. L. BUCHAN: Geological Society of America, Special Paper 352, p. 483–575.

EWART, A., MILNER, S. C., ARMSTRONG, R. A., and DUNCAN, A. R., 1998, Etendeka volcanism of the Goboboseb Mountains and Messum Igneous Complex, Namibia. Part I: geochemical evidence of Early Cretaceous Tristan plume melts and the role of crustal contamination in the Paraná–Etendeka CFB: Journal of Petrology, v. 39, p. 191–225.

FAURE, G., 1986, Principles of isotope geology (2nd edition): New York, John Wiley and Sons, 589p.

FREY, F. A., GREEN, D. H., and ROY, S. D., 1978, Integrated models of basalt petrogenesis: a study of quartz tholeiites to olivine melilites from southeastern Australia utilizing geochemical and experimental petrological data: Journal of Petrology, v. 19, p. 463–513.

GEE, R. D., de LAETER, J. R., and DRAKE, J. R., 1976, The geology and geochronology of altered rhyolite from the lower part of the Bangemall Group near Tangadee, Western Australia: Western Australia Geological Survey, Annual Report 1975, p. 112–117.

GÉLINAS, L., MELLINGER, M., and TRUDEL, P., 1982, Archaean mafic metavolcanics from the Rouyn–Noranda district, Abitibi greenstone belt, Quebec. 1. Mobility of the major elements: Canadian Journal of Earth Sciences, v. 19, p. 2258–2275.

GILL, J. B., 1981, Orogenic andesites and plate tectonics: Berlin, Springer-Verlag, 390p.

GLASS, L. M., 2002, Petrogenesis and geochronology of the North Australia Kalkarinji low-Ti continental flood basalt province: Australian National University, PhD thesis (unpublished).

GLAZNER, A., and USLER, W., 1988, Trapping of magma at midcrustal density discontinuities: Geophysical Research Letters, v. 15, p. 673–675.

GLIKSON, A. Y., STEWART, A. T., BALLHAUS, G. L., CLARKE, G. L., FEEKEN, E. H. T., LEVEL, J. H., SHERATON, J. W., and SUN, S-S., 1996, Geology of the western Musgrave Block, central Australia, with reference to the mafic–ultramafic Giles Complex: Australian Geological Survey Organisation, Bulletin 239, 206p.

GOODE, A., 2002, Tomkinson Ranges, *in* Musgrave Block — Proterozoic and Palaeozoic geology *edited by* C. H. H. CONNOR, A. CAMACHO, D. CLOSE, A. GOODE, R. MAJOR, and I. SCRIMGEOUR: Geological Society of Australia; 16th Australian Geological Convention, Excursion Guide C2.

GOODE, A. D. T., and HALL, W. D. M., 1981, The middle Proterozoic eastern Bangemall Basin, Western Australia: Precambrian Research, v. 16, p. 11–29.

GOODE, A. D. T., and KRIEG, G. W., 1967. The geology of Ewarara Intrusions, Giles Complex, central Australia: Geological Society of Australia, Journal, v. 14, p. 185–194.

GRAY, C. M., and GOODE, A. D. T., 1989. The Kalka layered intrusion, central Australia: a strontium isotopic history of contamination and magma dynamics: Contributions to Mineralogy and Petrology, v. 103, p. 35–43.

HALL, G. E. M., and PLANT, J. A., 1992, Analytical errors in the determination of high field strength elements and their implications in tectonic interpretation studies: Chemical Geology, v. 95, p. 141–156.

HALL, C. E., POWELL, C. McA., and BRYANT, J., 2001, Basin setting and age of the Late Palaeoproterozoic Capricorn Formation, Western Australia: Australian Journal of Earth Sciences, v. 48, p. 731–744.

HANSON, R. E., MARTIN, M. W., BOWRING, S. A., and MUNYANYIMA, H., 1998, U–Pb zircon age for the Umkondo dolerites, eastern Zimbabwe: 1.1 Ga large igneous province in southern Africa – East Antarctica and possible Rodinia correlations: Geology, v. 26, p. 1143–1146.

HERGT, J. M., PEATE, D. W., and HAWKESWORTH, C. J., 1991, The petrogenesis of Mesozoic Gondwana low-Ti flood basalts: Earth and Planetary Science Letters, v. 105, p. 134–148.

HICKMAN, A. H., and LIPPLE, S. L., 1978, Marble Bar, W.A.: Western Australia Geological Survey, 1:250 000 Geological Series Explanatory Notes, 24p.

HITZMAN, M. W., ORESKES, N., and EINAUDI, M. T., 1992, Geological characteristics and tectonic setting of Proterozoic iron oxides (Cu–U–Au–REE) deposits: Precambrian Research, v. 58, p. 241–287.

HOCKING, R. M., and JONES, J. A., 1999, Methwin, W.A. Sheet 3047: Western Australia Geological Survey, 1:100 000 Geological Series.

HOCKING, R. M., JONES, J. A., PIRAJNO, F., and GREY, K., 2000, Revised lithostratigraphy for Proterozoic rocks in the Earaheedy Basin and nearby areas: Western Australia Geological Survey, Record 2000/16, 22p.

HOCKING, R. M., and PIRAJNO, F., 2004, Lee Steere, W.A. Sheet 3346: Western Australia Geological Survey, 1:100 000 Geological Series.

HOFFMAN, P., 1991, Did the breakout of Laurentia turn Gondwana inside out?: Science, v. 252, p. 1409–1412.

HOOPER, P. R., 1997, The Columbia River flood basalt province: current status, *in* Large igneous provinces, continental, oceanic, and planetary flood volcanism *edited by* J. J. MAHONEY and M. F. COFFIN: American Geophysical Union, Geophysical Monograph 100, p. 1–27.

HYNES, A., 1980, Carbonatisation and mobility of Ti, Y, and Zr in Ascot Formation metabasalts, S.E. Quebec: Contributions to Mineralogy and Petrology, v. 75, p. 79–87.

IIZUMI, S., MAEHARA, K., MORRIS, P. A., and SAWADA, Y., 1994, Sr isotope data of some GSJ rock reference samples: Shimane University, Faculty of Science, Memoir, no. 28, p. 83–86.

IIZUMI, S., MORRIS, P. A., and SAWADA, Y., 1995, Nd isotope data for GSJ reference samples JB1-a, JB-3 and JG-1a and the La Jolla standard: Shimane University, Faculty of Science, Memoir, no. 29, p. 73–76.

IRVINE, T. N., and BARAGAR, W. R. A., 1971, A guide to the classification of the common volcanic rocks: Canadian Journal of Earth Sciences, v. 8, p. 523–548.

JOHNSTON, S. T., and THORKELSON, D. J., 2000, Continental flood basalts: episodic magmatism above long-lived hotspots: Earth and Planetary Science Letters, v. 175, p. 247–256.

KARLSTROM, K. E., AHALL, K. I., HARLAN, S. S., WILLIAMS, M. L., MCLELLAND, J., and GEISSMAN, J. W., 2001, Long-lived (1.8–1.0 Ga) convergent orogen in southern Laurentia, its extensions to Australia and Baltic, and implications for refining Rodinia: Precambrian Research, v. 111, p. 5–30.

KARLSTROM, K. E., HARALN, S. S., WILLIAMS, M. L., McLELLAND, J., GEISSMAN, J. W., and AHALL, K. I., 1999, Refining Rodinia: geologic evidence for the Australia–Western US connection in the Proterozoic: Geological Society of Australia, GSA Today, v. 9, p. 1–7.

KERR, A. C., WHITE, R. V., and SAUNDERS, A. D., 2000, LIP reading: recognizing oceanic plateaux in the geological record: Journal of Petrology, v. 41, p. 1041–1956.

KING, S. D., and ANDERSON, D. L., 1998, An alternative mechanism of flood basalt formation: Earth and Planetary Science Letters, v. 160, p. 289–296.

KLEWIN, K. W., and BERG, J. H., 1991, Petrology of the Keweenawan Mamainse Point Lavas, Ontario: petrogenesis, and continental rift evolution: Journal of Geophysical Research, v. 92, p. 457–464.

KRAPEZ, B., and McNAUGHTON, N. J., 1999, SHRIMP zircon U–Pb age and tectonic significance of the Paleoproterozoic Boolaloo Granodiorite in the Ashburton Province, Western Australia: Australian Journal of Earth Sciences, v. 46, p. 283–287.

LEAMAN, D. E., 1995. Mechanics of sill emplacement: comments based on the Tasmanian dolerites: Australian Journal of Earth Sciences, v. 42, p. 151–155.

LE MAITRE, R. W., (editor), 2002, Igneous rocks: a classification and glossary of terms: Cambridge, Cambridge University Press, 236p.

LE PICHON, X., and FRANCHETEAU, J., 1978, A plate tectonic analysis of the Red Sea – Gulf of Aden area: Tectonophysics, v. 46, p. 369–406.

LI, Z-X., LI, X. H., KINNY, P. D., and WANG, J., 1999, The breakup of Rodinia: did it start with a mantle plume beneath South China?: Earth and Planetary Science Letters, v. 173, p. 171–181.

LI, Z-X., LI, X. H., KINNY, P. D., WANG, J., ZHANG, S., and ZHOU, H., 2003, Geochronology of Neoproterozoic syn-rift magmatism in the Yangtze Craton, South China and correlations with other continents: evidence for a mantle superplume that broke Rodinia: Precambrian Research, v. 122, p. 85–109.

LI, Z-X., and POWELL, C. McA., 2001, An outline of the palaeogeographic evolution of the Australian region since the beginning of the Neoproterozoic: Earth Science Reviews, v. 53, p. 237–277.

LIGHTFOOT, P. C., and HAWKESWORTH, C. J., 1997, Flood basalts and magmatic Ni, Cu, and PGE sulphide mineralization: comparative geochemistry of the Noril'sk (Siberian Traps) and West Greenland sequences, *in* Large igneous provinces, continental, oceanic, and planetary flood volcanism *edited by* J. J. MAHONEY and M. F. COFFIN: American Geophysical Union, Geophysical Monograph 100, p. 357–380.

LIGHTFOOT, P. C., NALDRETT, A. J., GORBACHEV, N. S., DOHERTY, W., and FEDERENKO, V. A., 1990, Geochemistry of the Siberian Traps of the Noril'sk area, USSR, with implications for the relative contributions of crust and mantle to flood basalt magmatism: Contributions to Mineralogy and Petrology, v. 104, p. 631–644.

LINDSAY, J. F., 2002, Supersequences, superbasins, supercontinents — evidence from the Neoproterozoic – Early Palaeozoic basins of central Australia: Basin Research, v. 14, p. 207–223.

LUDDEN, J., GÉLINAS, L., and TRUDEL, P., 1982, Archaean metavolcanics from the Rouyn–Noranda district, Abitibi Greenstone belt, Quebec. 2. Mobility of trace elements and petrogenetic constraints: Canadian Journal of Earth Sciences, v. 19, p. 2276–2287.

LURIE, M. L., and MASAITIS, V. L., 1964, Plateau basalts: International Geological Congress 22: Moscow, p. 1–12.

MAHONEY, J. J., 1988, Deccan Traps, *in* Continental flood basalts *edited by* J. J. McDOUGAL: Norwell, Massachusetts, Kluwer Academic, p. 151–194.

MAJOR, R. B., and CONNOR, C. H. H., 1993, Musgrave Block, *in* The geology of South Australia *edited by* J. F. DREXEL, W. V. PREISS, and A. J. PARKER: Geological Survey of South Australia, Bulletin 54, p. 156–167.

MARSTON, R. J., 1979, Copper mineralisation in Western Australia: Western Australia Geological Survey, Bulletin 13, 208p.

MARTIN, D. McB., 2003, Peperite in the Backdoor Formation and its significance to the age and tectonic evolution of the Bangemall Supergroup: Western Australia Geological Survey, Annual Review 2002–03, p. 53–59.

MARTIN, D. McB., and THORNE, A. M., 2000, Another Jillawara-style sub-basin in the Bangemall Supergroup — implications for mineral prospectivity: Western Australia Geological Survey, Annual Review 1999–2000, p. 31–35.

MARTIN, D. McB., and THORNE, A. M., 2001, New insights into the Bangemall Supergroup: Western Australia Geological Survey, Record 2001/5, p. 1–2.

MARTIN, D. McB., and THORNE, A. M., 2002, Revised lithostratigraphy of the Bangemall Supergroup on the Edmund and Turee Creek 1:250 000 map sheets, Western Australia: Western Australia Geological Survey, Record 2002/15, 27p.

MARTIN, D. McB., and THORNE, A. M., 2004, Tectonic setting and basin evolution of the Bangemall Supergroup in the northwestern Capricorn Orogen: Precambrian Research, v. 128, p. 385–409.

MARTIN, D. McB., THORNE, A. M., and COPP, I. A., 1999, A provisional revised stratigraphy for the Bangemall Group on the Edmund 1:250 000 sheet: Western Australia Geological Survey, Annual Review 1998–99, p. 51–55.

MARTIN, D. McB., THORNE, A. M., and COPP, I. A., 2004, Elliot Creek, W.A. Sheet 2250: Western Australia Geological Survey, 1:100 000 Geological Series.

MARTIN, D. McB., THORNE, A. M., and OCCHIPINTI, S. A., 2002, Edmund, W.A. Sheet 2150: Western Australia Geological Survey, 1:100 000 Geological Series.

MATHISON, C. I., and AHMAT, A. L., 1996, The Windimurra Complex, Western Australia, *in* Layered intrusions *edited by* R. G. CAWTHORN: Amsterdam, Elsevier, p. 485–510.

MIYASHIRO, A., 1974, Volcanic rock series in island arcs and active continental margins: American Journal of Science, v. 274, p. 321–355.

MONTELLI, R., NOLET, G., DAHLEN, F. A., MASTERS, G., ENGDAHL, E. R., and HUNG, S-H., 2004, Finite-frequency tomography reveals a variety of plumes in the mantle: Science, v. 303, p. 338–343.

MOORES, E. M., 1991, Southwest US – East Antarctic (SWEAT) connection: a hypothesis: Geology, v. 19, p. 425–428.

MORRIS, P. A., 2000, Composition of Geological Survey of Western Australia geochemical reference materials: Western Australia Geological Survey, Record 2000/11, 33p.

MORRIS, P. A., McGUINNESS, S. A., SANDERS, A. J., and COKER, J., 2000, Geochemical mapping of the Stanley 1:250 000 sheet: Western Australian Geological Survey, 1:250 000 Regolith Geochemistry Series Explanatory Notes, 53p.

MORRIS, P. A., PIRAJNO, F., and SHEVCHENKO, S., 2003, Proterozoic mineralization identified by integrated regional regolith geochemistry, geophysics, and bedrock mapping in Western Australia: Geochemistry — Exploration, Environment, Analysis, v. 3, p. 13–28.

MUHLING, P. C., and BRAKEL, A. T., 1985, Geology of the Bangemall Group — the evolution of an intracratonic Proterozoic basin: Western Australia Geological Survey, Bulletin 128, 265p.

MUNYANYIWA, H., 1999, Geochemical study of the Umkondo dolerites and lavas in the Chimanimani and Chipinge Districts (eastern Zimbabwe) and their regional implications: Journal of African Earth Sciences, v. 28, p. 349–365.

MYERS, J. S., 1990, Wingelina Complex and Bentley Supergroup, *in* Geology and mineral resources of Western Australia: Western Australia Geological Survey, Memoir 3, p. 283–286.

MYERS, J. S., and HOCKING, R. M., 1998, Geological map of Western Australia 1:2 500 000 (13th edition): Western Australia Geological Survey.

MYERS, J. S., SHAW, R. D., and TYLER, I. M., 1996, Tectonic evolution of Proterozoic Australia: Tectonics, v. 15, p. 1431–1446.

NALDRETT, A. J., 1992, A model for the Ni–Cu–PGE ores of the Noril'sk region and its application to other areas of flood basalt: Economic Geology, v. 87, p. 1945–1962.

NALDRETT, A. J., FEDORENKO, V. A., LIGHTFOOT, P. C., KUNILOV, V. I., GORBACHEV, N. S., DOHERTY, W., and JOHAN, Z., 1995, Ni–Cu–PGE deposits of Noril'sk region, Siberia: their formation in conduits for flood basalts volcanism: Institute of Mining and Metallurgy, Transactions, B104, p. B18–B36.

NALDRETT, A. J., and LIGHTFOOT, P. C., 1993, Ni–Cu–PGE ores of the Noril'sk region, Siberia: a model for giant magmatic sulfide deposits associated with flood basalts, *in* Giant ore deposits *edited by* B. W. WHITING, C. J. HODGSON, and R. MASON: Society of Economic Geologists, Special Publication, no. 2, p. 81–124.

NELSON, D. R., 1995, Compilation of SHRIMP U–Pb dates, 1994: Western Australia Geological Survey, Record 1995/3, 244p

NELSON, D. R., 1998, Compilation of SHRIMP U–Pb zircon geochronology data, 1997: Western Australian Geological Survey, Record 1998/2, 242p.

NELSON, D. R., 2001, Compilation of geochronology data, 2000: Western Australia Geological Survey, Record 2001/2.

NELSON, D. R., 2002, Compilation of geochronology data, 2001: Western Australia Geological Survey Record 2002/2.

NESBITT, R. W., GOODE, A. D. T., MOORE, A. C., and HOPWOOD, T. D., 1970, The Giles Complex, central Australia: a stratified sequence of mafic and ultramafic intrusions, *in* Symposium on the Bushveld Igneous Complex and other layered intrusions: Geological Society of South Africa, Special Publication, no. 1:p. 547–564.

NICHOLSON, S. W., CANNON, W. F., and SCHULZ, K. J., 1992, Metallogeny of the Midcontinent rift system of North America: Precambrian Research, v. 58, p. 355–386.

NIKISHIN, A. M., ZIEGLER, P. A., ABBOTT, D., BRUNET, M–F., and CLOETINGH, S., 2002, Permo-Triassic intraplate magmatism and rifting in Eurasia: implications for mantle plumes and mantle dynamics: Tectonophysics, v. 351, p. 3–39.

NORRISH, K., and CHAPPELL, B. W., 1977, X-ray fluorescence spectrometry, *in* Physical methods in determinative mineralogy (2nd edition) *edited by* J. ZUSSMAN: London, Academic Press, p. 201–272.

NORRISH, K., and HUTTON, J. T., 1969, An accurate X-ray spectrographic method for the analysis of a wide range of geological samples: Geochimica et Cosmochimica Acta, v. 33, p. 431–453.

OCCHIPINTI, S. A., SHEPPARD, S., TYLER, I. M., and NELSON, D. R., 1999, Deformation and metamorphism during the c. 2000 Ma Glenburgh Orogeny and the c. 1800 Ma Capricorn Orogeny: Geological Society of Australia, Abstracts, v. 56, p. 26–29.

OKAJANGAS, R. W., MOREY, G. B., and GREEN, J. C., 2001, The Mesoproterozoic Midcontinent rift system, Lake Superior region, USA: Sedimentary Geology, v. 141–142, p. 421–442.

OPPLIGER, G. L., MURPHY, J. B., and BRIMHALL, G. H., 1997, Is the ancestral Yellowstone hotspot responsible for the Tertiary 'Carlin' mineralization in the Great Basin of Nevada?: Geology, v. 25, p. 627–630.

PEARCE, J. A., 1976, Statistical analysis of major element patterns in basalts: Journal of Petrology, v. 17, p. 15–43.

PEARSON, J. M., TAYLOR, W. R., and BARLEY, M. E., 1995, Geology of the alkaline Gifford Creek Complex, Gascoyne Province, Western Australia: Australian Journal of Earth Sciences, v. 43, p. 299–309.

PEATE, D. W., 1997, The Paraná – Etendeka Province, *in* Large igneous provinces, continental, oceanic, and planetary flood volcanism *edited by* J. J. MAHONEY and M. F. COFFIN: American Geophysical Union, Geophysical Monograph 100, p. 217–245.

PIPER, J. D. A., 2000, The Neoproterozoic supercontinent: Rodinia or Palaeopangea?: Earth and Planetary Science Letters, v. 176, p. 131–146.

PIRAJNO, F., 1992, Hydrothermal mineral deposits: Berlin, Springer-Verlag, 709p.

PIRAJNO, F., 1994, Mineral resources of anorogenic alkaline complexes in Namibia: a review: Australian Journal of Earth Sciences, v. 41, p. 157–168.

PIRAJNO, F., 1998, Geology and mineral deposits of Namibia: Australian Institute of Geoscientists, Bulletin 25, p. 61–66.

PIRAJNO, F., 2000, Ore deposits and mantle plumes: Dordrecht, Kluwer Academic Publishers, 556p.

PIRAJNO, F., 2004a, Hotspots and mantle plumes: global intraplate tectonics, magmatism and ore deposits: Mineralogy and Petrology, Special Issue, v. 82, p. 183–216.

PIRAJNO, F., 2004b, Metallogeny in the Capricorn Orogen, Western Australia; the result of multiple ore-forming processes: Precambrian Research, v. 128, p. 411–439.

PIRAJNO, F., and HOCKING, R. M., 2001, Mudan, W.A. Sheet 3247: Western Australia Geological Survey, 1: 100 000 Geological Series.

PIRAJNO, F., and HOCKING, R. M., 2002, Glenayle, W.A. Sheet 3347: Western Australia Geological Survey, 1: 100 000 Geological Series.

PIRAJNO, F., PHILLIPS, D., and ARMSTRONG, R. A., 2000, Volcanology and eruptive histories of the Erongo Volcanic Complex, Namibia: implications for mineral deposit styles: Geological Survey of Namibia, Communications Geological Survey of Namibia, v. 12, p. 301–312.

PISAREVSKY, S. A., WINGATE, M. T. D., and HARRIS, L. B., 2003a, Late Mesoproterozoic (ca 1.2 Ga) palaeomagnetism of the Albany–Fraser Orogen: no pre-Rodinia Australia–Laurentia connection: Geophysical Journal International, v. 155, p. F6–F11.

PISAREVSKY, S. A., WINGATE, M. T. D., POWELL C. McA., JOHNSON, S., and EVANS, D. A. D., 2003b, Models of Rodinia assembly and fragmentation: The Geological Society of London, Special Publications, no. 206, p. 35–55.

POWELL, C. McA., LI, Z-X., McELHINNY, M. W., MEERT, J. G., and PARK, J. K., 1993, Paleomagnetic constraints on timing of the Neoproterozoic breakup of Rodinia and the Cambrian formation of Gondwana: Geology, v. 21, p. 889–892.

PUFFER, J. H., 2001, Contrasting high field strength element contents of continental flood basalts from plume versus reactivated-arc sources: Geology, v. 29, p. 675–678.

PYKE, J., 2000, Minerals laboratory staff develop new ICP-MS preparation method: AGSO, Research Newsletter, v. 33, p. 12–14.

RAINBIRD, R. H., and ERNST, R. E., 2001, The sedimentary record of mantle-plume uplift: Geological Society of America, Special Paper, no. 352, p. 227–245.

RAMPINO, M. R. S., SELF, S., and STOTHERS, R. B., 1988, Volcanic winters: Annual Review of Earth and Planetary Sciences, v. 16, p. 73–99.

REYNOLDS, L. J., 2001, Geology of the Olympic Dam Cu–U–Au–Ag–REE deposit, *in* Hydrothermal iron oxide–copper–gold and related deposits — a global perspective *edited by* T. M. PORTER: Australian Mineral Foundation, v. 1, p. 93–104.

ROLLINSON, H., 1993, Using geochemical data: evaluation, presentation, interpretation: England, Longman, 352p.

RUDNICK, R. L., and FOUNTAIN, D. M., 1995, Nature and composition of the continental crust: a lower crustal perspective: Reviews of Geophysics, v. 33, p. 267–309.

RUPPEL, C., 1995, Extensional processes in continental lithosphere: Journal of Geophysical Research, v. 100, p. 24187–24215.

SAUNDERS, A. D., TARNEY, J., MARSH, N. G., and WOOD, D. A., 1980, Ophiolites as ocean crust or marginal basin crust: a geochemical approach, *in* Ophiolites *edited by* A. PANAYIOTOU: Ministry of Agriculture and Natural Resources, Cyprus, Geological Survey Department, International Ophiolite Symposium, Cyprus, 1979, Proceedings, p. 193–204.

SCHILLING, J-G., 1973, Iceland mantle plume: geochemical study of the Reykjanes Ridge: Nature, v. 242, p. 565–571.

SCHUBERT, G., TURCOTTE, D. L., and OLSON, P., 2001, Mantle convection in the Earth and planets: Cambridge, Cambridge University Press.

SCRIMGEOUR, I. R., CLOSE, D. F., and EDGOOSE, C. J., 1999, Petermann Ranges, N.T., Sheet SG 52-7:Northern Territory Geological Survey, 1:250 000 Geological Map Series Explanatory Notes: 59p.

SHARMA, M., 1997, Siberian Traps, *in* Large igneous provinces, continental, oceanic, and planetary flood volcanism *edited by* J. J. MAHONEY and M. F. COFFIN: American Geophysical Union, Geophysical Monograph 100, p. 273–295.

SHEPPARD, S., OCCHIPINTI, S. A., and TYLER, I. M., 2004, A 2005–1970 Ma Andean-type batholith in the southern Gascoyne Complex, Western Australia: Precambrian Research, v. 128, p 257–278.

SHEPPARD, S., and SWAGER, C. P., 1999, Geology of the Marquis 1:100 000 sheet: Western Australia Geological Survey, 1:100 000 Geological Series Explanatory Notes, 21 p.

SHERATON, J. W., and SUN, S-S., 1997, Mafic dyke swarms of the western Musgrave Block, central Australia: their geochemistry, origin, and relationships to the Giles Complex: AGSO, Journal of Geology and Geophysics, v. 16, p. 621–636.

SHETH, H. C., 1999, Flood basalts and large igneous provinces from deep mantle plumes: fact, fiction and fallacy: Tectonophysics, v. 311, p. 1–29.

SHIBATA, T., and NAKAMURA, E., 1997, Across-arc variations of isotope and trace element compositions from Quaternary basaltic volcanic rocks in northeastern Japan: implications for interaction between subducted oceanic slab and mantle wedge: Journal of Geophysical Research, v. 102, p. 8051–8064.

STEVENS, M. K., and APAK N., 1999, GSWA Empress 1 and 1A well completion report, Yowalga Sub-basin, Officer Basin, Western Australia: Western Australia Geological Survey, Record 1999/4, 110p.

SUN, S-S., and McDONOUGH, W. F., 1989, Chemical and isotopic systematics of oceanic basalts: implications for mantle composition and process, *in* Magmatism in the ocean basins, *edited by* A. D. SAUNDERS and M. J. NORRY: The Geological Society of London, Special Publication, no. 42, p. 313–345.

SUN, S-S., SHERATON, J. W., GLIKSON, A. Y., and STEWART, A. J., 1996, A major magmatic event during 1050–1080 Ma in central Australia and an emplacement age for the Giles Complex: AGSO, Research Newsletter 24, p. 13–15.

TAYLOR, S. R., and McLENNAN, S. M., 1985, The continental crust: its composition and evolution: Oxford, Blackwell Scientific Publications, 312p.

TESFAYE, S., HARDING, D. J., and KUSKY, T. M., 2003, Early continental breakup boundary and migration of the Afar triple junction, Ethiopia: Geological Society of America, Bulletin, v. 115, p. 1053–1067.

TOLAN, T. L., REIDEL, S. P., BEESON, M. H., ANDERSON, J. L., FECHT, K. R., and SWANSON, D. A., 1989, Revisions to the estimates of the areal extent and volume of the Columbia River Basalt Group, *in* Volcanism and tectonism in the Columbia River flood basalt province *edited by* S. R. REIDEL and P. R. HOOPER: Geological Society of America, Special Paper, no. 239, p. 1–20.

TRUMBULL, R. B., EMMERMANN, R., BÜHN, B., RERSTENBERGER, H., MINGRAM, B., SCMITT, A., and VOLKER, F., 2000, Insights on the genesis of the Cretaceous Damaraland igneous complexes in Namibia from a Nd- and Sr-isotopic perspective: Geological Survey of Namibia, Communications Geological Survey of Namibia, v. 12, p. 313–324.

TURCOTTE, D. L., EMERMAN, S. H., and SPENCE, D. A., 1987, Mechanics of dyke injection: Geological Association of Canada, Special Paper, no. 34, p. 25–30.

TYLER, I. M., and HOCKING, R. M., 2002, A revision of the tectonic units of Western Australia: Western Australia Geological Survey, Annual Review 2000–01, p. 33–44.

TYLER, I. M., and THORNE, A. M., 1990, The northern margin of the Capricorn Orogen, Western Australia — an example of an early Proterozoic collision zone: Journal of Structural Geology, v. 12, p. 685–701.

UNRUG, R., (editor), 1996, Geodynamic map of Gondwana: Council for Geosciences, Pretoria, South Africa and Bureau de Recherche Geologiques et Minieres, Orleans, France.

UNRUG, R., 1997, Rodinia to Gondwana: the geodynamic map of Gondwana Supercontinent assembly: Geological Society of Australia, GSA Today, v. 7, p. 1–6.

VANDERHOR, F., and FLINT, R. B., (compilers), 2001, Interpreted bedrock geology of Western Australia, preliminary edition (1:500 000 scale): Western Australia Geological Survey.

WAIGHT, T. E., MAAS, R., and NICHOLLS, I., 2000, Fingerprinting feldspar phenocrysts using crystal isotopic composition stratigraphy: implications for crystal transfer and magma mingling in S-type granites: Contributions to Mineralogy and Petrology, v. 139, p. 227–239.

WALTER, M. R., VEEVERS, J. J., CALVER, C. R., and GREY, K., 1995, Neoproterozoic stratigraphy of the Centralian Superbasin, Australia: Precambrian Research, v. 73, p. 173–195.

WHITE, R., and McKENZIE, D., 1995, Mantle plumes and flood basalts: Journal of Geophysical Research, v. 100, p. 17543–17585.

WILLIAMS, I. R., 1990, Bangemall Basin, *in* Geology and mineral resources of Western Australia: Western Australian Geological Survey, Memoir 3, p. 308–329.

WILSON, M. A., 1989, Igneous Petrogenesis: London, Unwin Hyman, 466p.

WINCHESTER, J. A., and FLOYD, P. A., 1976, Geochemical magma type discrimination: application to altered and metamorphosed basic igneous rocks: Earth and Planetary Science Letters, v. 28, p. 459–469.

WINDLEY, B. F., 1995, The evolving continents: Chichester, John Wiley and Sons.

WINDRIM, D. P., and McCULLOCH, M. T., 1986, Nd and Sr isotopic systematics of central Australian granulites: chronology of crustal development and constraints on the evolution of lower continental crust: Contributions to Mineralogy and Petrology, v. 94, p. 289–303.

WINGATE, M. T. D., 2001, SHRIMP baddeleyite and zircon ages for an Umkondo dolerite sill, Nyanga Mountains, eastern Zimbabwe: South African Journal of Geology, v. 104, p. 13–22.

WINGATE, M. T. D., 2002, Age and palaeomagnetism of dolerite sills intruded into the Bangemall Supergroup on the Edmund 1:250 000 map sheet, Western Australia: Western Australia Geological Survey, Record 2002/4, 48p.

WINGATE, M. T. D., 2003, Age and palaeomagnetism of dolerite intrusions of the southeastern Collier Basin and the Earaheedy and Yerrida Basins, Western Australia: Western Australia Geological Survey, Record 2003/3, 35p.

WINGATE, M. T. D., CAMPBELL, I. H., COMPSTON, W., and GIBSON, G. M., 1998, Ion microprobe U–Pb ages for Neoproterozoic basaltic magmatism in south-central Australia and implications for the breakup of Rodinia: Precambrian Research, v. 87, p. 135–159.

WINGATE, M. T. D., and EVANS, D. A. D., 2003, Palaeomagnetic constraints on the Proterozoic tectonic evolution of Australia: The Geological Society of London, Special Publication, no. 206, p. 77–91.

WINGATE, M. T. D., and GIDDINGS, J. W., 2000, Age and palaeomagnetism of the Mundine Well dyke swarm, Western Australia: implications for an Australia–Laurentia connection at 755 Ma: Precambrian Research, v. 100, p. 335–357.

WINGATE, M. T. D., PIRAJNO, F., and MORRIS, P. A., 2004, The Warakurna large igneous province: a new Mesoproterozoic large igneous province in west-central Australia: Geology, v. 32, p. 105–108.

WINGATE, M. T. D., PISAREVSKY, S. A., and EVANS, D. A. D., 2002, A revised Rodinia supercontinent: no SWEAT, no AUSWUS: Terra Nova, v. 14, p. 121–128.

WOOD, D. A., GIBSON, J. L., and THOMPSON, R. N., 1976, Elemental mobility during zeolite facies metamorphism of the Tertiary basalts of Eastern Iceland: Contributions to Mineralogy and Petrology, v. 55, p. 241–254.

WOODWARD, H. P., 1891, Geognosy: a general description of the Victoria, Murchison, Gascoyne, Ashburton, Fortescue, Roebourne, and de Grey districts: Western Australia Geological Survey, Western Australia Annual General Report of the Government Geologist for the year 1890, p. 6–12.

XIAO, L., XU, Y-G., XU, J-F., HE, B., and PIRAJNO, F., in press, Chemostratigraphy of flood basalts in the Ganze-Litang region and Zhoinga Block: implications for a western extension of the Emeishan Large Igneous Province, SW China: Acta Geologica Sinica.

ZHAO, J-X., and McCULLOCH, M. T., 1993a, Sm–Nd mineral isochron ages of Late Proterozoic dyke swarms in Australia: evidence for two distinct events of mafic magmatism and crustal extension: Chemical Geology, v. 109, p. 341–354.

ZHAO, J-X., and McCULLOCH, M. T., 1993b, Melting of subduction-modified continental lithospheric mantle: evidence from Late Proterozoic mafic dyke swarms in central Australia: Geology, v. 21, p. 463–466.

ZHAO, J-X., McCULLOCH, M. T., and KORSCH, R. J., 1994, Characterisation of a plume-related ~800 Ma magmatic event and its implications for basin formation in central-southern Australia: Earth and Planetary Science Letters, v. 121, p. 349–367.

ZIEGLER, P. A., 1993, Plate-moving mechanisms: their relative importance: The Geological Society of London, Journal, v. 150, p. 927–940.

ZINDLER, A., and HART, S. R., 1986, Chemical Geodynamics: Annual Review of Earth and Planetary Sciences, v. 14, p. 493–571.

ZOLUTUKHIN, V. V., and AL'MUKHAMEDOV, A. I., 1988, Traps of the Siberian Platform, *in* Traps of the Siberian Platform *edited by* J. D. McDOUGALL: Norwell, Massachusetts, Kluwer Academic, p. 273–310.

Appendix 1

Digital whole-rock chemistry (.csv digital dataset on Department's website)

Appendix 2

Analyses of the Bunbury Basalt reference material

Sample date	*Detection*	*08/02/2002*	*09/05/2002*	*12/08/2002*	*30/08/2002*	*30/08/2002*	*06/09/2002*	*06/09/2002*	*06/09/2002*	*06/09/2002*	*06/09/2002*	*06/09/2002*
							Percentage					
SiO_2	0.01	51.24	51.26	51.68	51.64	50.91	51.37	51.40	51.75	51.46	51.60	51.35
TiO_2	0.005	1.979	1.968	1.962	1.983	1.972	1.994	1.997	1.994	1.975	1.986	1.965
Al_2O_3	0.005	15.225	15.194	15.295	15.349	15.209	15.418	15.292	15.412	15.265	15.328	15.310
Fe_2O_3	0.005	2.948	2.934	3.081	3.351	3.222	3.483	3.445	3.322	3.027	3.019	3.131
FeO	0.01	8.06	8.22	8.07	7.86	7.83	7.87	7.83	7.93	8.21	8.16	8.06
MnO	0.005	0.160	0.171	0.158	0.159	0.155	0.161	0.155	0.160	0.160	0.158	0.158
MgO	0.005	4.513	4.650	4.013	4.070	4.036	4.112	4.067	4.082	4.063	4.086	4.041
CaO	0.01	8.46	8.63	8.72	8.75	8.66	8.81	8.70	8.77	8.73	8.77	8.71
Na_2O	0.01	2.93	2.96	3.01	3.00	2.98	3.04	2.98	3.05	3.04	3.01	2.99
K_2O	0.005	0.439	0.443	0.448	0.450	0.444	0.454	0.442	0.458	0.454	0.450	0.450
P_2O_5	0.005	0.246	0.265	0.266	0.269	0.258	0.265	0.267	0.265	0.266	0.263	0.268
SO_3	0.001	0.135	0.166	0.196	<0.001	<0.001	0.202	0.197	0.200	0.201	0.201	0.200
LOI	–	2.68	2.11	2.09	0.21	0.20	1.83	2.26	1.61	2.11	1.96	2.37
Total	**–**	**99.01**	**98.97**	**98.99**	**97.09**	**95.86**	**99.01**	**99.02**	**99.01**	**98.97**	**98.98**	**98.99**
							Parts per million					
Ag	0.01	<0.01	<0.01	<0.01	<0.01	<0.01	<0.01	<0.01	<0.01	<0.01	<0.01	<0.01
As	0.5	6.1	4.5	7.9	7.1	7.1	6.8	6.3	6.1	5.9	5.7	6
Ba	10	156	137	159	155	156	157	154	160	140	149	162
Be	0.1	0.7	0.3	0.8	0.4	0.7	0.6	1	0.7	0.8	1.1	0.7
Bi	0.1	<0.1	<0.1	<0.1	<0.1	<0.1	<0.1	<0.1	<0.1	<0.1	<0.1	<0.1
Cd	0.1	0.15	0.11	0.13	<0.1	<0.1	<0.1	<0.1	<0.1	<0.1	<0.1	<0.1
Ce	0.1	28.22	24.79	27.42	25.54	25.7	27.55	27.56	27.92	27.12	27.37	27.21
Cr	2	155	150	152	153	152	152	155	152	154	152	152
Cs	0.01	0.35	0.33	0.38	0.39	0.35	0.37	0.38	0.37	0.38	0.37	0.37
Cu	1	83	83	83	83	85	83	83	84	84	84	84
Dy	0.01	7.13	6.96	7.42	7.36	7	7.57	7.61	7.56	7.5	7.51	7.42
Er	0.01	3.81	3.87	3.94	3.93	3.92	3.97	3.97	3.87	3.95	3.99	3.93
Eu	0.001	2.003	1.845	2.069	1.97	2.091	2.063	2.018	2.044	2.064	1.989	2.022
F	50	411	381	408	431	432	412	441	421	423	432	451
Ga	0.2	23.6	22.7	23.8	24	24.3	23.3	23.1	23.3	23.3	22.9	22.8
Gd	0.01	7.63	7.33	7.66	7.44	7.42	7.76	7.84	7.68	7.59	7.69	7.79
Ge	0.1	1.6	1.5	1.4	1.6	1.6	1.5	1.5	1.5	1.4	1.6	1.4
Hf	0.1	3.7	3.9	4.1	4.2	4	3.9	4.1	4.1	4.1	4.1	4.1
Ho	0.01	1.44	1.33	1.58	1.52	1.48	1.63	1.64	1.62	1.58	1.59	1.58
La	0.02	11.24	10.28	11.29	10.63	10.67	11.13	11.16	11.13	11.01	11.14	10.96
Lu	0.01	0.43	0.43	0.53	0.51	0.49	0.54	0.53	0.53	0.53	0.55	0.53
Mo	0.1	2.7	3.5	1.7	1.8	1.9	1.5	1.6	1.6	1.5	1.6	1.5
Nb	0.1	7.7	7.6	7.5	8.7	8.7	7.7	7.7	7.5	7.5	7.4	7.5
Nd	0.01	18.97	17.91	19.38	18.53	19.36	19.63	19.54	19.6	19.47	19.54	19.23
Ni	2	48	49	47	47	49	46	49	47	49	48	47
Pb	0.5	4.3	3.8	4.7	2.7	5	3.1	3.9	4	3.5	4	3.3
Pr	0.01	3.74	3.61	3.55	3.28	3.34	3.52	3.57	3.56	3.55	3.53	3.49
Rb	0.3	10.6	10.9	11	10.6	11.1	10.8	10.6	11	11.3	10.7	11.3
Sb	0.1	0.3	<0.1	0.3	0.4	0.3	0.2	0.3	0.3	0.3	0.3	0.3
Sc	2	30	30	30	31	30	30	29	30	28	30	29
Sm	0.01	5.87	5.75	5.98	5.63	6.07	5.61	5.6	5.83	5.66	5.74	5.6
Sn	0.5	1.6	1.8	2.1	1.4	1.6	1.9	1.8	1.9	1.6	1.7	1.8
Sr	1	239	237.1	237.4	237.7	238.7	236.2	237.9	238	238.3	237.6	238.7
Ta	0.1	0.4	0.5	0.5	0.4	0.4	0.5	0.5	0.5	0.5	0.5	0.5
Tb	0.01	1.29	1.25	1.34	1.26	1.27	1.31	1.36	1.32	1.3	1.3	1.3
Th	0.1	1.5	1.7	1.8	1.7	1.7	1.9	1.9	1.9	1.9	1.9	1.9
U	0.01	0.29	0.31	0.31	0.29	0.29	0.32	0.33	0.34	0.32	0.32	0.31
V	5	254	257	204	207	201	206	202	206	203	204	200
Y	0.5	33.9	37	40.8	43.3	43.9	41.8	40.4	39.5	41	39.3	40.7
Yb	0.01	3.1	3.23	3.27	3.28	3.29	3.33	3.34	3.33	3.29	3.33	3.31
Zn	1	114.3	113	114	114	114	113	114	114	113	114	114
Zr	1	158	157	157	157	158	156	158	157	158	157	157

NOTE: RSD% percentage relative standard deviation

06/09/2002	06/09/2002	06/09/2002	06/09/2002	19/02/2003	19/02/2003	10/07/2003	10/07/2003	19/09/2003	19/09/2003	Average	Standard deviation	RSD%
						Percentage						
51.79	51.63	51.42	51.29	51.64	51.51	51.76	50.47	52.30	52.32	51.51	0.40	0.8
1.993	1.979	1.968	1.973	1.994	2.004	2.000	1.954	2.026	2.038	1.986	0.021	1.0
15.372	15.300	15.268	15.286	15.359	15.346	15.346	14.979	15.425	15.552	15.311	0.112	0.7
3.032	3.372	2.921	2.949	3.608	3.843	3.711	3.406	3.894	3.847	3.312	0.325	9.8
8.19	7.88	8.20	8.18	7.69	7.55	7.60	7.60	7.57	7.58	7.91	0.24	3.1
0.160	0.159	0.159	0.157	0.158	0.160	0.163	0.158	0.166	0.167	0.160	0.004	2.4
4.083	4.070	4.057	4.059	4.066	4.088	4.797	4.487	4.879	4.897	4.248	0.309	7.3
8.78	8.74	8.72	8.70	8.79	8.76	8.68	8.46	8.76	8.77	8.71	0.09	1.1
3.03	3.01	2.97	3.02	3.05	3.09	3.04	2.97	3.10	3.08	3.02	0.04	1.5
0.453	0.452	0.448	0.448	0.451	0.456	0.453	0.440	0.457	0.452	0.450	0.005	1.2
0.268	0.263	0.269	0.266	0.271	0.270	0.250	0.244	0.258	0.257	0.263	0.008	2.9
0.197	0.204	0.199	0.203	0.197	0.193	0.101	0.092	0.100	0.102	0.173	0.043	24.6
1.63	1.95	2.37	2.45	2.75	2.74	2.04	4.67	0.99	0.88	1.99	0.96	48.1
98.98	**99.01**	**98.97**	**98.98**	**100.03**	**100.02**	**99.94**	**99.94**	**99.92**	**99.93**	**–**	**–**	**–**
						Parts per million						
<0.01	<0.01	<0.01	<0.01	0.02	0.02	0.12	0.05	<0.01	<0.01	0.05	0.05	89.8
5.6	6	5.5	5.3	2.3	2.1	4.5	1.3	3	4.2	5.2	1.8	33.9
167	151	147	148	149	136	159	162	146	150	152	8	5.4
0.6	0.8	1.1	0.7	0.5	0.8	1.2	1.2	1.2	1.1	0.8	0.3	32.9
<0.1	<0.1	<0.1	<0.1	<0.1	<0.1	0.1	<0.1	<0.1	<0.1	0.1	–	–
<0.1	<0.1	<0.1	<0.1	<0.1	<0.1	0.12	0.17	0.42	0.12	0.2	0.1	63.3
27.24	27.81	27.39	26.98	25	25.04	25.35	26.4	23.71	24.92	26.5	1.3	4.9
154	151	153	150	153	150	146	151	147	146	151	3	1.7
0.36	0.38	0.36	0.36	0.34	0.32	0.33	0.31	0.32	0.3	0.35	0.03	7.4
84	83	84	84	84	84	87	83	89	88	84	2	2.0
7.51	7.48	7.3	7.36	7.19	6.91	6.75	6.85	7.06	6.82	7.25	0.28	3.9
3.93	3.93	3.9	3.95	4.01	3.89	3.81	3.92	4.09	3.99	3.93	0.06	1.6
2.043	2.078	2.102	2.045	1.993	2.043	2.054	2.09	1.953	1.944	2.02	0.06	3.0
427	396	416	416	438	420	407	408	423	402	419	16	3.9
22.6	23	22.8	22.6	23.6	23.7	23	23.3	23.5	22.9	23.2	0.5	2.0
7.79	7.69	7.59	7.62	7.1	6.75	6.85	7.06	6.96	6.59	7.42	0.38	5.1
1.5	1.5	1.4	1.4	1.4	1.4	1.5	1.4	1.6	1.5	1.5	0.1	5.3
4.2	4.2	4.2	4	4	4	3.8	4.6	3.9	3.7	4.0	0.2	4.9
1.6	1.59	1.56	1.58	1.41	1.37	1.33	1.46	1.38	1.33	1.50	0.11	7.2
10.99	11.09	11.06	10.9	10.37	10.32	10.48	10.74	10.03	9.94	10.79	0.41	3.8
0.52	0.53	0.55	0.52	0.47	0.47	0.47	0.49	0.47	0.43	0.50	0.04	7.9
1.5	1.5	1.5	1.5	1.8	1.9	1.7	1.9	1.4	1.6	1.8	0.5	27.3
7.4	7.4	7.3	7.3	7.4	7.4	7.2	7.7	7.2	7.1	7.6	0.4	5.5
19.45	19.54	19.58	19.43	18.49	18.59	18.73	18.55	17.67	17.78	19.00	0.64	3.4
48	47	49	47	49	47	45	47	46	46	47	1	2.5
3.6	4.6	5.3	3.8	1.9	2.1	4.2	4.8	3	6	3.9	1.0	26.1
3.53	3.58	3.48	3.48	3.71	3.72	3.96	3.85	3.63	3.7	3.59	0.16	4.3
10.8	10.5	11.1	11.1	10.4	10.8	11.8	10.8	11.9	11.9	11.0	0.4	4.0
0.3	0.3	0.3	0.3	0.2	0.2	0.7	0.2	0.2	0.2	0.3	0.1	37.3
30	30	31	29	30	31	28	32	27	28	30	1	4.0
5.9	5.81	5.82	5.79	5.75	5.85	5.67	5.49	5.51	5.34	5.73	0.17	3.0
1.7	1.7	2	1.6	1	1	1.6	2	1.5	1.4	1.7	0.3	17.4
239.2	238.3	239	237.7	238.7	238.1	237.7	235.7	238.4	237.5	238	1	0.4
0.5	0.5	0.5	0.5	0.5	0.5	0.3	0.5	<0.1	<0.1	0.5	0.1	11.9
1.3	1.34	1.31	1.29	1.16	1.15	1.19	1.2	1.12	1.11	1.26	0.07	6.0
1.8	1.9	1.9	1.8	1.7	1.7	1.5	1.5	1.6	1.6	1.8	0.1	8.4
0.31	0.31	0.32	0.31	0.29	0.29	0.27	0.3	0.26	0.27	0.30	0.02	6.8
202	208	201	208	205	207	202	206	194	200	208	16	7.7
38.2	39.3	39.7	39.1	39.7	40.5	39.9	33.1	38.6	38.9	39.5	2.5	6.4
3.32	3.4	3.33	3.29	3.33	3.37	3.2	3.17	3.36	3.2	3.29	0.07	2.2
114	114	114	114	114	114	114	113	114	114	114	0	0.4
158	158	158	157	158	157	155	156	155	155	157	1	0.7

Based on SHRIMP U–Pb geochronology, field relations, and geochemistry, dolerite sills intruding the Mesoproterozoic Bangemall Supergroup belong to either a 1465 or 1070 Ma magmatic event. The 1070 Ma sills and related volcanic rocks cover an area of about 1.5 million km^2 forming the Warakurna Large Igneous Province (LIP). The sills are variably fractionated, with uniform incompatible-element ratios and REE patterns, apart from some crustally contaminated sills in parts of the eastern Bangemall Supergroup. Isotope and trace element data support derivation of the sills from a subduction-modified lithospheric source induced by a mantle plume. The mineral potential of the Warakurna LIP includes magmatic Ni–PGE deposits of the Noril'sk type, and magmatic-hydrothermal deposits related to felsic anorogenic magmatism.

This Report is published in digital format (PDF) and is available online at: www.doir.wa.gov.au/gswa/onlinepublications. Laser-printed copies can be ordered from the Information Centre for the cost of printing and binding.

Further details of geological publications and maps produced by the Geological Survey of Western Australia are available from:

Information Centre
Department of Industry and Resources
100 Plain Street
East Perth, WA 6004
Phone: (08) 9222 3459 Fax: (08) 9222 3444

www.doir.wa.gov.au/gswa/onlinepublications

MORRIS, PIRAJNO

Mesoproterozoic sill complexes in the Bangemall Supergroup, Western Australia: geology, geochemistry, and mineralization potential

REPORT 99